7-1-2016

Arciero vs. LaPrade: A Biomechanical Study Comparison of Two Techniques for Knee Posterolateral Corner Reconstruction

Gabriel Ortiz

Gabriel T. Ortiz

Candidate

Mechanical Engineering

Department

This thesis is approved, and it is acceptable in quality and form for publication:

Approved by the Thesis Committee:

Christina Salas , Chairperson

Mahmoud Taha

Yu-Lin Shen

Robert Schenck

Arciero vs. LaPrade: A Biomechanical Comparison of Two Techniques for Knee Posterolateral Corner Reconstruction

by

Gabriel T. Ortiz

B.S., Mechanical Engineering

THESIS

Submitted in Partial Fulfillment of the
Requirements for the Degree of

Master of Science
Mechanical Engineering

The University of New Mexico

Albuquerque, New Mexico

July, 2016

Dedication

To my mother and father, whose love and responsibility has shaped my life and led me to a promising future. I will forever be gracious and thankful for your example. I will honor and cherish the time I have shared with you as your son. I love you so much.

Acknowledgments

My thanks to my committee members Dr. Shen, Dr. Taha, and Dr. Schenck.

I would like to acknowledge the Mountain West Clinical Translational Research Infrastructure Network (grant 1U54GM104944) and UNM Clinical & Translational Science Center (CTSC) (grant UL1TR001449) for their assistance with this study's data analysis.

I would like to thank the UNMH Orthopaedic Dept. and the University of New Mexico for their resources, funding, and support of this study. My thanks to the residents of the study: Heather Menzer, Kieth Gill, and Paul Johnson. And special thanks to Dr. Treme and Dr. Schenck for guiding and facilitating the study.

Finally, I would like to thank my mentor Christina Salas. Dr. Salas has been an invaluable source of knowledge, guidance, patience, and understanding. She has demonstrated the utmost example of self-motivation, determination, attention to detail, and professionalism in the work environment. I greatly appreciate the time and energy Dr. Salas has spent with me as an advisor for my graduate career at UNM and cannot thank her enough for her constant support.

Arciero vs. LaPrade: A Biomechanical Comparison of Two Techniques for Knee Posterolateral Corner Reconstruction

by

Gabriel T. Ortiz

B.S., Mechanical Engineering

M.S. Mechanical Engineering, University of New Mexico, 2016

Abstract

The purpose of this study is to biomechanically compare the effectiveness of restoring stability to a deficient Posterolateral Corner (PLC) using two different PLC reconstruction techniques, Arceiro and LaPrade. Stabilization of the PLC is the outcome of three soft tissue structures: the Fibular Collateral Ligament (FCL), the Popliteofibular Ligament (PFL), and the Polpliteus Tendon (PLT). For this study, these three structures were sectioned to simulate a deficient PLC. 10 paired fresh frozen lower extremity cadaveric specimens were used for experimentation. One limb from each pair was reconstructed using the LaPrade technique and the other with the Arciero technique using the Achilles tendon as graft material. A custom made testing fixture was created to isolate and test for a 10 Nm Varus Angulation (VA) moment and a 5 Nm External Rotation (ER) torque at 0°, 20°, 30°, 60°, and 90° of flexion about the knee joint. Testing was performed in the following order: prior to PLC sectioning, post sectioning, post reconstruction, and post sectioning of either the tibiofibular ligament or the ACL. Five of the paired cadaveric specimens had

their tibiofibular ligament sectioned, the remaining five specimens had their ACL's sectioned. Sectioning of the tibiofibular ligament or ACL was randomized to ensure that there was no repetition or bias during the study. We hypothesize that the LaPrade reconstruction will yield superior results because it attempts to simulate the repair of all three soft tissue structures whereas the Arciero technique aims repair of only the FCL and the PLT.

Contents

List of Figures

List of Tables

Glossary

anterior Front

bipennate Muscle with a central tendon where fibers converge from either side

distal Location farthest from the trunk of the body

iliac One of four spines of the ilium

intracapsular Situated or occuring within a capsule

lateral Away from midline

linea aspera Longitudinal ridge running down the posterior surface of the femur

medial Toward midline

posterior Back

prone Facing downward

proximal Location closest to the trunk of the body

supine Facing upward

supracondylar Above a condyle

superior Situated above or directed upwards

tuberosity An elevation or protuberance

Chapter 1

Introduction

1.1 Introduction

The Posterolateral Corner (PLC) is an area of the knee that does not receive adequate research recognition despite its functionality and contribution to the overall stability of the knee. Until recently, its anatomy and biomechanics have been poorly understood and the need for diagnosis and treatment have been in a constant state of evolution. This has led to the creation of multiple reconstruction methods. The two most commonly used techniques are the Arciero and LaPrade reconstructions. Both have shown promising outcomes, but the two techniques have never been compared against each other from a biomechanical perspective. Advantages of the Arciero technique include: a relatively straight-forward procedure for reconstruction of the fibular collateral ligament (FCL) and popliteofibular ligament (PFL) that requires less time as compared to other techniques. The LaPrade technique benefits from the inclusion of popliteus tendon (PLT) graft which produces added reinforcement to the PLC. The objective of this study is to identify which reconstruction technique best restores stability to an isolated PLC injury in addition to an injury to the tibiofibular

ligament or Anterior Cruciate Ligament (ACL).

1.2 Motivation and Methods

The PLC is rarely an isolated injury and is commonly injured in conjunction with one or both cruciate ligaments. Though an uncommon occurrence, there has also been evidence that the tibiofibular joint becomes jeopardized in the event of a PLC injury in part because the most distal aspect of the Fibular Collateral Ligament (FCL) and Popliteofibular Ligament (PFL) attach to the fibular head. Multiple PLC reconstruction techniques exist but none have proven to perform best for complete repair and biomechanical functionality. There has been great interest in two specific PLC techniques, Arciero and LaPrade. These two techniques have shown promising clinical outcomes and have been compared against alternate techniques but never against each other. The present study aims at elucidating which technique best restores stability and function to an isolated PLC injury and injuries involving the tibiofibular ligament or ACL.

1.3 Structure of Thesis

This thesis is structured as followed: Chapter 2 describes the anatomy of the primary and secondary static stabilizers of the PLC. In addition, Chapter 2 describes different clinical tests used to determine the severity of a PLC injury. Finally we describe the surgical procedures and distinguish the differences between the Arciero and LaPrade PLC reconstructions.

Chapter 3 summarizes the experimental methods of the study. We describe the testing fixture design including all of its individual components, the torque/force

applicators, the Optitrack Motion Capture software, specimen preparation, and testing protocol. The experimental results are explained and compared accordingly in Chapter 4. Chapter 5 discusses the conclusions of the study, findings that should be addressed, and future work.

Chapter 2

Literature Review

2.1 Anatomy of the Posterolateral Corner

The Posterolateral Corner (PLC) is often called the "dark side" of the knee due to its complexity and the minimal amount of research performed to better understand its anatomy and biomechanics. Recently, great strides by Dr. LaPrade and others have helped to shed light and characterize its anatomy and complicated function. The PLC consists of multiple structures in the knee; bones that include the femur, tibia, and fibula, and soft tissue structures such as the fibular collateral ligament (FCL), popliteus tendon (PLT), popliteofibular ligament (PFL), lateral gastrocnemius tendon, iliotibial band, and the biceps femoris tendon. Though not located in the posterolateral aspect of the knee, the Anterior Cruciate Ligament (ACL) and Posterior Cruciate Ligament (PCL) act as secondary stabilizers that resist internal and external rotation.

The combination of all the previously mentioned primary and secondary structures help to stabilize the posterolateral corner of the knee. Research has demonstrated that the primary static stabilizers consist of the FCL, the PLT, and the PFL.

These three soft tissue structures stabilize the PLC at varying degrees of flexion and extension by resisting varus gapping in combination with external rotation at the knee joint. Internal rotation about the knee has also been investigated but research has shown that a compromised PLC has little effect in terms of this area of concern. The FCL, PLT, and PFL will be the primary focus of concern when analyzing the biomechanics of the PLC for this study.

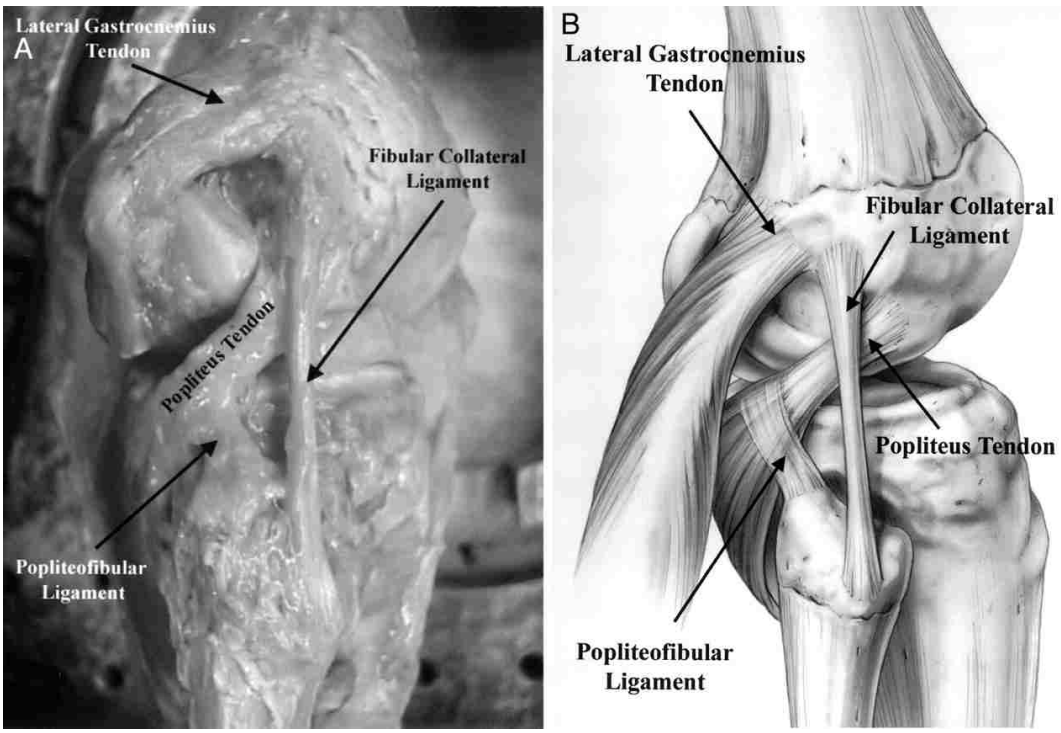

Figure 2.1: Gross anatomy (A) and illustration (B) of the Posterolateral Corner highlighting the Fibular Collateral Ligament, Popliteus Tendon, Popliteofibular Ligament, and the Lateral Gastrocnemius Tendon. [23]

2.2 Primary Structures that Stabilize the PLC

2.2.1 The Fibular Collateral Ligament

Serving as the predominant ligament tissue structure in the lateral aspect of the knee, the FCL, also known as the lateral collateral ligament, is one of three central stabilizers that provides stability in the PLC. The FCL has a mean length of 57.8 $\pm$ 5.5 mm and a cross sectional area of 11.9 $\pm$ 2.9 mm^2. On average, the femoral attachment site is located in a depression proximal (1.4 mm) and posterior (3.1 mm) to the lateral femoral condyle (Figure 2.2) [1,2,27,28]. The FCL then inserts at the lateral aspect of the fibular head posterior (8.2 mm) to the anterior margin and distal (28.4 mm) to the fibular styloid process with an average cross sectional area of attachment of 43 mm^2 (Figure 2.2) [1,2,27,28]. The FCL serves as the primary structure that resists varus gapping between the distal femur and proximal tibia in the lateral aspect of the knee joint. It is the most commonly injured structure in the PLC.

2.2.2 The Popliteus Tendon

The PLT serves and the main contributor for resisting external rotation about the knee joint. The origin of the PLT is located on the most anterior aspect of the popltiteus sulcus (Figure 2.2). It originates from the lateral femoral condyle with an average distance of 18.5 mm distal and posterior to the FCL origin. Studies have found the mean length of the PLT to be 34.3 $\pm$ 5.5 mm with an average cross sectional area of 21.9 $\pm$ 3.9 mm^2 and an average area of attachment of 59 mm^2 [1,2,27,28]. Other studies have found the mean length to vary substantially. A study by LaPrade et al reported a range of 50.5 mm to 61 mm with an average length of 54.5 mm[3]. Due to this variability, the true mean length of the PLT fluctuates and

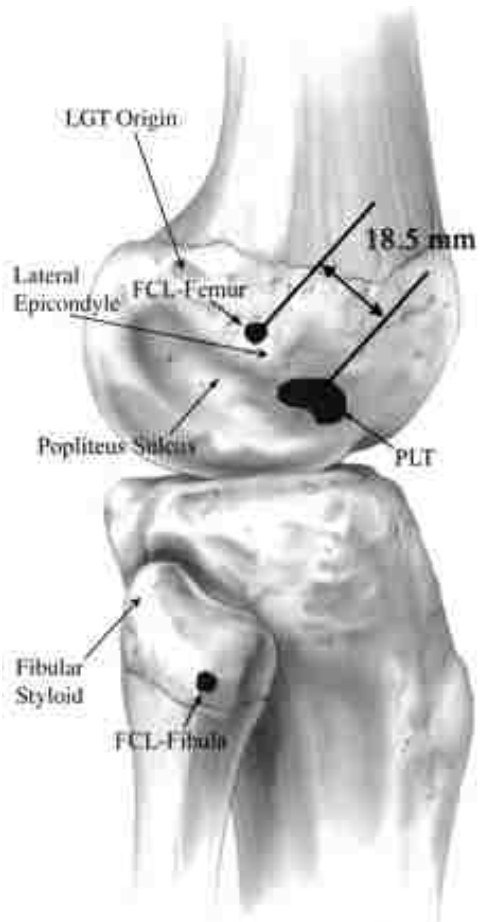

Figure 2.2: PLC illustration highlighting the origins and areas of attachment for the FCL, PLT, and PFL. [23]

will be dependent on the size of the specimens used for the study. The distal end of the PLT inserts at the musculotendious junction of the popliteus muscle which runs posterior and medial to the proximal tibia and is a dynamic stabilizer for the lateral aspect of the knee[1,27,28]. The PLT possesses superior mechanical properties and can undergo the largest load to failure as compared to other primary static stabilizers because of its structural composition as a tendon rather than a ligament.

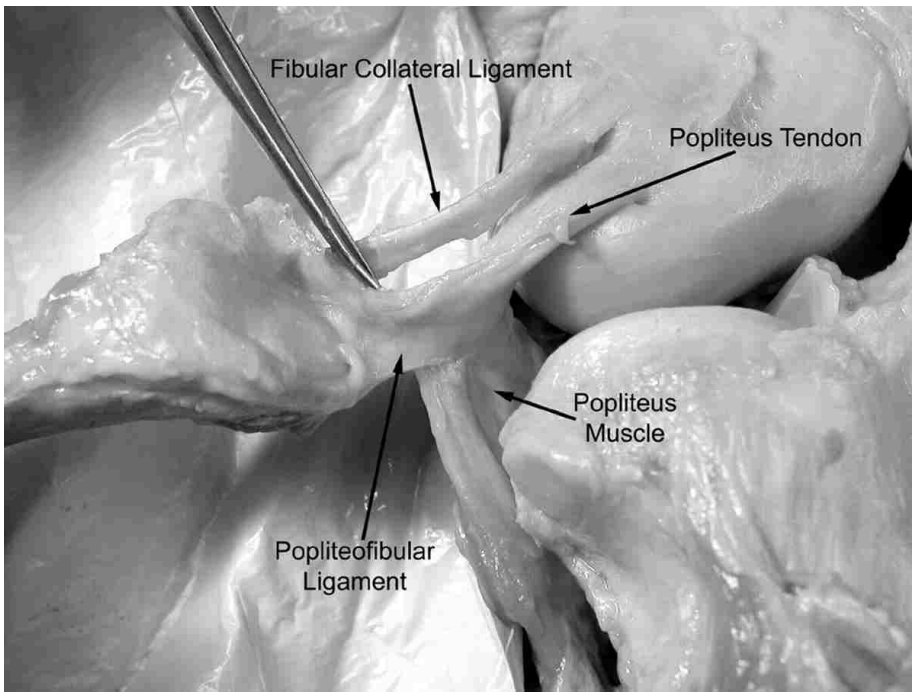

Figure 2.3: Isolated PLC Structures. The tibiofibular ligament has been disarticulated to show individual primary structures in the PLC: FCL, PLT, and PFL. [2]

2.2.3 The Popliteofibular Ligament

The PFL originates from the musculotendinous junction of the popliteus structure and attaches distally and anterior onto the fibular styloid process at an average angle of 83° with a range from 78° to 88° [3]. Studies have shown the mean length of the PFL to be $14.7 \pm 2.5\ mm$ with an average cross-sectional attachment area of $17.9 \pm 1.9\ mm^2$ [2,27,28]. It joins the PLT at the musculotendious junction of the popliteus structure. The PFL is the shortest of the three primary static stabilizers, in addition it has the lowest Young's Modulus at 24.8 ± 14.5 MPa but the largest strain to failure at 0.64 ± 0.5 [1]. All three primary structures can be viewed individually from each other in Figure 2.3. Additional mechanical properties of the primary static structures can be seen in Figure 2.1

Mechanical Properties of the Posterolateral Structures of the Knee						
	Ultimate Tensile Load, N	Stiffness N/m	Max Stress, MPa	Strain %	E MPa	Cross-sectional Area, mm^2
FCL	295±96	33.5±13.4	26.9±11.7	.16±.05	183.5±110.7	11.9±2.9
PFL	298.5±144.1	28.6±13.6	12.8±6.0	.64±.40	24.8±14.5	17.9±1.9
PLT	700.3±231.7	83.7±24.3	32.0±13.1	.27±.18	130.9±37.0	21.9±3.9

Table 2.1: Mean failure properties (± SD) of the Fibular Collateral Ligament (FCL), Popliteofibular Ligament (PFL), and Popliteus Tendon (PLT)

2.3 Secondary Structures

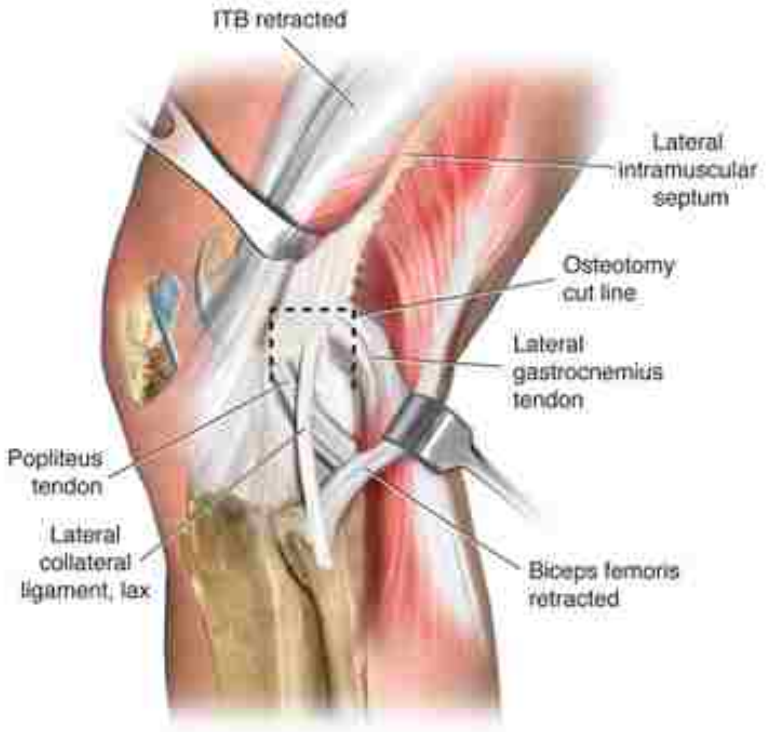

Figure 2.4: Lateral view of the knee highlighting the secondary structures of the PCL. This includes the Lateral Gastrocnemius Tendon, Iliotibial Band, and the Biceps Femoris. [35]

2.3.1 The Lateral Gastrocnemius Tendon

The gastrocnemius structure (Figure 2.4) is a bipennate muscle with a medial and lateral head. The medial head originates from the medial femoral condyle while the lateral head forms about the lateral femoral condyle and inserts at their respective musculotendinous junctions. The gastrocnemius muscle contributes to the knee biomechanially by flexing the calf muscle about the knee joint and is primarily involved during running and jumping. The lateral gastrocnemius tendon has an attachment site located at the supracondylar process of the distal femur and is located 13.8 mm posterior to the FCL, 28.4 mm posterior to the PLT insertion, and is nearly inseparable from the meniscofemoral portion of the posterior capsule [5].

2.3.2 The Iliotibial Band

The ITB (Figure 2.4) originates from the anterior superior iliac spine and the anterior part of the external lip of the iliac crest and inserts onto the anterolateral aspect of the lateral tibial plateau [5]. Its primary function is to stabilize the knee when in extension. It is used constantly and contributes to stabilization of the lateral aspect of the knee as well. Though the IT Band is a structural component of the PLC and is constantly used during everyday activities, it plays a significantly less important role as compared to other posterolateral structures.

2.3.3 The Biceps Femoris

The Biceps Femoris (Figure 2.4) is a muscle that consists of a long and short head and is a component of the hamstring muscle group. The long head originates from the ischial tuberosity and is part of the common hamstring origin whereas the short head originates slightly medial to the linea aspera of the distal femur, and is innervated

by the peroneal division of the sciatic nerve [5]. Its basic function is to flex the leg at the knee joint, in addition it is a secondary stabilizer for internal and external rotation. The Biceps Femoris tendon is the structure associated with the PLC and is found approximately 1.5 to 2 cm distal to fibular styloid.

2.3.4 The Tibiofibular Ligament

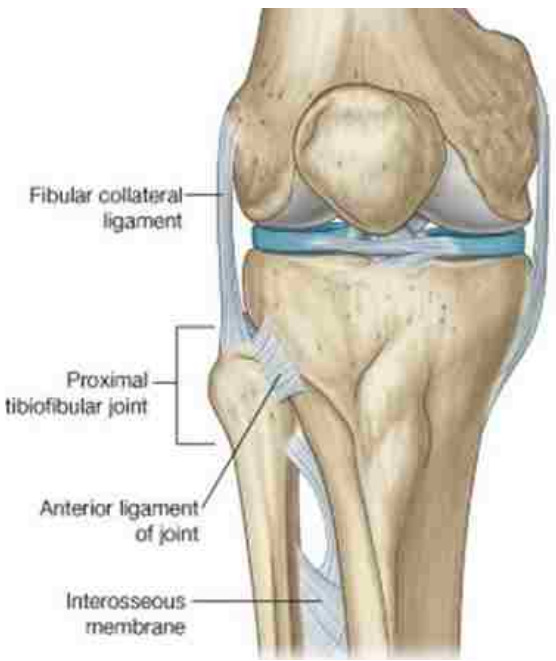

Figure 2.5: Tibiofibular joint with respect to the fibula and tibia. [36]

The proximal head of the fibula serves as the most distal point of attachment for two of the primary soft tissue structures comprised of the PLC, the FCL and PFL [2,3,27,28]. The tibiofibular joint is the area in which the proximal fibular head attaches to the lateral condyle of the tibia (Figure 2.5). It is required that this structure/component remain intact for lateral-sided knee reconstructions. Specifically for the majority of PLC reconstructions, an anterior to posterior tunnel is reamed through the proximal fibular head in order to pass the respective FCL graft which

is secured to the fibular tunnel during the surgical process by an interference screw. Jabara [26] et al has mentioned that there is a frequency of proximial tibiofibular joint instabilities when presented with patients who have suffered multiligament knee injuries. Jabara also suggests that the lack of diagnosis for a dislocated tibiofibular joint may be the cause of failed PLC reconstructions.

2.3.5 The Anterior Cruciate Ligament (ACL) and Posterior Cruciate Ligament (PCL)

There are two intracapsular cruciate ligaments that stabilize the human knee, they are the anterior cruciate ligament (ACL) and the posterior cruciate ligament (PCL). The ACL's primary function is to stabilize the knee by resisting anterior translation and medial rotation. It is the most commonly injured knee ligament [6,20]. Injury is normally induced in non-contact circumstances when moments of instantaneous acceleration or deceleration cause the femur and tibia to twist in opposite directions [20,22,28,31]. This produces a shearing force about the ACL which causes it to tear. This commonly occurs in sports that require a lot of running, stopping, jumping, and cutting such as basketball, soccer, volleyball, and skiing [31,32]. The ACL is commonly injured in conjunction with other knee ligaments such as the medial collateral ligament (MCL), PCL, and PLC.

The second cruciate ligament is the PCL. It resists posterior translation and provides minor external rotation stabilization of the tibia with respect to the femur. It is the stronger of the two cruciates and is an uncommonly injured ligament compared to the ACL. Injury occurs at its largest point of vulnerability which is when the knee is flexed at 90° and a large blunt force is directed at the proximal anterior face of the tibia [34]. This stresses the PCL beyond its ultimate tensile strength and causes it to rupture. Methods of injury include hyper extension and car injuries where the

Figure 2.6: Anterior view showing the respective locations of the ACL and PCL with respect to the femur and tibia. [37]

knee strikes the dashboard at high velocities [34]. Both the ACL and PCL can be viewed in Figure 2.6.

2.4 Injury to the Posterolateral Corner

The PLC is primarily responsible for resisting varus angulation and external rotation in addition to posterior displacement of the tibia. When compromised, the deficient PLC causes the individual to experience instability in posterior and lateral motions. It causes higher levels of stress to be induced onto the ACL and PCL which are the primary stabilizers to anterior and posterior translation, respectively. It is uncommon for the PLC to be an isolated injury. It is usually injured in conjunction with one or both cruciate ligaments or the tibiofibular joint [6,11,20,22,26]. When misdiagnosed or untreated, the lack of a structurally sufficient PLC induces more stress on adjacent

structures in knee reconstructions, this is a primary cause of graft failure for ACL or PCL reconstructions [6]. It is extremely important that the functionality of the PLC and tibiofibular joint be checked along with other clinical tests when diagnosing a knee injury.

Injury to the PLC commonly occurs in multiple ways, one example is due to a blunt force applied perpendicular to the anteromedial aspect of the knee while the distal tibia is grounded or fixed. This causes varus stress on the PLC which results in gapping or lateral angulation of the knee. This condition induces the most stress in the FCL (as compared to other posterolateral structures) whose primary function it to resist varus angulation [1,2,3,5,27,28]. When these blunt forces overcome the overall yield strength of the PLC, it can either be strained or completely ruptured. Another mechanism of injury occurs when the distal tibia is grounded or fixed and large amounts angular force is exerted about the knee joint causing external rotation. This puts increased tensile stress on both the FCL and the PLT. These mechanisms of injury are commonly caused by athletic traumas, motor vehicle accidents, and falls [4].

2.5 Diagnosis

There are multiple methods to evaluate the severity of a PLC injury. One of the first methods used to identify a compromised PLC is through gait analysis. Gait analysis is a physical examination that compares a patient's altered walking pattern to a universal standard. Often when a patient's lower extremity is injured, their gait pattern is modified to an extent that the patient cannot employ a muscular compensation strategy to effectively stabilize the knee [6, 8]. For a PLC injury, the patient may walk with slight knee flexion to prevent hyperextension and reduce pain associated with the lateral compartment. This altered gait pattern is a clear

indicator that structural damage may exist in the PLC and further testing should be conducted to determine the severity of the injury. It has also been noted that when standing, a patient may exhibit a varus alignment as compared to their corresponding limb [7].

A second method for evaluation is the use of radiograph imaging. Magnetic Resonance Imaging (MRI) and X-ray imaging are both excellent indicators for diagnosis, though MRI is the preferred imaging modality [7]. MRI's are especially useful for injury assessment because they can identify individual soft tissue structures whereas X-ray images cannot. In addition, MRI's can identify alternative soft tissue structures that may have been injured in combination with the PLC. The primary use of X-rays are to determine varus misalignment/gapping in the lateral compartment.

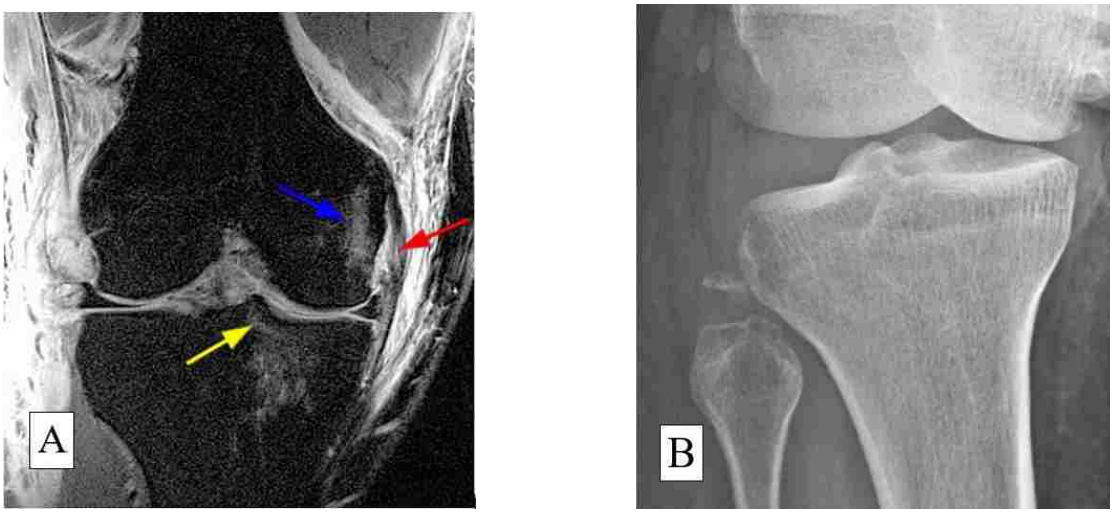

Figure 2.7: Radiograph imaging of an injured PLC. (A) MRI showing a strained FCL. (B) X-Ray showing lateral gapping between the lateral aspects of the distal femur and proximal tibia. [13]

2.6 Specialized Clinical Tests

To help confirm diagnosis, clinicians use 6 specialized tests to evaluate stability in the PLC. These six tests are the Posterolateral Drawer Test, Dial Test, External Recurvatum, Varus Stress, Reverse Pivot Shift Test, and Standing Apprehension [6].

2.6.1 Posterolateral Drawer Test

This test is conducted with the patient in the supine position with the knee flexed at 80° to 90° and the foot externally rotated at 15° [6, 7, 8]. With the patient's foot stabilized, the clinician applies a posterolateral drawer force and looks for increased posterolateral rotation compared to the contralateral knee [6]. A posterolateral drawer force includes a light posterior drawer force combined with external rotation about the knee joint. Increased rotation compared to the contralateral knee indicates injury to the popliteus complex. If extremely large posterolateral rotation is shown, this may indicate an injury not only to the popliteus complex, but also to the PCL.

2.6.2 External Rotation Recurvatum

For this test, the patient lies supine while the clinician stabilizes the thigh, grabs the big toe, and lifts. The amount of genu recurvate is observed against the normal knee. Genu recurvature is defined as excessive hyper extension where the knee bends backwards at the tibialfemoral joint. The clinician looks to compare for differences in lateral hyperextension, varus, and tibial external rotation [7]. This test is used to detect a concomitant PCL-ACL injury or a PLC bicruciate injury [6, 8].

2.6.3 Reverse Pivot-Shift

This test has been described as dynamic posterolateral drawer test, in this case the patient lies supine as the clinician flexes the knee at approximately 45° to 60° with the foot externally rotated and a valgus stress applied [8]. The clinician extends the patient's knee to 0° in a slow manner and looks for subluxation as he/she extends the leg. A positive test is confirmed when subluxation is felt at approximately 25° of flexion, this is compared to the opposite knee for verification[6].

2.6.4 Standing Apprehension Test

The standing apprehension test is assessed with the patient standing on his/her injured leg with slight flexion at the knee. The clinician applies a small force to the anterolateral portion of the lateral femoral condyle. If rotation of the lateral condyle about the tibia is noted in addition to the patient feeling as though their knee may "give out", this is indicative of a positive test [6]. This test is usually performed in conjunction with gait analysis. Often the amount of pain a patient experiences from a PLC injury prohibits the clinician from administering the standing apprehension test, because of this the standing apprehension test is one of the least common tests used for PLC evaluation.

2.6.5 Dial Test

The Dial test is performed with the patient in either the prone or supine position with the knee flexed at 30° and the thigh stabilized. While flexed, the foot is externally rotated and the position of the tibial tubercle is recorded relative to the opposite knee. External rotation of the tibial tubercle greater than or equal 10° is considered positive for a PLC injury [6, 7, 8]. The same test is repeated with the knee flexed

at 90°, if both tests show greater than 10° of external rotation, this may suggest an injury to both the PLC and the PCL. If a positive dial test is found at 30° of knee flexion but negative at 90° of flexion, this may indicate an isolated PLC injury [6]. This is an important clinical test because it helps to isolate the integrity of the PLC by specifically testing for rotational instability, ie. disarticulation of the PLT and PFL.

2.6.6 Varus Stress

The varus stress test is performed at both 30° and 0° with the patient lying in the supine position. The clinician allows the knee to be flexed at 30° off of the table and applies a varus stress by stabilizing the proximal femur and pulling the foot/ankle inwards which creates a moment about the lateral joint. This test is considered positive if the clinician feels an increased amount of translation or gapping about the lateral compartment as compared to the contralateral knee [6]. If large varus angulation is noted about the lateral joint, this is indicative of a complete tear of the FCL [6, 8]. The injury is graded accorded to how much gapping is recorded. A grade I FCL sprain shows mild gapping (0-5 mm) with a firm endpoint, grade II shows moderate gapping (5-10 mm), and grade III is scored when gapping is equal to or greater than 10 mm [6, 8]. The same test is repeated at 0° of flexion. If a positive varus stress test is found at 0° of flexion, this may suggest an injury to the PCL as well [6].

2.7 Reconstruction Techniques

Injuries to the posterolateral corner may be repaired or reconstructed in a variety of ways, yet there is no technique that separates itself amongst the wide variety. Unlike

the surgical improvements made for anterior and posterior reconstructions in the past decades, the posterolateral corner has seen little advancement in comparison. Residual laxity, instability and graft failure still exist post operatively in present day outcomes [15,19,26]. In this study we compared two widely used PLC reconstruction techniques: Arciero and LaPrade. The reconstruction techniques and biomechanical evaluations of each technique are described below.

2.7.1 Arciero Posterolateral Corner Reconstruction

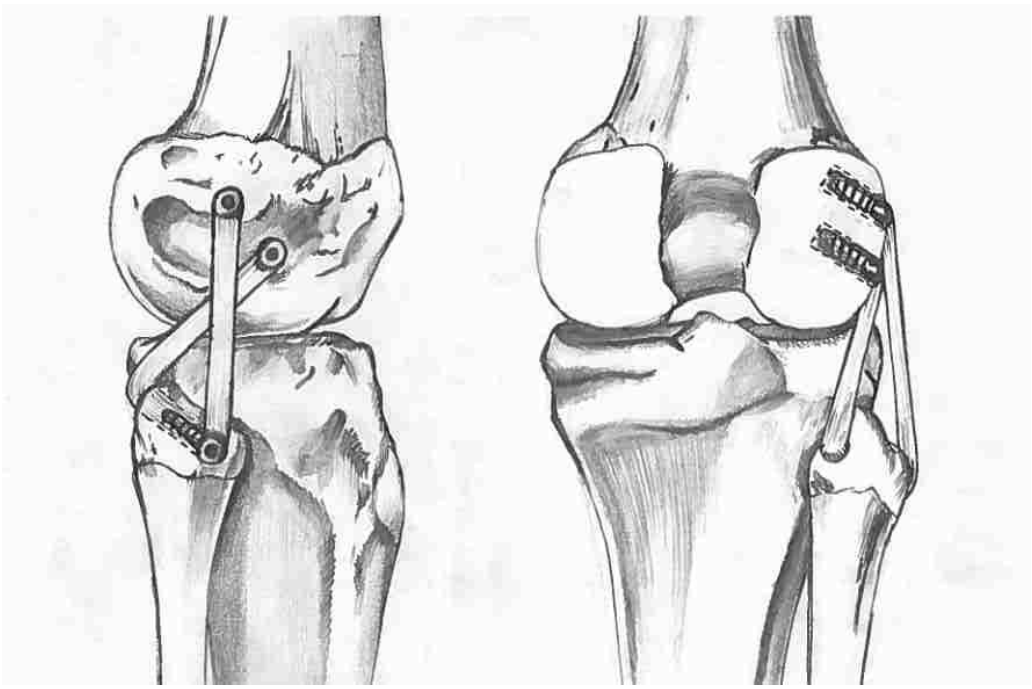

Figure 2.8: Arciero Reconstruction showing the anatomical locations for graft passage and insertion. The Arciero is distinguished by two femoral sockets and one fibular tunnel using a single graft to reconstruct the PLC [12]

The Arciero PLC Reconstruction technique is described in complete detail in a technical note written by Arciero in the Journal of Arthroscopic and Related Surgery 2005 [10]. The main attributes that distinguish this technique from others are the

use of dual femoral sockets and an anterior to posterior tibiofibular tunnel [10]. A single graft (commonly the Achilles tendon) is used to create two supporting limbs that act as the FCL and PFL. A Polyetheretherketone (PEEK) bioabsorbable interference screw is used to anchor the free end of the graft into the anterior fifth of the popliteus sulcus while the opposite end of the graft is tunneled through the tibiofibular joint. An additional PEEK interference screw is placed into the fibular tunnel to ensure complete tension. The opposite end of the graft is tensioned while the knee is flexed to 30° before it is secured. Finally the free end of the graft is then secured by another bioabsorbable screw into the femoral socket where the native FCL once originated. The Arciero technique does not attempt to recreate all three primary PLC stabilizers. The two limbs of the graft function as the FCL and the PFL. An anatomical reconstruction of the PLT is not attempted.

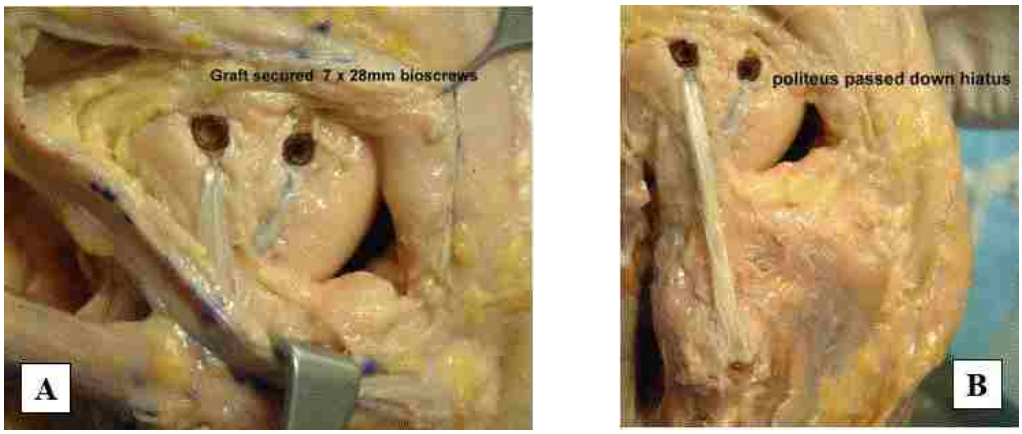

Figure 2.9: Arciero cadaveric PLC reconstrution. (A) Graft fixation using two bioabsorbable interference screws in the corresponding femoral sockets. (B) Vertical view showing the graft being passed through the fibular tunnel and then reinserting into the femoral sockets. Modified from [10]

Biomechanical tests have been conducted using the Arciero method in comparison with other techniques. Studies done by Po-Yan Ho et al. [12] and Thomas Nau et al [20] have used the Arciero PLC reconstruction method to compare varus laxity and external rotation at 0° and 30° of knee flexion. Po-Yan Ho et al. compared the

Arciero reconstruction against the Larson reconstruction. The Larson technique is similar to Arciero with respect to the single fibular tunnel. Larson differs by reaming only one femoral socket in the lateral femoral condyle where the two limbs of the graft are secured [20,28], as seen in Figure 2.10. They tested their specimens using a 5 Nm varus moment about the knee for varus laxity and 5 Nm rotational torque for external rotation. At 0° and 30° of flexion, intact varus laxity was measured to be 2.3° and 4° for Arciero and Larson, respectively. The final varus angulation was measured to 7.9° and 12.8°, respectively, when sectioned. On average after the Arciero reconstruction, varus laxity was reduced to 2° and 4.9° for 0 and 30 degrees of flexion, respectively [12]. The Larson technique restored varus laxity to 1° and 6.4° for 0 and 30 degrees of flexion, respectively. Due to standard deviation, Po-Yan Ho et al. concluded that statistically there was no difference between the two techniques. Additionally they found the average external rotation of intact knees to be 11.2° at 30° of flexion and 15° at 90° of flexion. After sectioning the PLC the specimens exhibited significant amounts of external rotation, 24.6° and 26.6°, respectively. After reconstruction using the Arciero technique, external rotation was measured to be 10.2° and 18.8° respectively. At 30 and 90 degrees of flexion, the Larson technique failed to restore stability as well as Arciero. They reported 14° and 20.2° at 30 and 90 degrees of flexion, respectively. In terms of external rotation, Po-Yan Ho et al. declared the Arciero technique to be superior.

The study conducted by Thomas Nau et al. compared the Arciero technique against a modified 4-Strand Larson PLC reconstruction; the modified Larson technique can be seen in Figure 2.11. They measured external rotation and varus laxity after both reconstructions at 0°, 30°, and 90° of flexion. They concluded that both techniques were statistically the same.

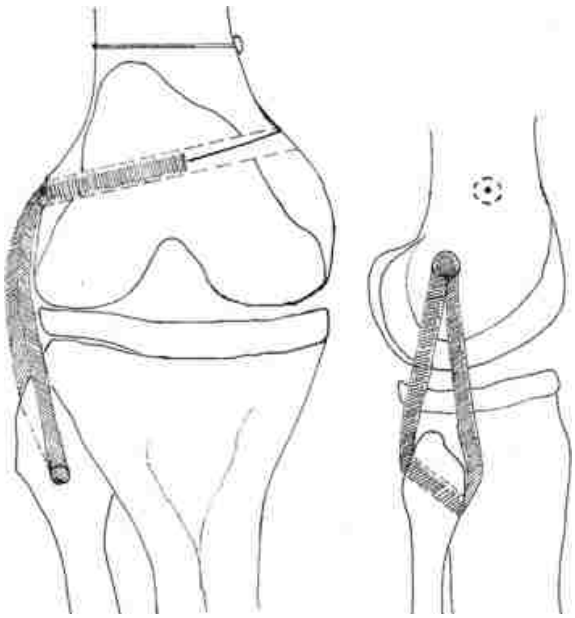

Figure 2.10: Larson PLC reconstruction. The Larson technique uses a single femoral socket to secure a single graft. It aims to reconstruct the FCL and a pseudo PLT [11].

Figure 2.11: Modified 4-Strand Larson PLC Reconstruction. This technique uses three grafts that reconstruct each individual primary PLC structure: FCL, PLT, and PFL by using dual femoral sockets, a fibular tunnel, and a tibial tunnel. [20]

2.7.2 LaPrade Posterolateral Corner Reconstruction

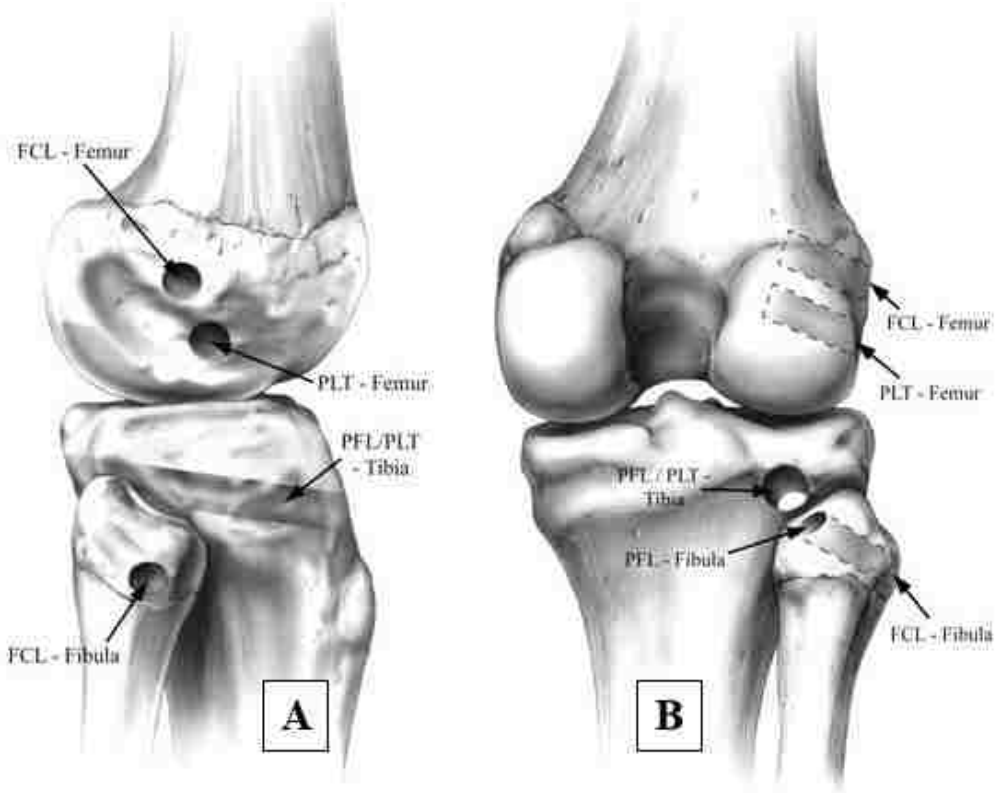

Figure 2.12: (A) Illustrates a lateral view of the femoral, fibular, and tibial tunnels where the corresponding grafts will be inserted. (B) Illustrates these same tunnels and insertion points but from the posterior aspect of the knee. Modified from [11]

The LaPrade PLC reconstruction is described in complete detail by LaPrade in the article: An Analysis of an Anatomical Posterolateral Knee Reconstruction in 2004 [11]. Unlike other PLC reconstruction techniques the LaPrade technique aims to reconstruct all three anatomic PLC stabilizers. It has been suggested that the anatomic reconstruction of the PFL leads to over-constraint of the PLC and will cause subluxation, but an additional study by McCarthy et al. [23] found that the LaPrade reconstruction with the tibial tunnel for the PFL significantly improved normal knee kinematics and did not lead to over-constraint. This technique has been described as "a technically challenging procedure with a definite learning curve,"

but clinical outcomes show promise for optimal post-op functionality. Cadaveric specimens with this PLC reconstruction have demonstrated knee performances that are biomechanicaly better or equivalent to a grade I PLC injury after complete PLC secioning.

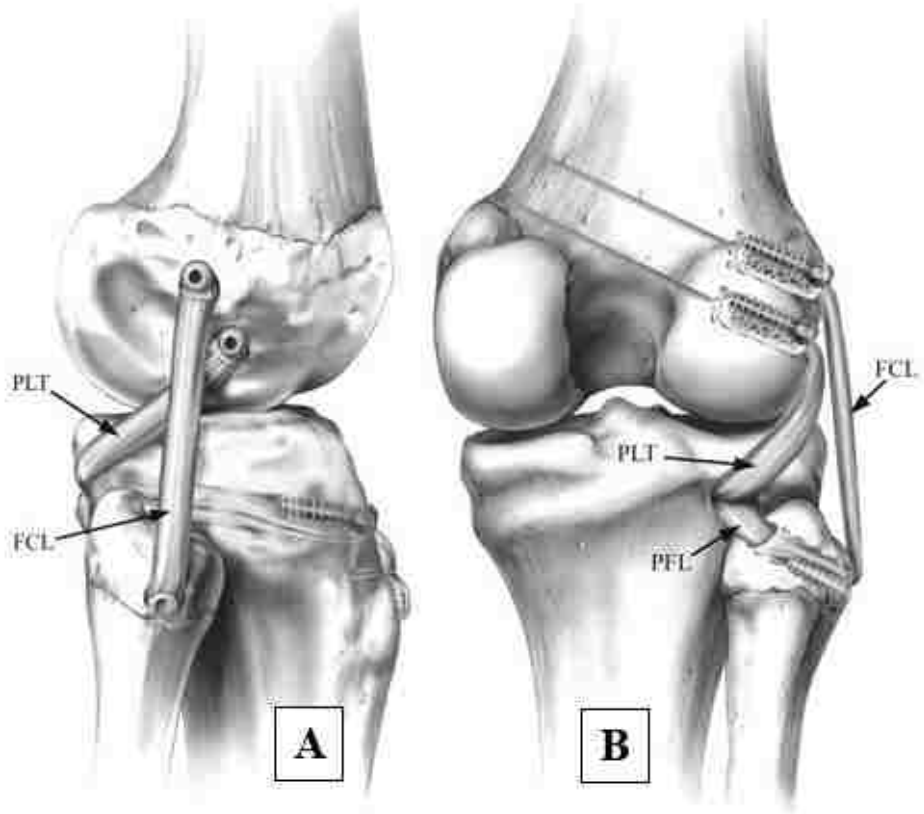

Figure 2.13: (A) Lateral view and (B) posterior view, illustrates Figure 2.12 but with their corresponding grafts secured in their respective insertion points. Modified from [11]

Like the Arciero technique, two femoral sockets are created. The first socket is located on the anterior fifth of the popliteus sulcus for the PLT, and the second tunnel is located at the native FCL attachment site. A tibiofibular tunnel is also reamed for passage of the FCL and PFL graft. In addition, a tibial tunnel is drilled on the posterior aspect of the proximal tibia. Rather than a single graft, two 22

cm length grafts are used for this reconstruction. This is achieved by splitting the harvested Achilles tendon at its midline (lengthwise imaginary line that separates the achilles tendon into two equal halves.) creating two equal 22 *cm* grafts. The first graft is secured into the popliteus sulcus femoral socket by an interference screw. The remaining end of the graft travels through the posterior aspect of the tibial tunnel with the free end of the graft protruding out the anterior face of the tibia. The second graft is anchored into the femoral socket of the FCL attachment site by an interference screw and is then passed through the tibiofibular tunnel. The free end of this graft is then passed through the posterior tibial tunnel in conjunction with the first graft [10]. With the knee flexed at 30°, the two grafts are simultaneously tightened by anteriorly loading the free ends of the grafts protruding from the tibia. Bioabsorbable interference screws are placed into the tibiofibular and tibial tunnels to fix the two grafts into place. A lateral and posterior view of this reconstruction can be seen in Figures 2.14 and 2.15, respectively.

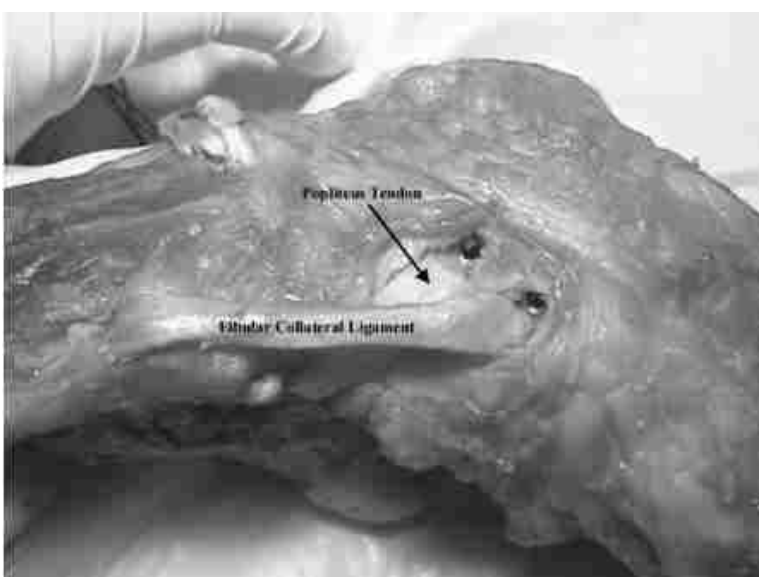

Figure 2.14: Cadaveric PLC LaPrade Reconstruction from a lateral view and. The figure highlights the reconstructed FCL, PLT, and PFL [11]

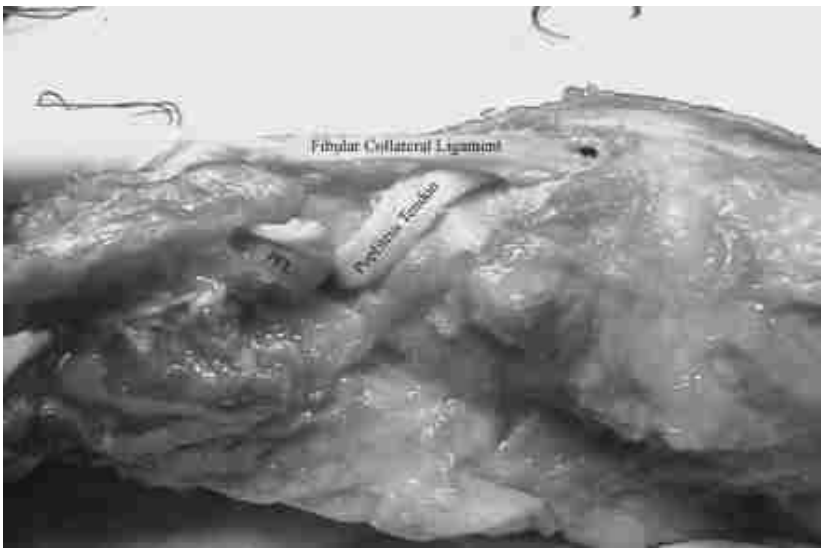

Figure 2.15: Cadaveric PLC LaPrade Reconstruction from a posterior view. The figure highlights the reconstructed FCL, PLT, and PFL [11].

Multiple LaPrade PLC studies [11, 22, 23] have been carried out to test varus angulation and external rotation at 0°, 20°, 30°, 60°, and 90° of flexion. LaPrade et al. [11] used a pilot study to determine the limit of loading for varus and external rotation. A 60 Nm anterior and posterior load was applied to test the strength of the specimens. From the pilot study, they concluded that loosening occurred over time to the fibular head graft from a 12 Nm varus load because of osteoporotic bone and the elderly age of the specimens they were using for testing. They adjusted the varus load to 5 Nm in order to eliminate the occurrence of loosening in the graft. A 5 Nm torque was used for external rotation. They concluded that the PLC is most vulnerable at 30° and 60° of flexion. At these angles, they posted the largest variability in terms of varus laxity and external rotation. For an intact specimen, measurements did not exceed 10° in terms of varus gapping and external rotation. Only after the PLC had been sectioned did the outcome measures exceed 10° unlike other studies which posted outcome measures larger than 10° when the knee specimen was still intact. From their results, they found that the LaPrade reconstruction was

capable of restoring stability back to the specimens original unaltered state within a small margin of error.

McCarthy et al. [23] followed a similar methodology except a 10 Nm varus load was applied. For this study they compared the LaPrade reconstruction against a modified version of the LaPrade technique. They labeled the standard LaPrade technique as group I and the modified version as group II as seen in Figure 2.16. The modified technique does not aim to reconstruct the PFL. The remaining limb of the graft is sutured to the base of the FCL graft at the proximal fibular head. Motion capture was used to track the displacement of the knee as loads were being applied. Like other studies, they concluded that the PLC was most vulnerable between 30° to 60° of flexion. They note that at 30° of flexion, both the intact, sectioned, and reconstructed specimens demonstrated more instability than any other angle based on their findings. Additionally McCarthy et al. found that the standard LaPrade reconstruction was able to restore varus laxity and external rotation close to that of the intact specimen more so than the modified technique.

An additional study by Serbino et. al. [38] investigated the the effect that the LaPrade technique in terms of varus and rotational stability at 0°, 30°, 60°, and 90° of flexion. Instead of using the Achilles tendon as an allograft, only the gracilis and semitendinosus tendons were using as grafts. Serbino et. al. reported that the LaPrade technique was able to restore varus stability close to initial conditions but partially restored rotational instability. They hypothesize that external rotation may have been affected by graft choice. Serbino et. al. state that the PLT and PFL are thicker structures compared to the gracilis and semitendinosus which were used to reconstruct them [38]. They suggest that it would be more appropriate to use the achilles tendon, quadriceps, or double semitendinosus tendons as suitable allografts.

Results from LaPrade and McCarthy [11, 23] tests showed the LaPrade technique restores stability to the grade III PLC injury through a reconstructed PLC. Both

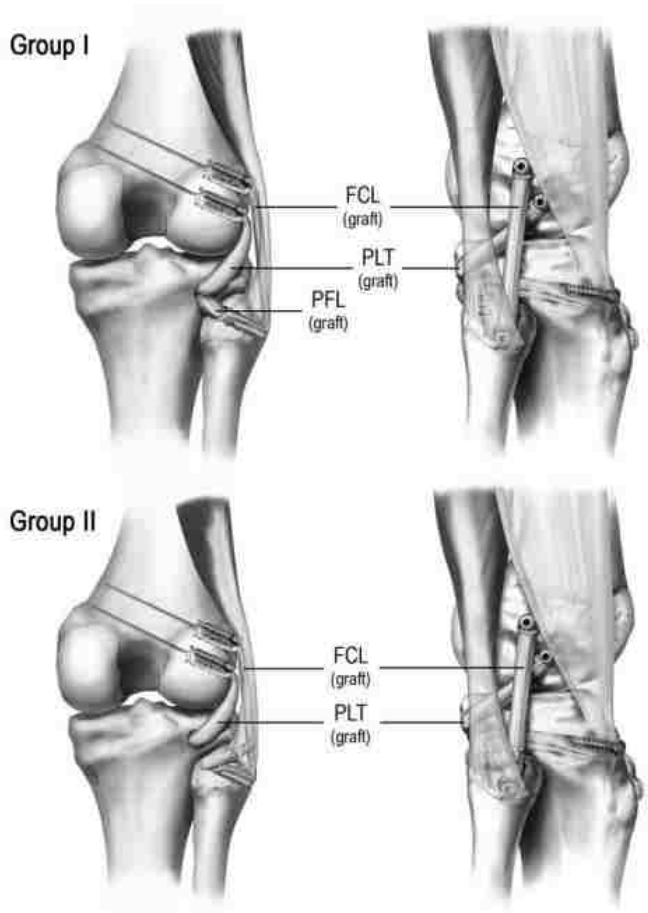

Figure 2.16: Group I: Modified LaPrade reconstruction where the PFL is not included in the reconstruction. Group II: Standard LaPrade reconstruction with all three primary structures being reconstructed. Modified from [23].

the Arciero and LaPrade biomechanical testing outcomes have shown comparable results even though their anatomical reconstructions differ. The Arciero technique reconstructs the FCL and PFL while neglecting the need for a PLT structure. The presence of a reconstructed PLT in addition with the FCL and PFL is thought to lead to over constraint, though later studies proved this concept otherwise insignificant. The LaPrade technique aims for a full anatomical reconstruction of all three PLC structures. The two techniques have not been compared to each other in an individual study despite their recognition of providing stabilization to the injured PLC.

Chapter 3

Materials and Methods

3.1 Methods

This is a biomechanical study simulating a dial and varus stress test in order to compare two Posterolateral Corner (PLC) reconstruction techniques: Arciero and LaPrade. To provide statistically significant data, a total of 10 paired cadaveric specimens were used for this study. 2 pairs were used for preliminary testing, while the following 8 pairs were used for data acquisition. For each pair, 1 leg was reconstructed with the Arciero technique, while the contralateral limb was reconstructed with the LaPrade technique. Varus stress and external torque were applied using a custom made testing fixture at 0°, 20°, 30°, 60°, and 90° of flexion. Reflective markers were used with motion capture cameras to measure varus angulation and external rotation about the lateral compartment for data analysis. Finally, one specimen from each pair was evaluated with sectioned tibiofibular ligament or a torn anterior cruciate ligament.

Figure 3.1: Completed Posterolateral Corner testing fixture.

3.2 Testing Fixture Design

The PLC testing fixture (Figure 3.1) was created in order to replicate clinical tests that measure varus stress and external rotation about the lateral compartment of the knee joint. The design of the testing fixture is inspired from previous fixtures used to study the biomechanics of the PLC. The fixture is composed of eleven parts: the base plate, two side plates, two dial plates, two extension arms, the end piece, the torque/force rod, and the vise.

3.2.1 Base and Side Plates

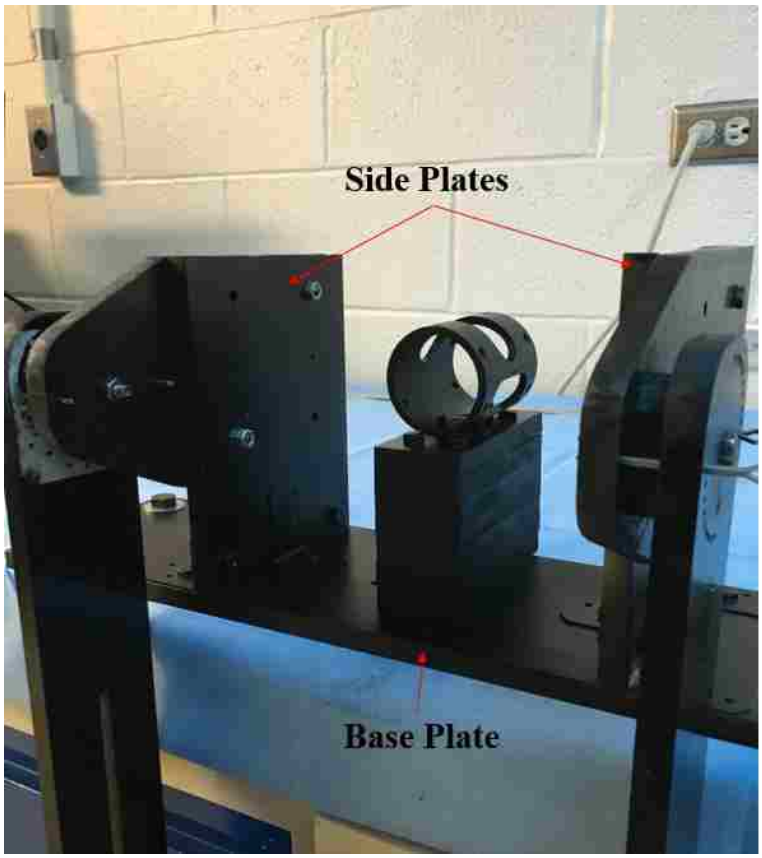

Figure 3.2: Mounted testing fixutre. The base and two side plates are highlighted.

The base plate and two side plates (Figure 3.2) are made from 6061-T6 Aluminum Alloy. The 6061-T6 Aluminum was selected as the suitable material for these components (In order to support the overall weight of both the fixture and the cadaveric specimen) because of rigidity, strength, and low cost. The base plate is 1/2 inch thick x 23 inch length x 6 inch height. The side plates are located 6.25 inches from each end of the base plate, respectively. Both side plates are attached to the base plate with three aluminum elbows for each side plate. The two side plates are separated by 10 inches to allow adequate space for the specimen to fixed at the center of the base plate. Finally the base plate is anchored to the table with two 1/2 inch bolts.

Dimensional drawings for each component can be found in Appendices B.3 and B.7.

3.2.2 Torque/Force Rod

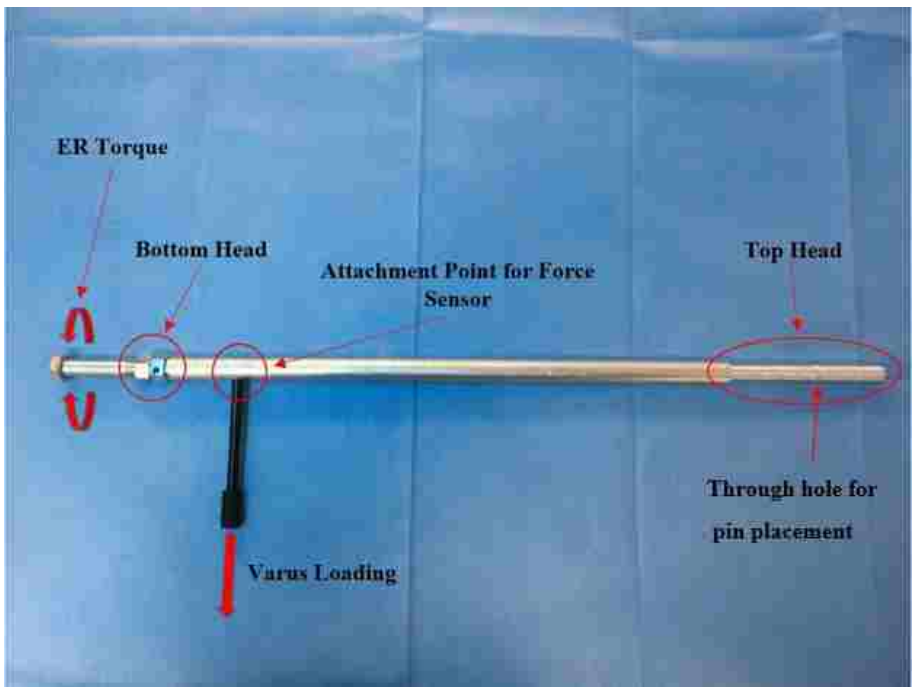

Figure 3.3: Torque/force rod showing the points of varus loading and ER torque. Also the location for pin placement and the attachment point for the force sensor.

The torque/force rod (Figure 3.3) was created in order to apply both the varus and torsional loads on the cadaveric specimen. It has an overall length of 15 inches with a 1/2 inch diameter shaft. The top head of the rod has diameter of .3149 inches (8mm) which extends 3 inches below the head of the rod. This is to ensure that the head of the rod can fit inside the reamed tibial canal and fixed into place once the specimen has been prepared. This 8mm diameter also allows the rod to slide through the slot of the end plate with minimal. A 9/64 inch through hole is located 1.5 inch below the head of the rod. This allows for the placement of a 1/8 inch pin which passes through the distal tibia of the rod. This secures the rod into the medullary

canal of the distal tibia allowing for both external rotation and varus angulation to be applied. Located 1.5 inches above the bottom head of the rod is an M6 tapped holed which also lies parallel to the 1/8 inch hole. This is the attachment point for the force sensor. Finally at the bottom face of the rod, a 3/8 inch tapped hole was made for the placement of a bolt. The tapped hole was filled with epoxy, the bolt was inserted and the epoxy was allowed to dry. This prevented the bolt from loosening during the applied torsion. A torque wrench was used to apply a 5 Nm torque to the head of the bolt. The fixation of the bolt in the rod allows for external rotation in both left and right legs when the torque wrench is used. Dimensional drawings for the rod can be found in Appendix Figure B.4.

The remaining components of the testing fixture are made from ABS polymer. Its lightweight properties combined with easy machinability and tensile strength proved to be an acceptable material for supporting the weight of the cadaveric specimen in the testing fixture. The remaining components of the fixture consisted of two Dial Plates, two Extension Arms, two Spacers, and one End Piece.

3.2.3 Dial Plate

A single Dial Plate (Figure 3.4) is attached to the outside face of one Aluminum Side Plate with the other Dial plate attached to the outside face of the opposite Side plate. These plates allow for changing the flexion angles of the specimen. The joint line of the knee is centered between the two dial plates. A 1/4 inch diameter through hole located 1.5 inches inside the outermost rounded feature of the Dial Plate served as the axis of rotation for knee flexion. Two additional 1/8 inch through holes parallel with the joint line were created as pin locations in order to secure the Extension Arms at a specific angles which can be seen in Figure 3.4. Using a zero degree reference plane, one pin location was made 1.25 inches to the left and right of the joint line.

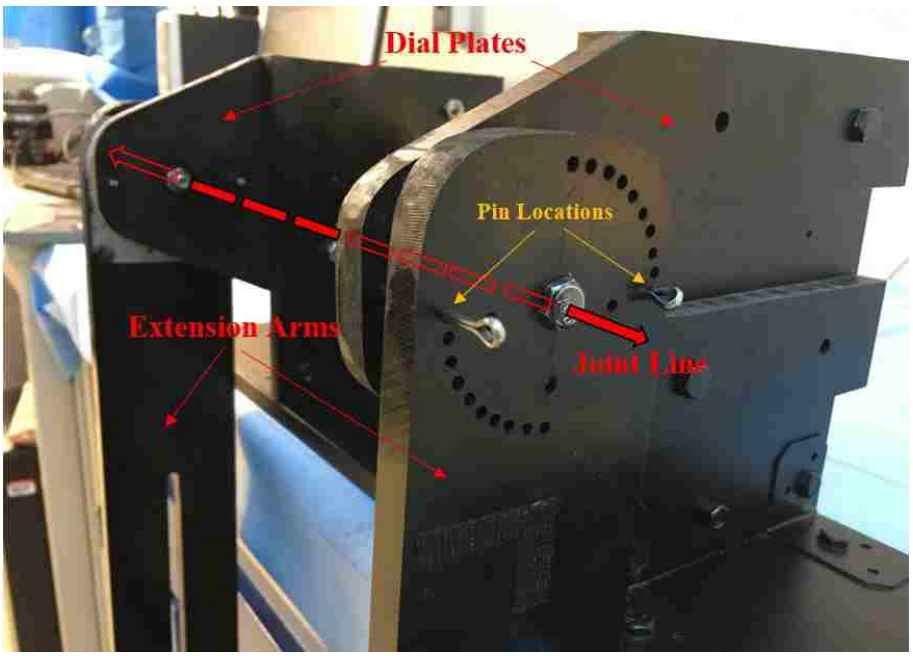

Figure 3.4: Dial Plate and Extension Arm pinned at 90° of flexion. The two Dial Plates, two Extension Arms, pin locations, and joint line are highlighted.

Dimensional drawings of the dial plate can be found in Appendix B.8.

3.2.4 Extension Arms

The extension arms (Figure 3.4 and Figure 3.5) serve the purpose of changing the knee flexion angle for testing purposes and to support the weight of the tibia. 1/8 inch through holes were positioned at coincident along a 1.25 radius from the joint line made in increments of 10° from 0° to 90° and from 180° to 270°. As the Extension Arm rotates about the joint line, the individual through holes would align with the dial plate pin locations where two pins were inserted to maintain the correct flexion angle during testing. In order to accommodate the varying lengths of specimens, the Extension Arm has an overall length of 21 inches from the joint line to the farthest end of the extension slot. This value was chosen based on the average length of

the human tibia which is 15 inches. The extension slot provides a line of reference that ensures the tibia lies in plane at the correct flexion angle, it also allows for adjustability of the End Piece depending on the length the specimen. Dimensional drawings of the extension arms can be found in Appendix B.9.

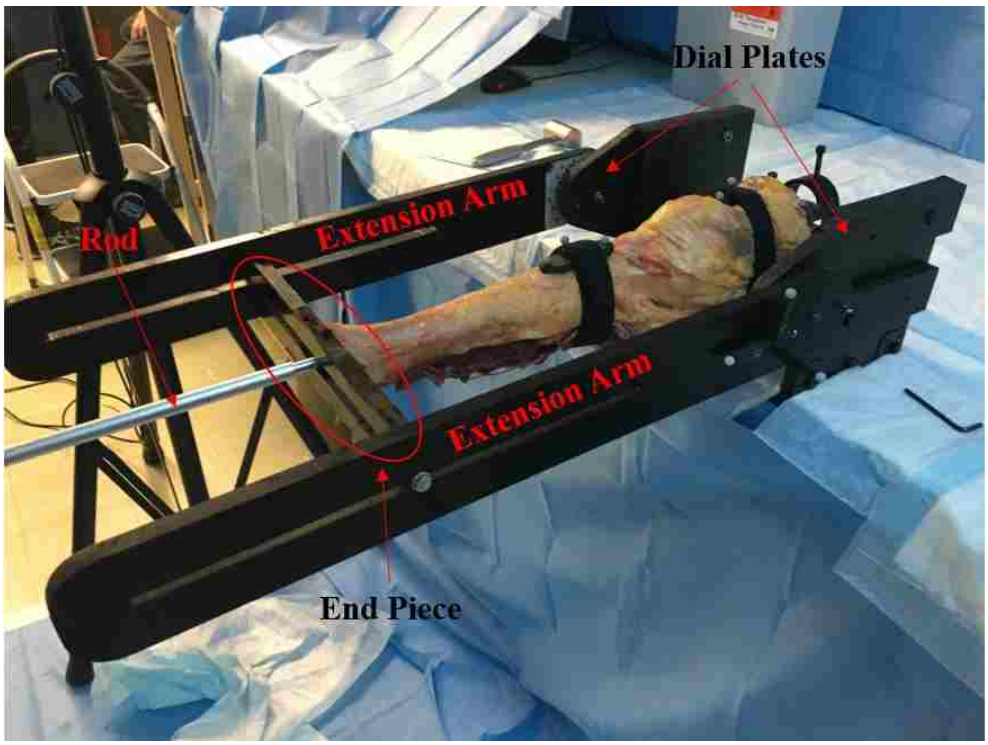

Figure 3.5: Side view of the testing fixture with the specimen mounted at 0° of flexion. The Dial Plates, Extension Arms, End Piece, and Rod are highlighted.

3.2.5 End Piece

The End Piece (Figure 3.5) attaches to the two extension arms at each end. Using the extension slot of the arms, the end piece is adjusted to position it against the distal end of the tibia. A slot through the center of the End Piece allows for the Rod to be inserted into the distal tibia. The slot allows for a maximum of 11 inches of horizontal translation when applying varus angulation in either direction. The slot

also restricts the movement of the rod to only translate in the horizontal direction while keeping both the rod and the specimen in the same plane of the extension slot in the arms. Dimensional drawings of the end piece can be found in Appendix B.6.

3.2.6 Vise and Spacer

Figure 3.6: Vise and Spacer mounted on the Base Plate

The final component of the testing fixture is the vise (Figure 3.6). The vise is made from stainless steel. It is a cylindrically shaped device with an inside diameter

of 2 inches and an outside diameter of 2.13 inches. The approximate diameter of the human femur is 1.5 inches, therefore it was determined that the vise would provide the ample space for which to secure the femur. The vise has 10 M6 tapped holes, five arranged at the front end and five at the back end. Each set of 5 tapped holes were arranged in a pattern on the outside surface of the vise located at 30°, 60°, 90°, 120°, and 210° about the outside diameter projected inwards to the center line of the Vise. M6 socket head bolts were used to fix the femur in-line with the vise and the ends of the socket head bolts were grinded to a sharp point so that thev restrain the femur shaft along the centerline of the vise. In order to position the specimen at the same height as the dial plate, a 3.5 inch ABS polymer spacer was secured to the center of base plate using 1/4-20 bolts. The vise, which secures the Femur into place, was anchored to the top face of the spacer. At this height, the center line of the cylindrically shaped vise aligned normal to the line of the dial plate. This ensures that when extension arms are situated at 0° the leg lies fully extended, where both the femur and tibia of the specimen are and in-line with each other.

3.3 Torque/Force Applicators

3.3.1 Varus Moment Applicator

Figure 3.7: (A) Nidec-SHIMPO FG-3008 Force Gauge. (B) 5 Nm Torque Wrench.

A NIDEC-SHIMPO FG-3008 Digital Force Gauge (Figure 3.7) was used to apply a 10 Nm varus moment about the knee joint. The FG-3008 force gauge has a capacity of 500 N with an accuracy of ± 0.3 percent. It is equipped with a M6 male attachment that connects near the bottom head of the Torque/Force Rod. In order to calculate the applied force needed at the load cell attachment, the specimen is first measured from the knee joint line to the point of attachment of the Force Gauge. To create a 10 Nm varus moment (M) acting about the joint of the knee, the moment (10 Nm) was divided by the length to determine the applied varus load required at the distal tibia. The application of a 10 Nm varus moment can be seen in Figure 3.8.

$$\frac{Moment\,(Nm)}{Length\,(m)} = Force\,(N) \tag{3.1}$$

Figure 3.8: 10 Nm varus moment being applied at 90° of flexion.

3.3.2 Torque Applicator

A standard torque wrench (Figure 3.7) set at a 5 Nm limit was used to apply torque on the Rod using the head of the 3/8 inch bolt located on the bottom face. This allowed for consistent and repeatable torque applications during testing.

3.4 Specimen Preparation and Implants

3.4.1 Allograft Preparation

Preparation was required for each cadaveric specimen in order to achieve the required conditions for each reconstruction. It was necessary for the Gracilis, Semitendinosus, and Achilles tendons to be harvested from each specimen to be used as allografts for the reconstructions. For this procedure the frozen specimen was left to thaw overnight for 24 hours before preparation. Once thawed, the surgeon made an incision at the point where the Gracilis and Semitendinosus tendon attach to the anterior face of the tibia, 3 *cm* medial to the tibial tubercle as seen in Figure 3.9. Using the Stipper/Pig's Tail surgical instrument, the surgeon removed the entire length of the Gracilis and Semitendinosus tendons. The remaining muscle left on the grafts were stripped and removed leaving only the tendinous soft tissue intact. The Arciero reconstruction requires the use of only one of these tendons with an optimal length of 20 *cm*. Each graft was then measured to ensure that at least one of the graft's overall length equaled 20 *cm*. The Semitendinosus graft is longer than the Gracilis and was nominally chosen each time as the suitable allograft.

Next the surgeon made an incision along the skin from the most distal aspect of the Gastrocnemius muscle to the calcaneus and the full length of the Achilles tendon was exposed. Using a reciprocating saw, a portion of the calcaneus was separated from the rest of the foot with the attachment site of the Achilles tendon at the bone left undisturbed. The entirety of the bone/tendon tissue was removed from the specimen and cleaned thoroughly. All three grafts (Achilles, Gracilis, and Semitendinosus) were laid out and cleaned (Figure 3.10). The Achilles tendon was then separated into two equal halves with their respective bone plugs still intact. Using bone cutters, the outside surface of the bone plugs were chipped away carefully to create cylindrically shaped bone plugs that would be later used for fixation at the

Figure 3.9: Isolation of the Gracilis and Semitendinosus

femoral and fibular tunnels of each reconstruction (Figure 3.11). A Bone Plug Sizer was used to determine the correct dimensions of the final bone plugs. It was required that each bone plug be approximately 20 mm in length and fit semi-loosely into a size 9.0 mm bone plug tunnel. This is demonstrated in Figure 3.12.

Except for the bone plugs, the ends of all three allografts (the two separated Achilles tendons, Gracilis, and Semitendinosus) were "whip-stiched" following the harvest process. The four grafts were sprayed with Saline and placed together in a zip lock bag and stored in a freezer for the day that they would be used for their respective reconstructions.

3.4.2 Tissue Removal

On the day of testing the entirety of the foot was disarticulated in order to expose the distal articular surface of the tibia. The tibial medullary canal was then reamed through the articular surface to a depth of 12 cm to allow placement of the Rod. The skin and subcutaneous fat was removed from the tibia before all surgical procedures

Figure 3.10: From top to bottom: Achilles, Gracilis, and Semitendinosus allografts

commenced. All soft tissue was removed from the proximal femur to allow fixation of the bone into the vise. This prevented the specimen from moving laterally or horizontally during testing.

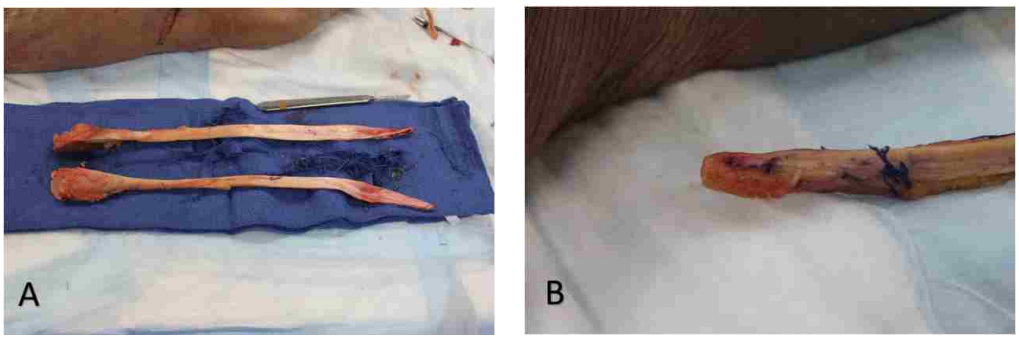

Figure 3.11: Achilles Allografts. (A) Achilles tendon split down the centerline with bone blocks remaining. (B) Finished bone plug ready for sizing.

Figure 3.12: Bone Plug sizing

3.4.3 Implants

Three different types of bio-compatible screws were used for their respective reconstructions: a 11x23 mm PEEK-OPTIMA® polymer Round Delta Tapered Interference Screw, a 7x23 mm PEEK-OPTIMA® polymer PEEK Interference Screw, and a 7x20 mm Titanium Cannulated Interference Screw as seen in Figure 3.13.

Figure 3.13: From left to right: (A) Round Delta Tapered Interference Screw, (B) PEEK Interference Screw, (C) Cannulated Interference Screw.

The Arciero reconstruction required one 7x23 *mm* PEEK Interference Screw fixed in the fibular tunnel while the remaining two screws were fixed in their respective

femoral tunnels. The screws were secured at 30° of flexion. For the LaPrade Reconstruction, four screws were used to repair the PLC which required the use of all three types of screws. One 11x28 *mm* Round Delta Tapered Interference screw was secured in the tibial tunnel on the anterior face of the tibia. Two 7x28 *mm* Cannulated Interference Screws were fixed in their respective femoral tunnels, and one PEEK Interference Screw was placed in the fibular tunnel. The fixation of the bio-compatible screws was done at 30° of flexion.

3.5 High Resolution Motion Capture

3.5.1 Cameras and Software

High resolution motion capture cameras were used to record the translation and rotation of the tibia when the appropriate forces were applied to the knee. Because the degree at which the tibia translates in millimeters, a very accurate and sensitive motion capture program was needed in order to obtain these measurements. Optitrack Motive Body Software with Prime 13 cameras were chosen as a suitable source of motion capture technology because of its ability to isolate defined rigid bodies and describe their dynamic movements to within a millimeter of displacement. For this study we used eight Prime 13 cameras (Resolution: 1.3MP 1280x1024, 240 FPS) which were positioned at varying heights on tripods all aimed at the specimen and the testing fixture. Four tripods were placed in a rectangular fashion about the testing fixture with each tripod housing two motion capture cameras. For each tripod, one camera was placed at a height of approximately 7.5 ft and the other at a height of 6 ft from the ground. This camera orientation ensured that all defined rigid bodies remain visible throughout the testing procedure.

Motive Body Software describes data in the following fashion: For position (trans-

lation), the defined rigid bodies are described by x,y,z global coordinates (in meters) relative to their distance from the origin (Equation 3.2). The origin is defined during the calibration process when the ground plane is set. The point at which the X axis and the Z axis intersects on the Ground Plane represents the origin in space. For rotation (Equation 3.3), the software defines rigid bodies locally in terms of Euler angles (yaw α, pitch β, roll γ) with respect to their centroids.

$$Postion = (X, Y, Z) \quad Global \tag{3.2}$$

$$Rotation = (X(\alpha)Y(\beta)Z(\gamma)) \quad Local \tag{3.3}$$

3.5.2 Marker Sets

For this study, 10 mm diameter markers grouped as triads were used to define rigid bodies (Figure 3.14). The markers are retro reflective and reflect light generated by the Optitrack camera lenses back to camera detectors. During the calibration process, the user must remove other reflective surfaces from every camera's line of sight. This prevents the cameras from confusing other markers for defined rigid bodies. Three rigid body marker sets were used to identify landmarks on the specimen. Each marker set was constructed using ABS Polymer as the base for which 3 individual markers are placed on top. The motion capture software allows the user to select a cluster of individual marks and define them as a single rigid body so long as each rigid body is comprised of at least 3 markers. It is important when defining the rigid body that the markers lie in a unique orientation that allows the software to distinguish it from other rigid bodies. Also it is required that the markers that define the rigid body not be co-linear or equidistant. This can lead to a misunderstanding in the orientation and direction of the rigid body while conducting data analysis.

Figure 3.14: Rigid Body Markers. From left to right (Tibia, Femur, Origin)

The marker sets were placed at the following locations: tibial tuberosity, 15cm proximal from the most distal end of the femur, and the outside face of the extension arm, along its centerline, 5.08cm away from the center pin. As loading occurs the tibial tuberosity marker set moves in conjunction with the tibia, only its initial and final positions in space are needed for data analysis. From the motion capture data, PLC instability and laxity will be interpreted by the change in angle/degrees from the varus moment and external rotation. The purpose of the femur rigid body was to measure its pitch and ensure that the leg lies horizontal in the testing fixture during varus and external rotation loading. Because the distal femur is fixed to the vise, there should be no difference between the initial and final positions of this marker set during testing. The origin rigid body was used for vector analysis to determine flexion angle and the total varus angulation during varus loading.

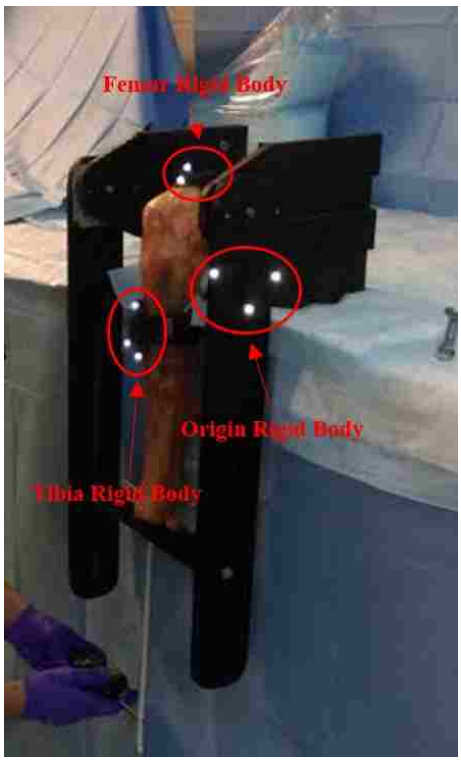

Figure 3.15: Rigid Body Marker attached during data acquisition for Varus Angulation at 90° of flexion. The positions of the Tibia, Origin, and Femur rigid body sets are highlighted.

3.5.3 Vector Analysis

Vector analysis was conducted in order to determine the amount of varus angulation. An initial vector was created by the tibia and origin rigid body sets. A final tibia-origin vector was determined after a 10 Nm moment was created. To solve for the change in θ (varus angulation) the angle between the two vectors was computed in the following manner: First, by virtually translating the origin rigid body set 165.1 mm in the negative x direction (global coordinates). This distance was chosen because this (virtually) puts the origin marker set approximately halfway between the two dial plates. Next the distance between the tibia rigid body and the new origin rigid body was computed using the distance formula where x,y,z are the global coordinates

of the Origin (O) and Tibia (T) which can be seen in Equation 3.4. Next the total translation in the x direction (Δx) was calculated. Finally, varus angulation was determined by Equation 3.5.

$$Distance = \sqrt{(O(x) - T(x))^2 + (O(y) - T(y))^2 + (O(z) - T(z))^2} \quad (millimeters) \tag{3.4}$$

$$Varus\ Angulation = \arctan(\frac{\Delta x}{Distance}) \cdot (\frac{180}{\pi}) \quad (degrees) \tag{3.5}$$

Optitrack defines rotation in Euler angles (local coordinates) which automatically derives the external rotation of the tibia based on the initial and final position of the tibia marker set and defines that rotation in terms of yaw, pitch, and roll. The total external rotation is solved by subtracting the final roll from the initial roll as described by Equation 3.6.

$$External\ Rotation = Roll_F(z) - Roll_I(z) \tag{3.6}$$

3.5.4 Statistical Analysis Methods

Multivariate Analysis of Variance (MANOVA) was used to find statistically significance at the four phases of the study by analyzing the differences in means between the two reconstruction methods at varying degrees of flexion. MANOVA is used when there are two or more dependent variables. For this study, the five varying degrees of flexion were the dependent variables and the two reconstruction methods were the two groups being analyzed. There are multiple statistics that may be used

for MANOVA analyses. The Wilks' Lambda statistic was used because it is the most commonly used statistic and is the most powerful for MANOVA when solving for P. The Wilks' Lambda statistic (λ) is a monotone function of F and can be transformed to an approximate F distribution [40] as shown in Equation 3.7. This F value is used to calculate a P value. The P value is then used to determine significance. Values of P<0.05 reject the null hypothesis while values of P>0.05 accept the null hypothesis. For this study, if P>0.05 we interpret the analysis between the two dependent variable to be statistically indifferent. Other statistics include the Pilai's Trace, Hotelling-Lawley Trace, and Roy.

$$Wilks' \ Lambda \ Statistic \quad (\lambda) = f(F) \quad F \ Statistic \tag{3.7}$$

3.6 Testing Protocol

To examine the significance of PLC instability, it is required that we investigate instability by inducing similar loading conditions to the PLC that are conducted during clinical examinations. For this study, the varus and dial Tests were selected as the tests that would best identify PLC injury and lateral knee instability. The complete testing procedure is comprised of four parts described in Figure 3.16. First, the specimens were tested with intact PLC's. Next, the PLC is destabilized by sectioning the primary static stabilizers and retested. The specimens were repaired using one of the selected PLC reconstruction techniques, Arciero or LaPrade, and then tested. Finally the tibiofibular joint or ACL was sectioned and the specimen was retested. All phases are conducted at 0°, 20°, 30°, 60°, and 90° of flexion. Figures 3.17 and 3.18 show a front view and a sideview, respectively, of a specimen being prepared for testing.

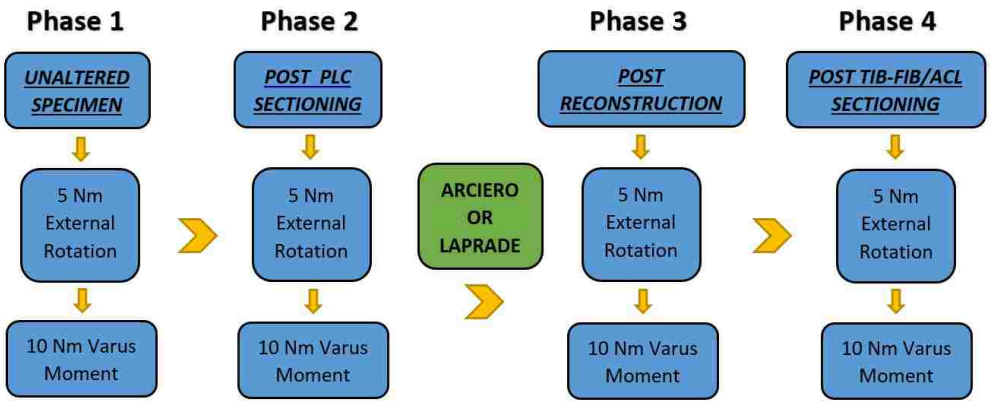

Figure 3.16: Testing Procedure. For each pair, one leg underwent the LaPrade reconstruction while the other underwent Arciero. Each Phase consists of a 5 Nm torque and 10 Nm varus moment being applied at 0°, 20°, 30°, 60°, and 90° of flexion. Each specimen underwent the same testing procedure except at Phase 4, where half of the specimen's tibiofibular joints were sectioned while the other half had their ACL's secitoned.

Figure 3.17: Front view of the prepared specimen mounted in the testing fixture at 0° of flexion.

Figure 3.18: Side view of the prepared specimen mounted in the testing fixture at 30° of flexion.

Chapter 4

Experimental Results

4.1 Initial Testing

In order to accurately compare both techniques, the baseline cumulative averages of the paired specimens at initial testing needed to be statistically equal at all tested flexion angles. The raw external rotation (ER) and varus angulation (VA) data at initial testing was compiled for each paired set of specimens. During testing, one specimen had extreme osteoarthritis at the knee joint and was unable to reach full extension at 0°. We decided not to include this specimen or the contralateral leg in final tests. The outcome measures from the two preliminary tests were included with the 7 other paired specimens for data analysis. Data for nine paired specimens is reported. Table 4.1 shows the raw data for one paired specimen. All additional raw data can be found in Appendix C.1. The means of all specimens at initial testing at each flexion angle for ER and VA was calculated for every paired specimen (Table 4.2).

INITIAL TESTING: SPECIMEN ID#1				
	Arciero		**LaPrade**	
Flexion Angle	ER (Degrees)	VA (Degrees)	ER (Degrees)	VA (Degrees)
0	6.50	3.88	6.14	3.89
	6.87	4.36	6.37	5.11
	6.61	5.85	6.82	4.67
20	13.09	6.11	13.74	6.31
	14.29	6.37	15.03	3.56
	11.82	6.74	15.41	7.41
30	17.99	8.95	18.00	8.12
	15.15	7.06	17.90	6.56
	16.29	8.15	20.46	7.63
60	15.95	10.78	16.60	9.56
	17.29	11.45	16.20	10.25
	17.76	8.66	18.97	9.33
90	14.47	9.68	16.25	9.45
	14.13	8.34	17.04	8.11
	15.45	9.45	17.08	8.52

Table 4.1: Paired ER and VA raw data for Specimen#1 at varying flexion angles. The first paired leg set to undergo the Arciero reconstruction, (left), compared to the corresponding leg set to undergo the LaPrade reconstruction, (right).

INITIAL TESTING: SPECIMEN#1 (MEANS)			
	Flexion Angle	**ER (Degrees)**	**VA (Degrees)**
LaPrade	0	6.44	4.56
	20	14.73	5.76
	30	18.79	7.44
	60	17.26	9.71
	90	16.79	8.69
Arciero	0	6.66	4.70
	20	13.07	6.41
	30	16.48	8.05
	60	17.00	10.30
	90	14.68	9.16

Table 4.2: Mean paired ER and VA data for Specimen#1 at 0°, 20°, 30°, 60°, and 90° of flexion.

4.1.1 External Rotation

An ER distribution was taken for the two techniques and compared against each other to ensure that both reconstructions had equal graphical profiles. A statistically equal initial testing baseline allows us to argue that all paired specimens, regardless of which technique would be used, had similar initial mechanical conditions. The mean Arciero ER distributions with upper and lower 99% confidence levels are shown in Figure 4.1 and Table 4.3, respectively.

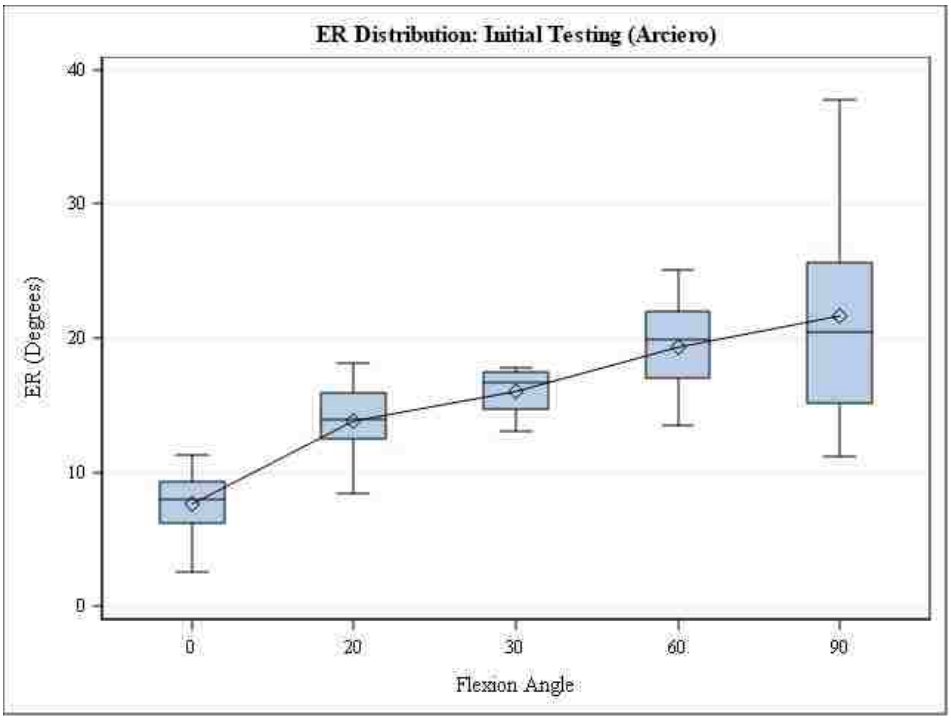

Figure 4.1: ER distribution at initial testing for Arciero specimens. This shows a graphical profile depicting ER trends and averages at 0°, 20°, 30°, 60°, and 90° of flexion. The distribution is described by a box and whisker plot where the diamond represents the mean, the center line represents the median, and the whiskers represent the upper and lower quartiles of the sample size at certain flexion angles.

ER: Initial Testing (Arciero)			
Flexion Angle	Mean (Degrees)	Lower Mean 99% CL	Upper Mean 99% CL
0	7.62	4.45	10.79
20	13.87	10.58	17.16
30	16.03	13.96	18.11
60	19.32	15.29	23.34
90	21.65	12.17	31.13

Table 4.3: Initial testing ER (Arciero) means with lower and upper 99% confidence levels.

The mean outcome measures of the LaPrade specimens at initial testing with upper and lower 99% confidence levels are shown in Figure 4.2 and Table 4.4.

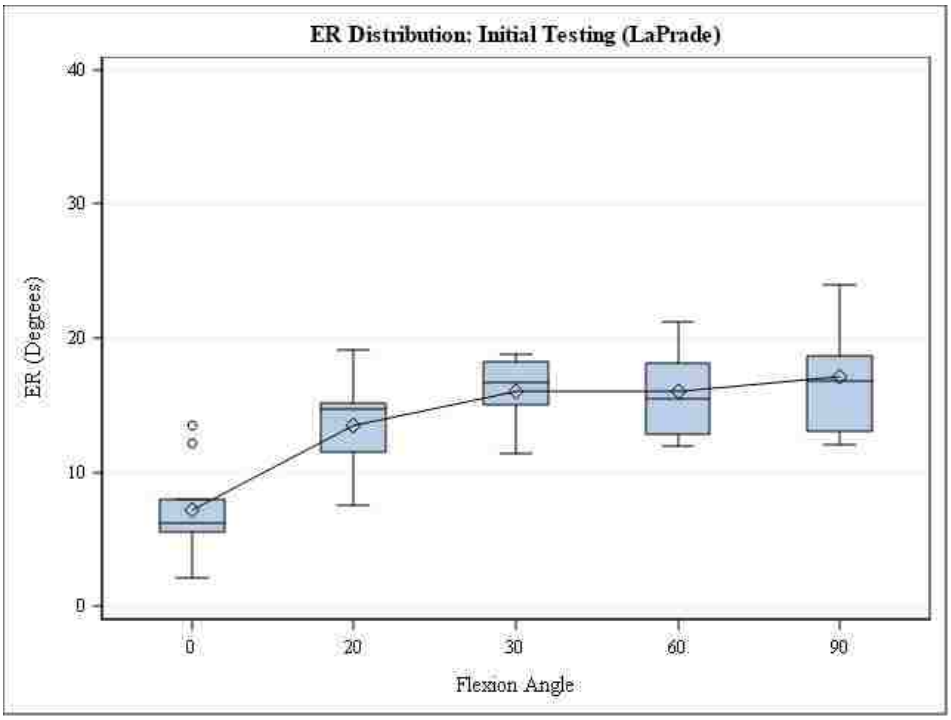

Figure 4.2: ER distribution at initial testing for LaPrade specimens. This shows a graphical profile depicting ER trends and averages at 0°, 20°, 30°, 60°, and 90° of flexion. The distribution is described by a box and whisker plot where the diamond represents the mean, the center line represents the median, and the whiskers represent the upper and lower quartiles of the sample size at certain flexion angles.

ER: Initial Testing (LaPrade)			
Flexion Angle	Mean (Degrees)	Lower Mean 99% CL	Upper Mean 99% CL
0	7.15	3.11	11.19
20	13.44	9.52	17.35
30	16.06	13.19	18.94
60	16.06	12.37	19.76
90	17.16	12.45	21.87

Table 4.4: Initial testing ER (LaPrade) means with lower and upper 99% confidence levels.

The Arciero and LaPrade ER graphical profiles were combined into one graph for comparison in Figure 4.3.

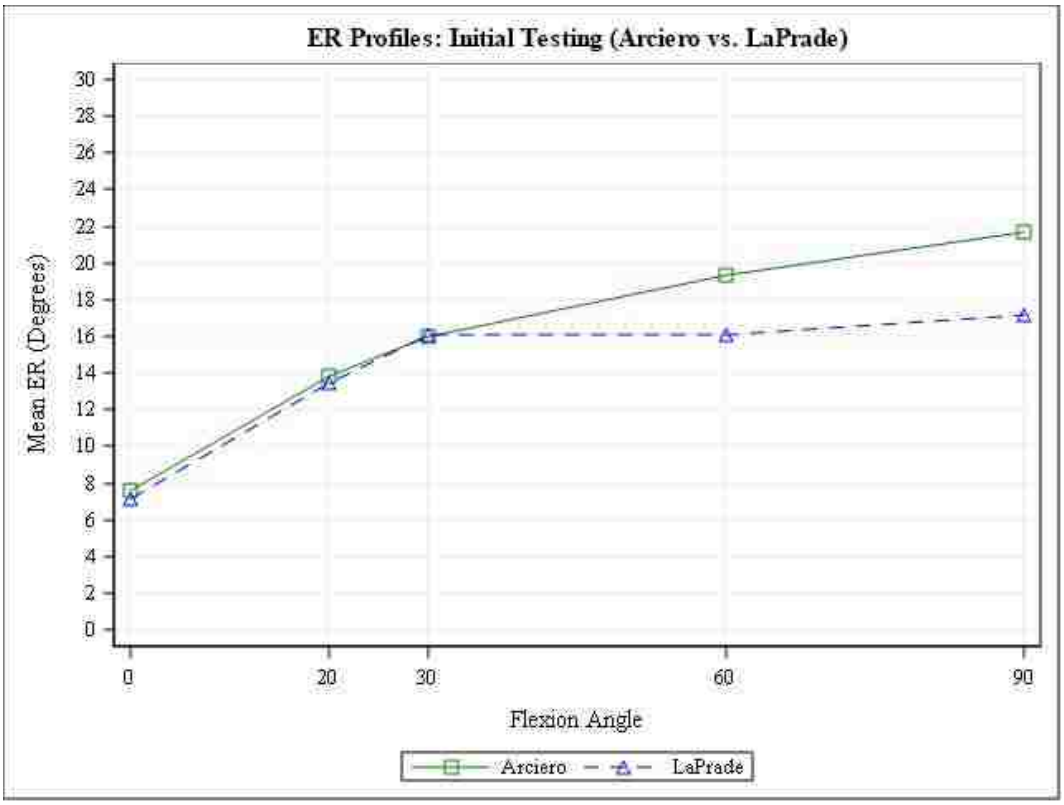

Figure 4.3: Arciero and LaPade ER profiles.

Figure 4.3 suggests that at initial testing, the Arciero and LaPrade means were nearly identical at 0°, 20°, and 30° of flexion. Using Multivariate Analysis of Variance

(MANOVA), a Wilks' Lambda statistic of 0.7496 and P = .5697 was found indicating no statistical difference between Arciero and LaPrade profiles.

4.1.2 Varus Angulation

A VA distribution was measured and compared across the two reconstruction techniques. Again, prior to PLC reconstruction, a baseline at initial testing must be measured to compare which technique, in terms of VA, restores stability to an injured PLC. The mean Arciero VA distributions with upper and lower 99% confidence levels can be seen in Figure 4.4 and Table 4.5.

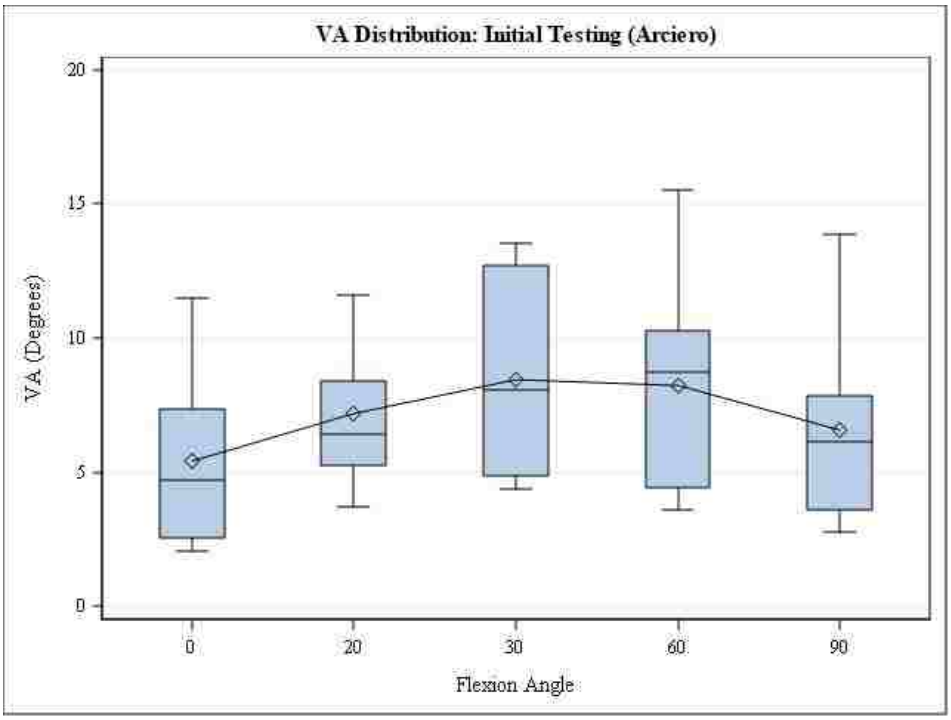

Figure 4.4: VA distribution at initial testing for Arciero specimens. This shows a graphical profile depicting VA trends and averages at 0°, 20°, 30°, 60°, and 90° of flexion. The distribution is described by a box and whisker plot where the diamond represents the mean, the center line represents the median, and the whiskers represent the upper and lower quartiles of the sample size at certain flexion angles.

VA: Initial Testing (Arciero)			
Flexion Angle	Mean (Degrees)	Lower Mean 99% CL	Upper Mean 99% CL
0	5.43	1.68	9.18
20	7.18	3.94	10.41
30	8.43	4.16	12.70
60	8.24	3.37	13.11
90	6.55	2.70	10.40

Table 4.5: Initial testing VA (Arciero) means with lower and upper 99% confidence levels.

The mean VA outcome measures of the LaPrade specimens at initial testing with upper and lower 99% confidence levels can be seen in Figure 4.5 and Table 4.6. The Arciero and LaPrade profiles were combined into Figure 4.6 for comparison.

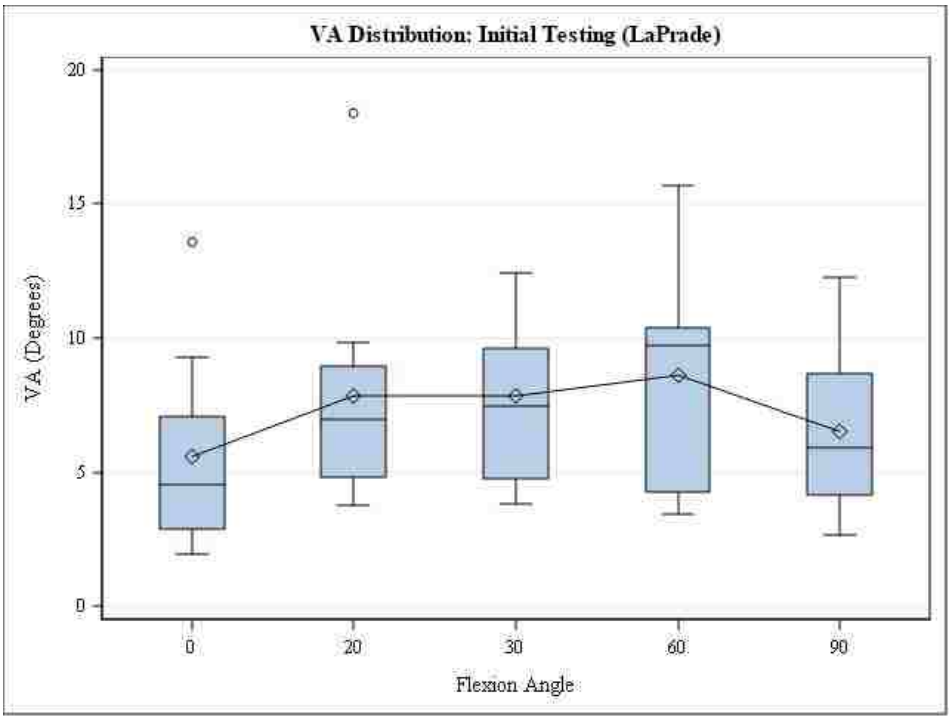

Figure 4.5: VA distribution at initial testing for LaPrade specimens. This shows a graphical profile depicting VA trends and averages at 0°, 20°, 30°, 60°, and 90° of flexion. The distribution is described by a box and whisker plot where the diamond represents the mean, the center line represents the median, and the whiskers represent the upper and lower quartiles of the sample size at certain flexion angles.

VA: Initial Testing (LaPrade)			
Flexion Angle	Mean (Degrees)	Lower Mean 99% CL	Upper Mean 99% CL
0	5.58	1.26	9.89
20	7.86	2.91	12.81
30	7.82	4.08	11.56
60	8.61	3.51	13.70
90	6.5	2.95	10.05

Table 4.6: Initial testing VA (LaPrade) means with lower and upper 99% confidence levels.

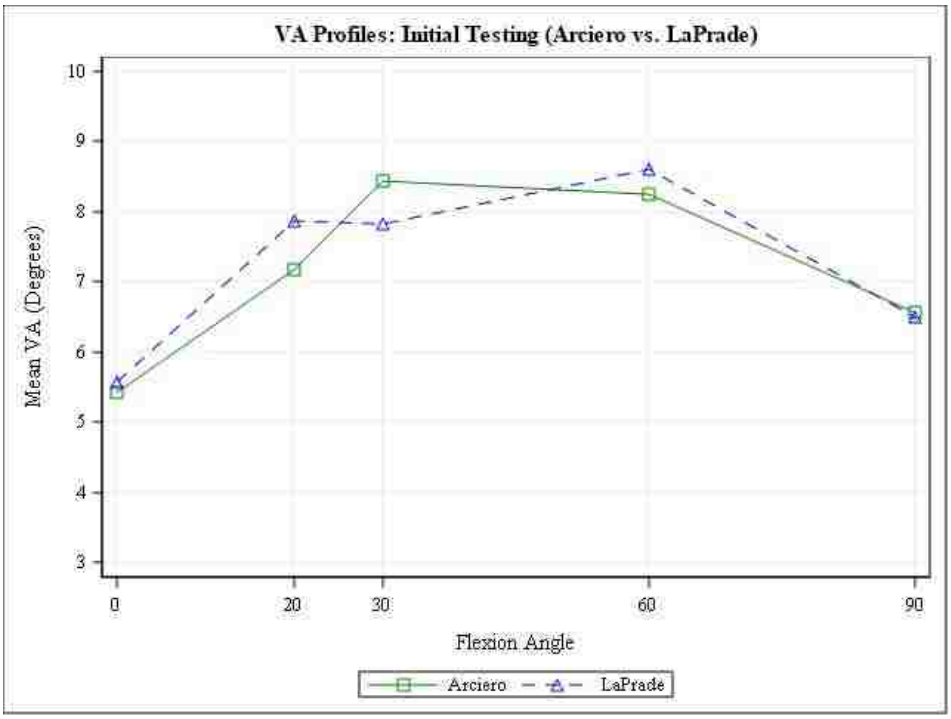

Figure 4.6: Arciero and LaPrade VA profiles.

At initial testing, the Arciero and LaPrade mean graphical profiles showed little to no parity at each flexion angle. The Arciero and LaPrade VA profiles were compared against each other at every flexion angle. Using MANOVA to assess the differences, a Wilks' Lambda statistic of 0.8293 and P=0.7749 were found indicating that the Arciero and LaPrade VA profiles are statistically equal at all flexion angles.

Finally, two separate graphical profile for ER and VA were created that combined the Arciero and LaPrade specimens together to show the overall ER and VA means at initial testing. It is acceptable to group the two profiles together because MANOVA shows no statistical difference between the two profiles. The combined profiles will be used to compare against the post sectioning profile and the post reconstruction profiles. Figures 4.7, 4.8, and Table 4.7 show the combined ER and VA means of both the Arciero and LaPrade specimens. The ER and VA profiles will serve as baselines for comparison against all other phases (Post Sectioning, Post Reconstruction, Post Tibiofibular Joint Sectioning, and Post ACL Sectioning) of the study.

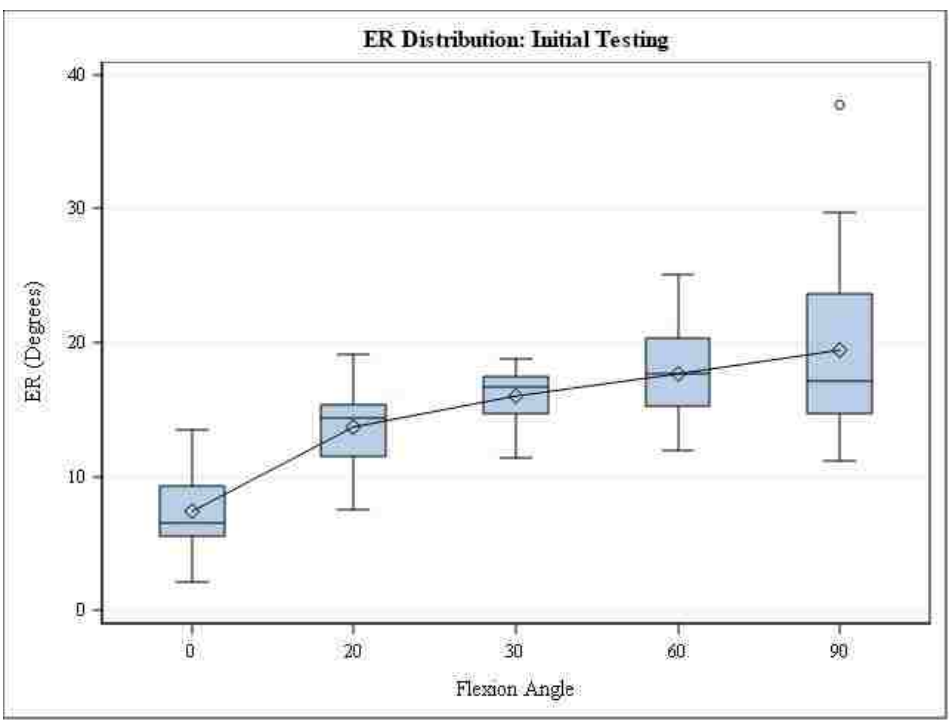

Figure 4.7: Combined mean ER profile of Arciero and LaPrade specimens at initial testing.

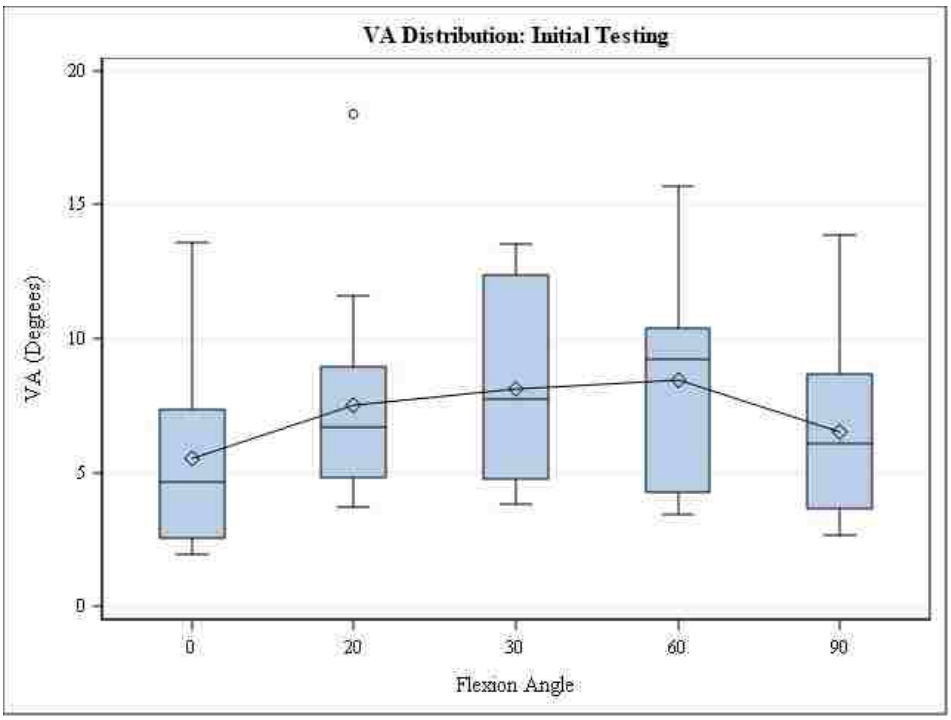

Figure 4.8: Combined mean VA profile of Arciero and LaPrade specimens at initial testing.

ER & VA Distribution: Initial Testing		
Flexion Angle	Mean ER (Degrees)	Mean VA (Degrees)
0	7.75	5.44
20	13.66	7.48
30	16.17	7.94
60	17.50	8.22
90	19.63	6.28

Table 4.7: ER and VA mean values at initial testing at 0°, 20°, 30°, 60°, and 90° of flexion.

4.2 Post Sectioning

Table (4.8) shows Specimen#1 mean ER and VA outcome measures. All additional tables for specimens 2-9 can be found in Appendix C.2. At post sectioning, each paired specimen's outcome measures for ER and VA were drastically larger than their initial. These measures are indicative of a ruptured PLC.

POST SECTIONING: SPECIMEN#1 (MEANS)			
	Flexion Angle	**ER (Degrees)**	**VA (Degrees)**
LaPrade	0	9.39	10.56
	20	27.57	12.95
	30	29.72	15.69
	60	27.94	15.06
	90	18.43	13.11
Arciero	0	8.62	12.16
	20	25.74	13.38
	30	30.02	15.43
	60	29.99	15.29
	90	21.58	14.19

Table 4.8: Mean paired ER and VA data for Specimen#1 at 0°, 20°, 30°, 60°, and 90° of flexion.

4.2.1 External Rotation

ER Distribution: Post Sectioning	
Flexion Angle	Mean ER (Degrees)
0	12.36
20	22.36
30	27.68
60	30.92
90	29.30

Table 4.9: ER mean values at post sectioning at 0°, 20°, 30°, 60°, and 90° of flexion.

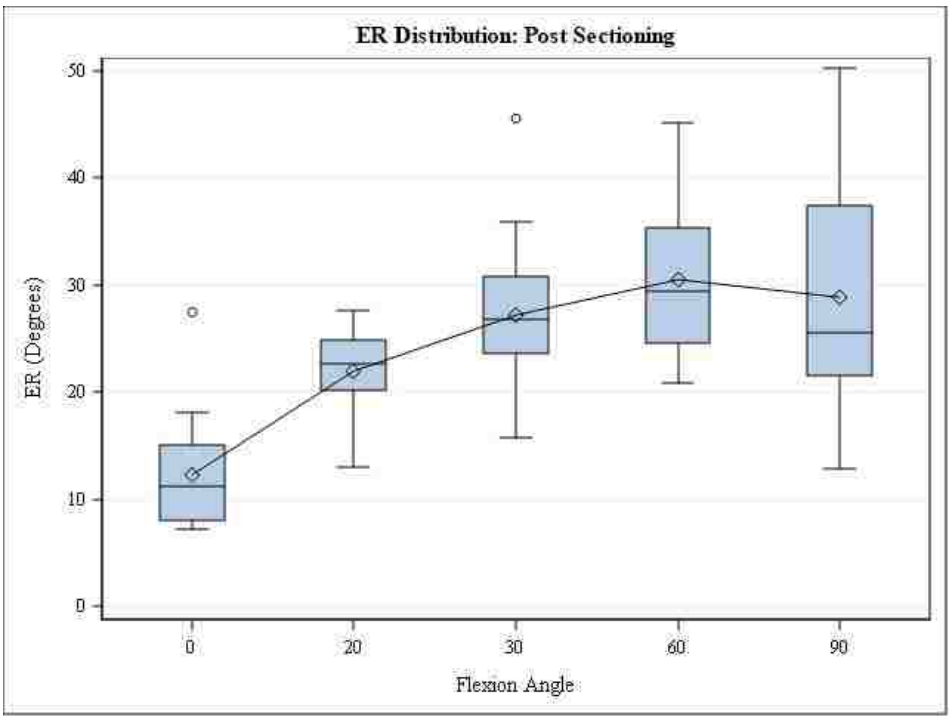

Figure 4.9: Combined mean ER profile of Arciero and LaPrade specimens at post sectioning.

We compared the initial and post sectioning ER profiles against each other. Figure 4.10 shows the initial testing vs. post sectioning mean ER profile comparison. We found a significant difference ($P<0.0001$) when comparing the two profiles across all flexion angles. The largest ER difference between the initial and post sectioning profiles was at 60° with an overall difference of 13.4 degrees between the two means. It also had the largest mean ER value (30.9 degrees) compared all other flexion angles. This may suggest that the knee is most susceptible to rotational instability at 60° of flexion with an injured PLC.

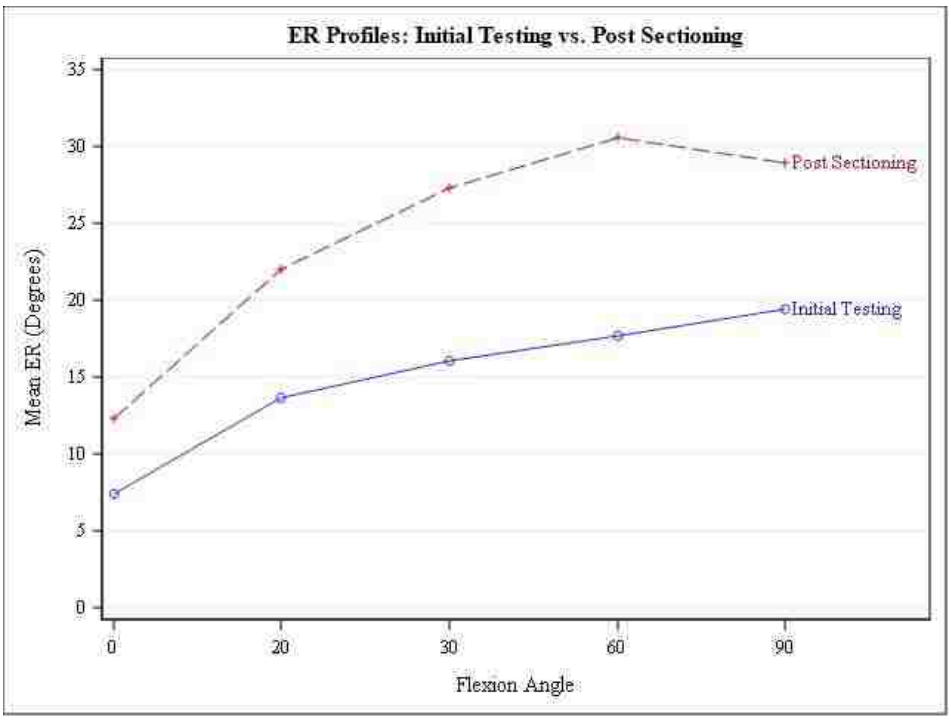

Figure 4.10: Initial Testing vs. Post Sectioning mean ER profiles at 0°, 20°, 30°, 60°, and 90° of flexion.

4.2.2 Varus Angulation

Figure 4.11 and Table 4.10 show the VA distribution and mean values, respectively, at post sectioning for all specimens.

VA Distribution: Post Sectioning	
Flexion Angle	Mean ER (Degrees)
0	9.42
20	12.66
30	12.27
60	11.94
90	10.10

Table 4.10: VA mean values at post sectioning at 0°, 20°, 30°, 60°, and 90° of flexion.

Figure 4.12 shows the two VA profile comparisons for initial and post sectioning.

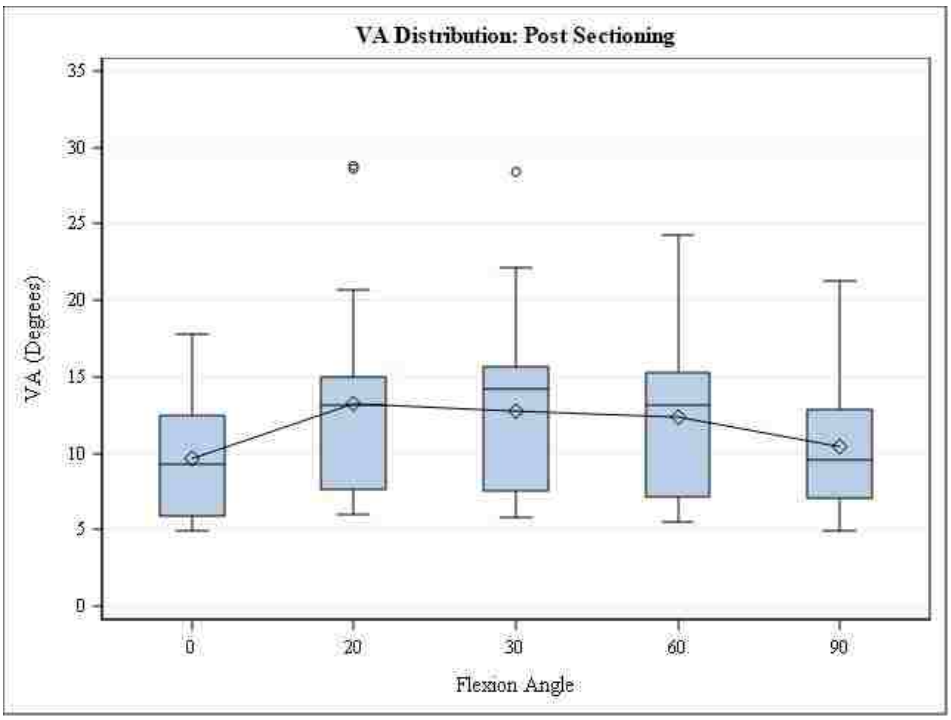

Figure 4.11: Comibined mean VA profile of Arciero and LaPrade specimens at post sectioning.

A Wilks' Lambda statistic of 0.6432 and P=0.0165 was found indicating that there is a significance difference between the initial and post sectioning profiles for VA. The largest difference between the two profiles was at 20° with a value of 5.18 degrees. It also had the largest mean VA value at 12.66 degrees. This may suggest, in terms of lateral gapping, the knee may be most vulnerable at 20° of flexion.

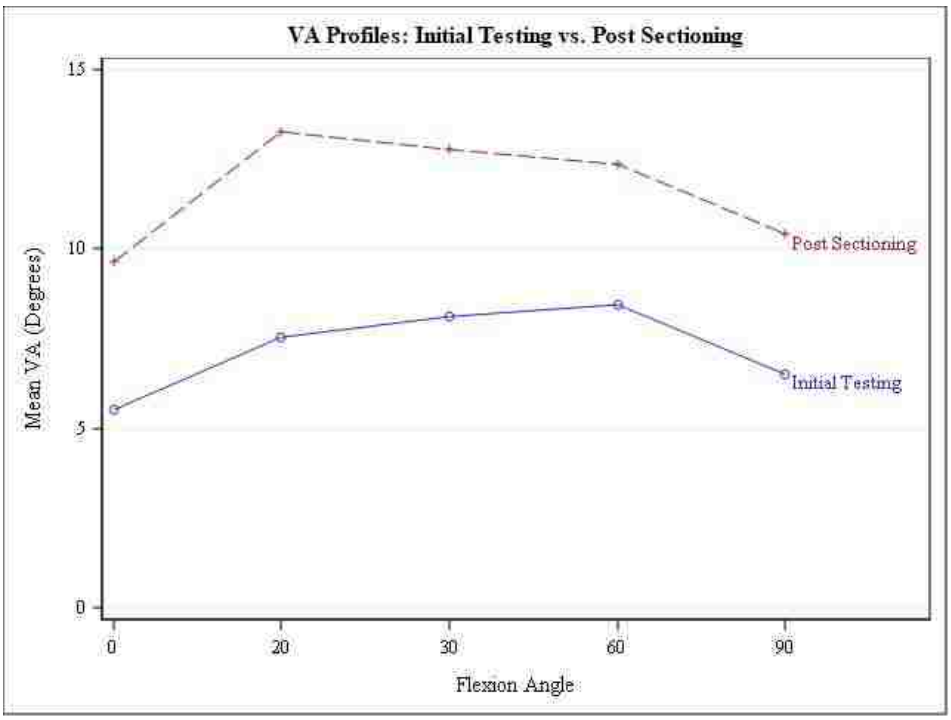

Figure 4.12: Initial Testing vs. Post Sectioning mean VA profiles at 0°, 20°, 30°, 60°, and 90° of flexion. A statistical difference was found between the two profiles with $P<0.05$. The greatest destabilization at post sectioning was found at 20° of flexion. Both profiles show parallelism.

4.3 Post Reconstruction

Table 4.11 shows Specimen#1 mean ER and VA outcome measures at post reconstruction. All additional specimen mean ER and VA tables at post reconstruction can be found in Appendix D.3. At this phase of the study, the respective Arciero and LaPrade specimens were separated and compared against their contralateral limbs. Like the previous phases, the reconstructions were tested and measured at 0°, 20°, 30°, 60°, and 90° of flexion.

POST RECONSTRUCTION: SPECIMEN#1 (MEANS)			
	Flexion Angle	**ER (Degrees)**	**VA (Degrees)**
LaPrade	0	7.81	4.97
	20	12.74	5.21
	30	16.34	9.53
	60	13.97	9.12
	90	13.22	7.64
Arciero	0	5.08	5.26
	20	11.70	6.19
	30	12.29	9.87
	60	15.34	8.83
	90	15.35	9.59

Table 4.11: Mean paired ER and VA data for Specimen#1 at 0°, 20°, 30°, 60°, and 90° of flexion.

4.3.1 External Rotation

Arciero ER Distribution: Post Reconstruction		
Flexion Angle	Initial Mean ER (Degrees)	Post-Recon. Mean ER (Degres)
0	7.75	7.66
20	13.66	15.71
30	16.17	17.74
60	17.50	19.85
90	19.63	21.44

Table 4.12: Arciero ER Initial vs. Post Reconstruction means.

Figure 4.13 and Table 4.12 show the combined ER distribution for Arciero specimens after post reconstruction. Except at 20° and 60° of flexion, the Arciero technique was able to restore ER within 2° of rotation. At 20° and 60° flexion, ER was restored to within 3° of rotation when compared to initial testing outcome measures.

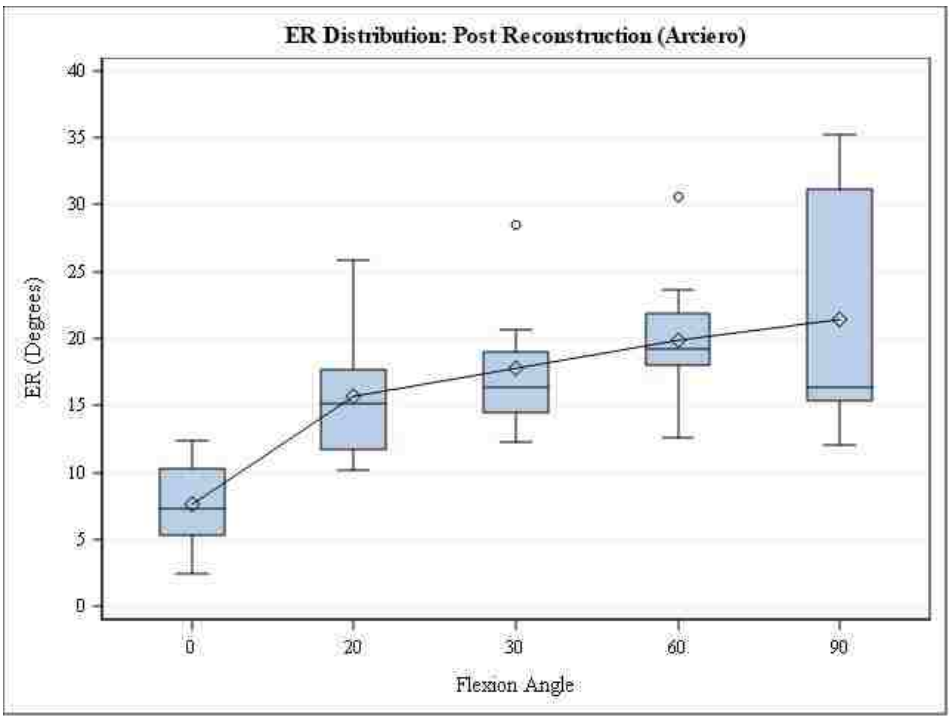

Figure 4.13: Mean post reconstruction ER distribution of Arciero specimens at 0°, 20°, 30°, 60°, and 90° of flexion.

LaPrade ER Distribution: Post Reconstruction		
Flexion Angle	Initial Mean ER (Degrees)	Post-Recon. Mean ER (Degres)
0	7.75	7.65
20	13.66	15.37
30	16.17	16.58
60	17.50	19.84
90	19.63	19.12

Table 4.13: LaPrade ER Initial vs. Post Reconstruction means.

Figure 4.14 and Table 4.13) show the LaPrade post reconstruction means. At 0° and 90° of flexion, the LaPrade technique was able to restore and resist rotation better than at initial testing. At all other flexion angles, ER was restored to within less than 3° of rotation when compared to initial conditions.

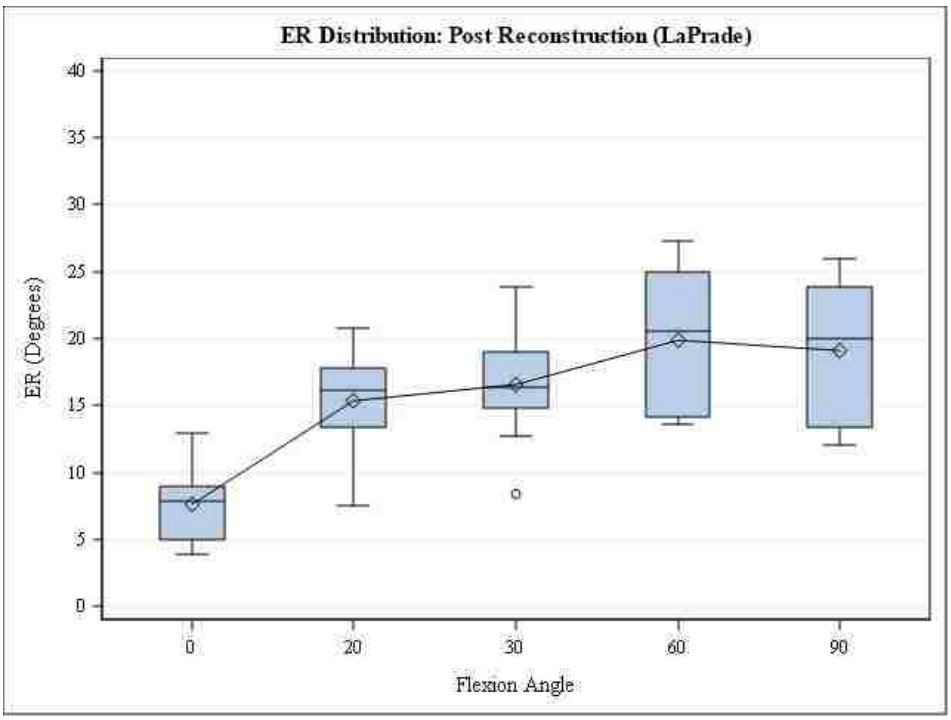

Figure 4.14: Mean post reconstruction VA distribution of LaPrade specimens at at 0°, 20°, 30°, 60°, and 90° of flexion.

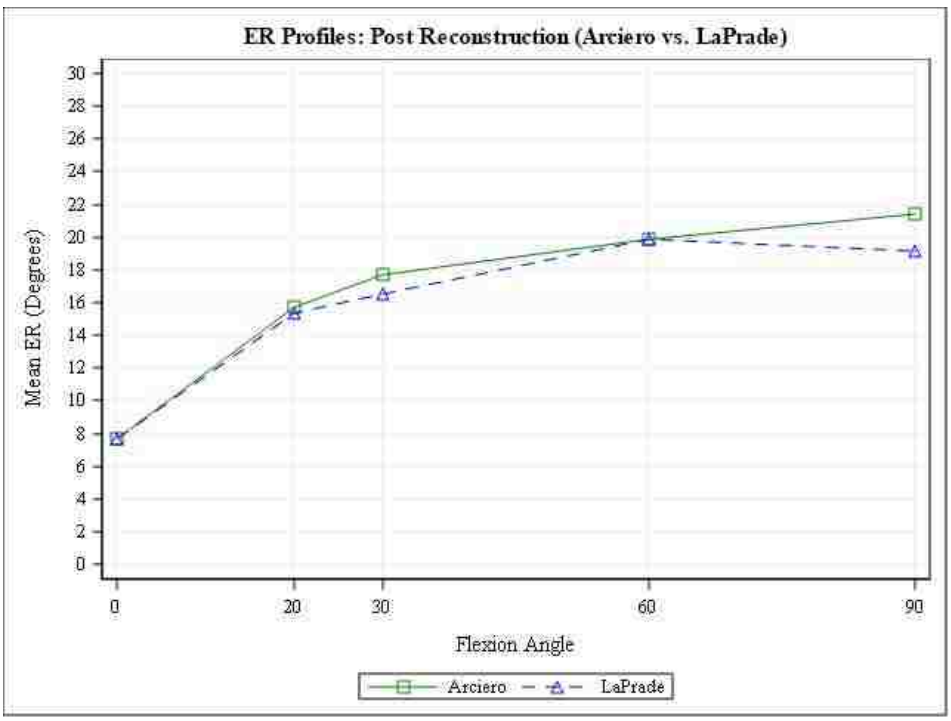

Figure 4.15: Arciero vs. LaPrade ER means at post reconstruction at 0°, 20°, 30°, 60°, and 90° of flexion.

The Arciero and LaPrade ER post reconstruction profiles were almost identical (Figure 4.15). A Wilks' Lambda statistic of .7792 and P=0.4812 was found indicating there was no statistical difference between the two ER profiles.

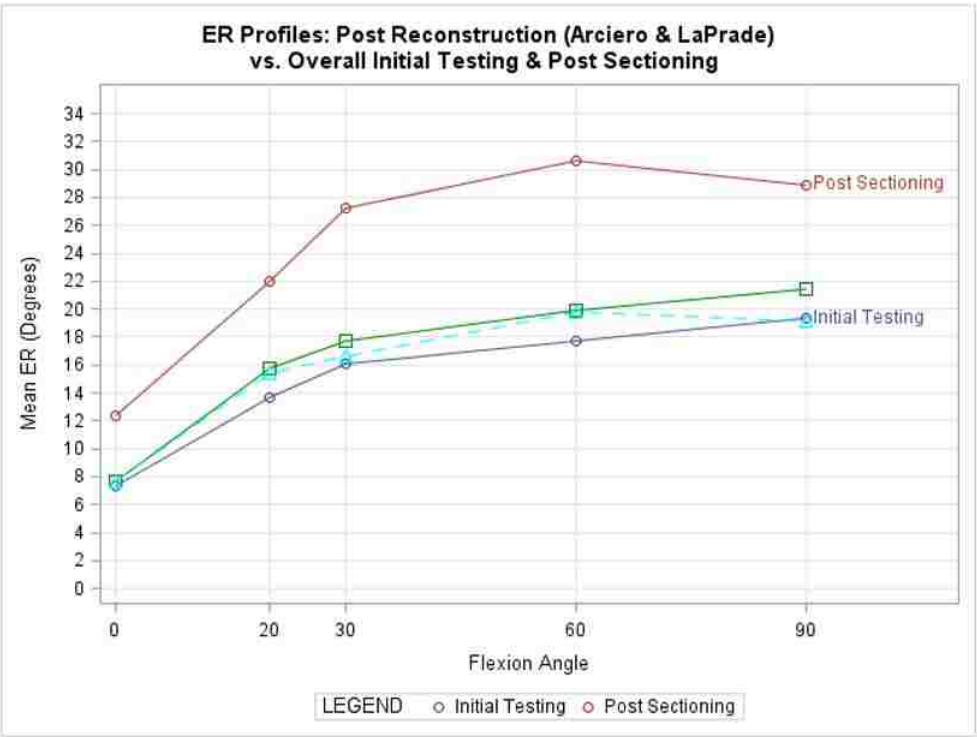

Figure 4.16: ER profile comparison at initial and post sectioning vs. Ariero and LaPrade specimens at post reconstruction. The cyan △ indicates the LaPrade ER profile. The green box indicates the Arciero ER profile.

Figure 4.16 shows the ER profile comparison of the intact and sectioned specimens vs. the Arciero and LaPrade specimens at post reconstruction.

4.3.2 Varus Angulation

The combined VA distribution and means across all flexion angles of Arciero specimens can be found in Figure 4.17 and Table 4.14. The Arciero technique was able to restore varus gapping to within 1° when compared to all flexion angles at initial

conditions except at 0° of flexion. At 0° of flexion, the mean VA value was less than that of the initial testing value.

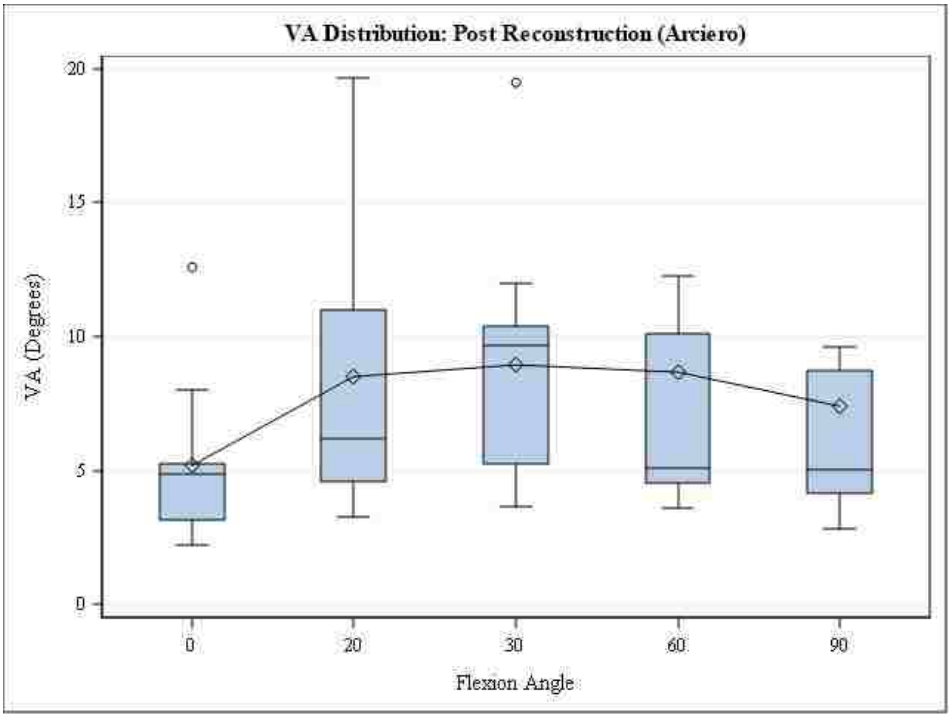

Figure 4.17: Mean post reconstruction VA distribution of Arciero specimens at 0°, 20°, 30°, 60°, and 90° of flexion.

Arciero VA Distribution: Post Reconstruction		
Flexion Angle	Initial Mean ER (Degrees)	Post-Recon. Mean ER (Degres)
0	5.58	5.21
20	7.86	8.50
30	7.82	8.94
60	8.61	8.69
90	6.50	7.39

Table 4.14: Arciero VA Initial vs. Post Reconstruction means.

The LaPrade VA outcome measures were better than initial testing means except at 30° of flexion. At all other flexion angles, the LaPrade reconstruction not only

restored varus gapping, but was able to reduce varus laxity that was either less than or closely comparable to initial measures.

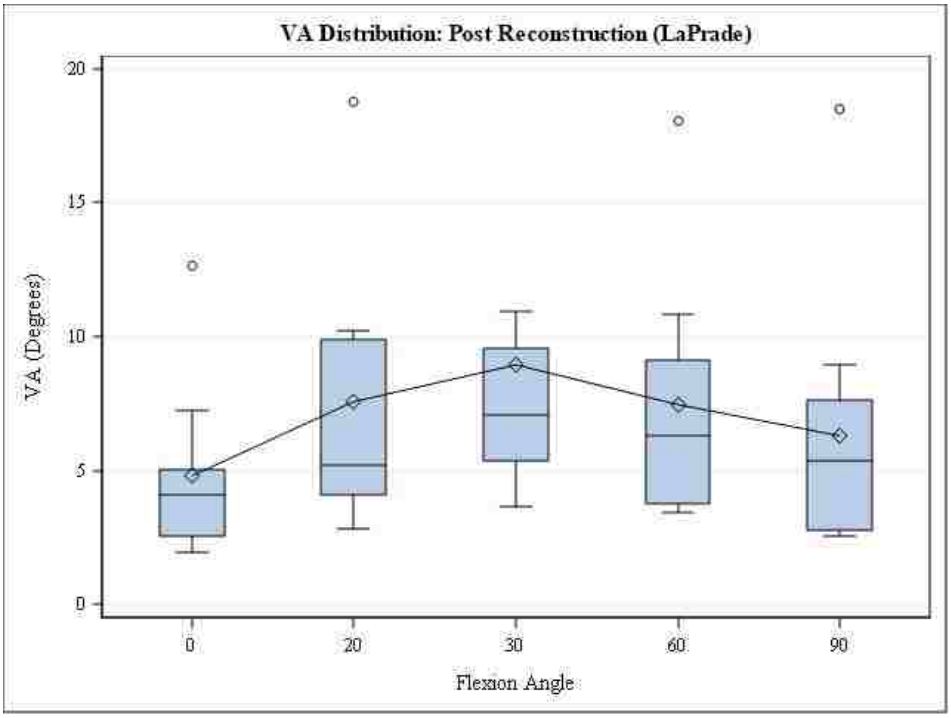

Figure 4.18: Mean post reconstruction VA distribution of LaPrade specimens at 0°, 20°, 30°, 60°, and 90° of flexion.

LaPrade VA Distribution: Post Reconstruction		
Flexion Angle	Initial Mean ER (Degrees)	Post-Recon. Mean ER (Degres)
0	5.58	4.82
20	7.86	7.58
30	7.82	8.93
60	8.61	7.48
90	6.50	6.29

Table 4.15: LaPrade VA Initial vs. Post Reconstruction means.

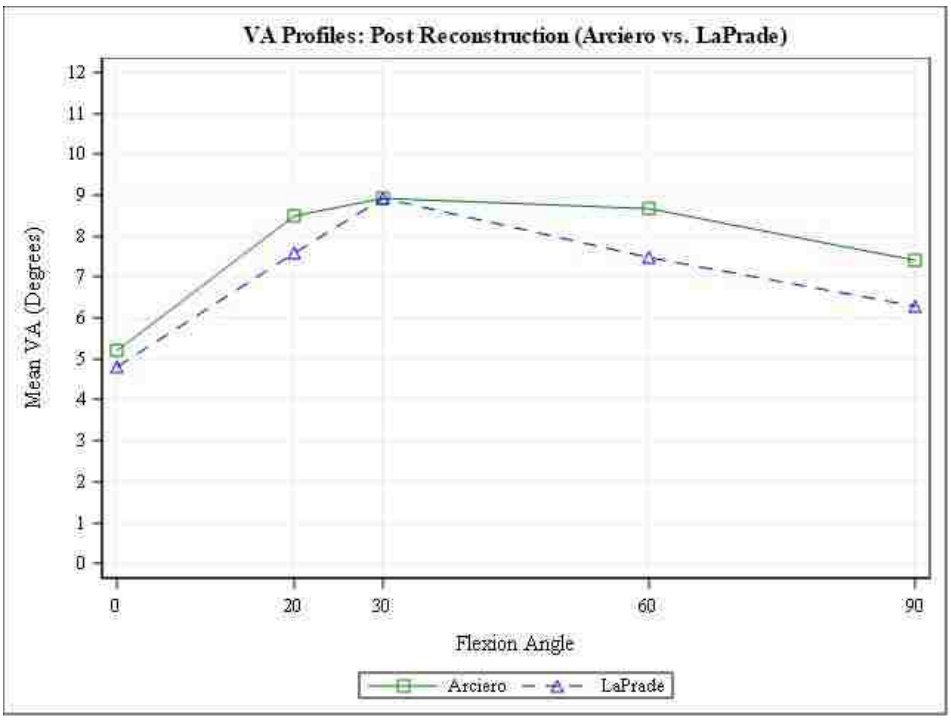

Figure 4.19: Arciero vs. LaPrade VA means at post reconstruction at 0°, 20°, 30°, 60°, and 90° of flexion.

The Arciero and LaPrade VA post reconstruction profiles showed parallelism except at 30° of flexion. At all other flexion angles, the LaPrade technique exhibited better outcome measures. A Wilks' Lambda statistic of .8627 and P=0.7248 was found indicating that there is no statistical difference between the two techniques. Figure 4.20 shows the VA profile comparison of the intact and sectioned specimens vs. the Arciero and LaPrade specimens at post reconstruction.

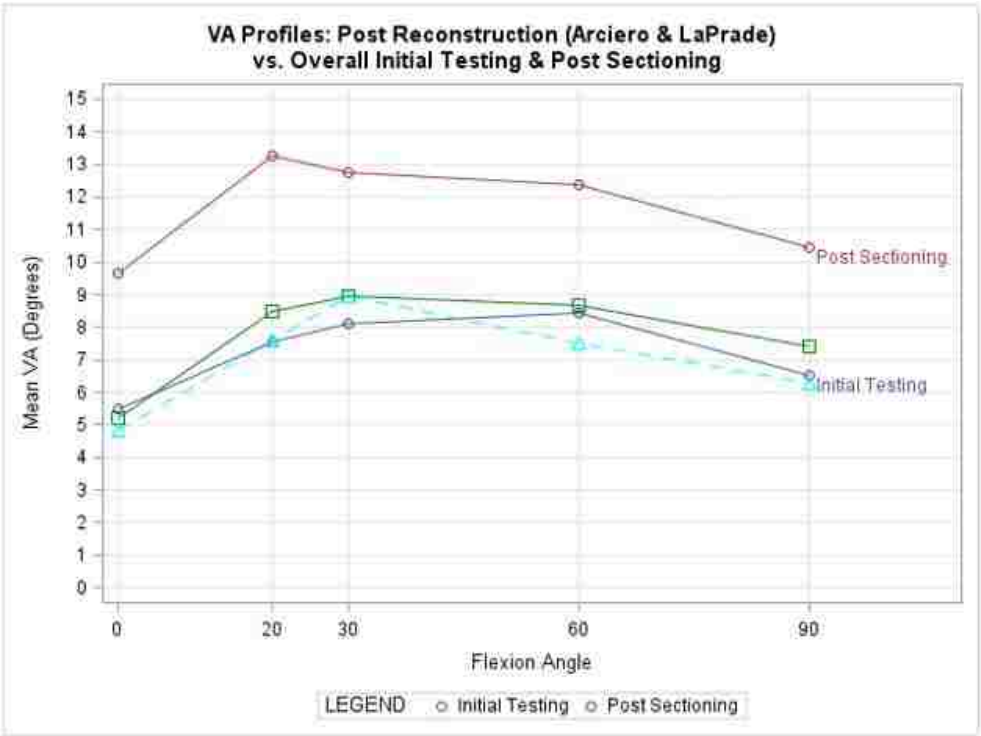

Figure 4.20: VA profile comparison at initial and post sectioning vs. Arciero and LaPrade specimens at post reconstructioin. The cyan △ indicates the LaPrade VA profile. The green box indicates the Arciero VA profile.

4.4 Post Tib-Fib Sectioning

Table 4.16 shows Specimen#5 mean ER and VA outcome measures at post tib-fib sectioning. All additional specimen mean ER and VA tables at post tib-fib sectioning can be found in Appendix D.4.

4.4.1 External Rotation

Rotational instability was greatly increased in all Arciero specimens across all flexion angles after sectioning of the tibiofibular ligament (Figure 4.21 and Table 4.17). Mean

POST TIB-FIB SECTIONING: SPECIMEN#5 (MEANS)			
	Flexion Angle	**ER (Degrees)**	**VA (Degrees)**
LaPrade	0	8.39	2.95
	20	13.82	4.72
	30	12.25	4.54
	60	19.29	4.70
	90	23.03	5.93
Arciero	0	9.16	4.99
	20	22.71	7.29
	30	23.02	5.42
	60	28.57	10.18
	90	28.98	8.03

Table 4.16: Mean paired ER and VA data for Specimen#1 at 0°, 20°, 30°, 60°, and 90° of flexion.

values were comparable or greater than the outcome measures at post sectioning.

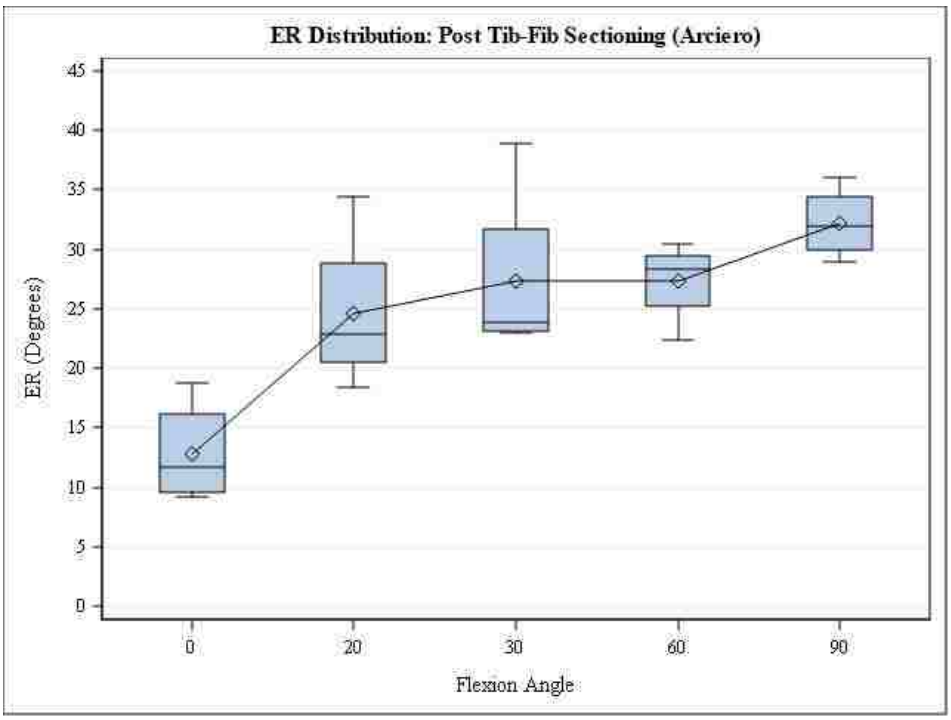

Figure 4.21: Mean post tib-fib sectioning ER distribution of Arciero specimens at 0°, 20°, 30°, 60°, and 90° of flexion.

Arciero ER Distribution: Post Tib-Fib Sectioning	
Flexion Angle	Mean ER (Degrees)
0	12.84
20	24.67
30	27.39
60	27.40
90	32.23

Table 4.17: Mean Arciero ER distribution at post tib-fib sectioning.

The LaPrade ER distribution and means are shown in Figure 4.22 and Table 4.18. Rotational instability was greatly increased at all flexion angles and the LaPrade technique was unable to provide satisfactory rotational stability to the PLC.

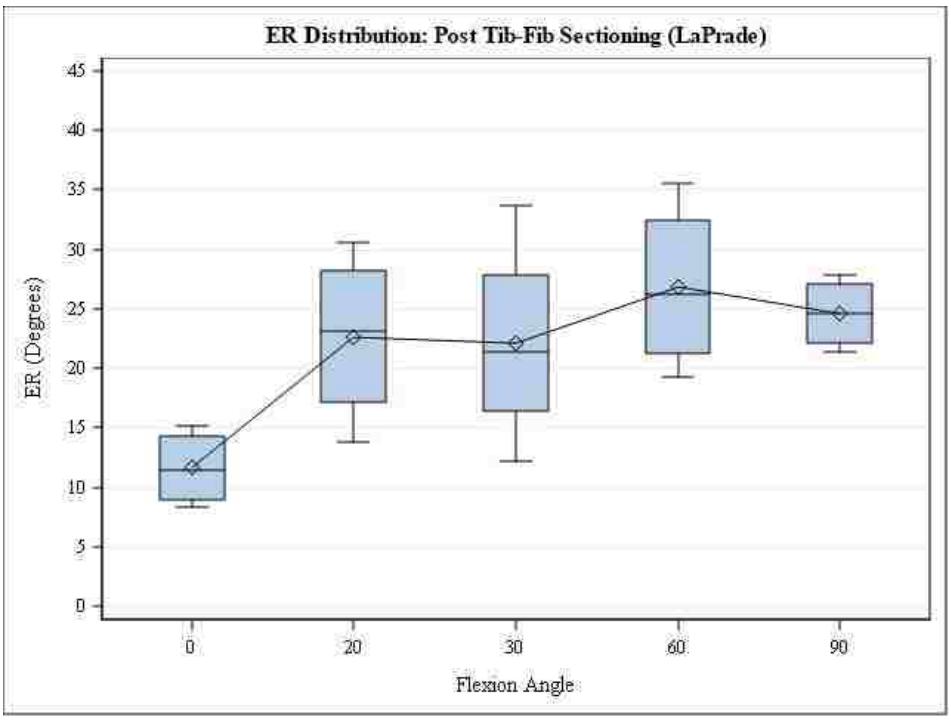

Figure 4.22: Mean post tib-fib sectioning ER distribution of LaPrade specimens at 0°, 20°, 30°, 60°, and 90° of flexion.

Arciero ER Distribution: Post Tib-Fib Sectioning	
Flexion Angle	Mean ER (Degrees)
0	11.63
20	22.68
30	22.16
60	26.82
90	24.61

Table 4.18: Mean LaPrade ER distribution at post tib-fib sectioning.

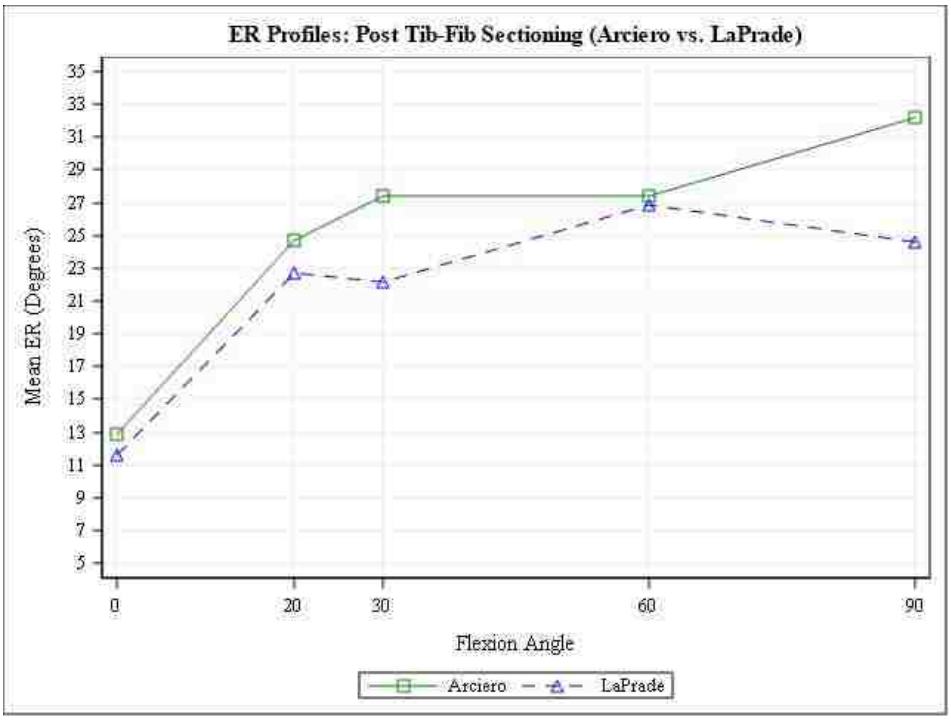

Figure 4.23: Arciero vs. LaPrade ER means at post tib-fib sectioning at 0°, 20°, 30°, 60°, and 90° of flexion.

Figure 4.23 shows the Arciero vs. LaPrade ER comparison at post tib-fib sectioning. A Wilks' Lambda statistic of .0989 and P=.2293 was found indicating the two profiles are statistically indifferent. A post hoc analysis using ANOVA revealed a statistical difference at 90° of flexion with a value of P=0.0115. But all other flexion angles had P values greater that 0.05.

4.4.2 Varus Angulation

Figure 4.24 and Table 4.19 show the Arciero VA profile and means, respectively. Figure 4.25 and Table 4.20 show the LaPrade VA profile and means, respectively.

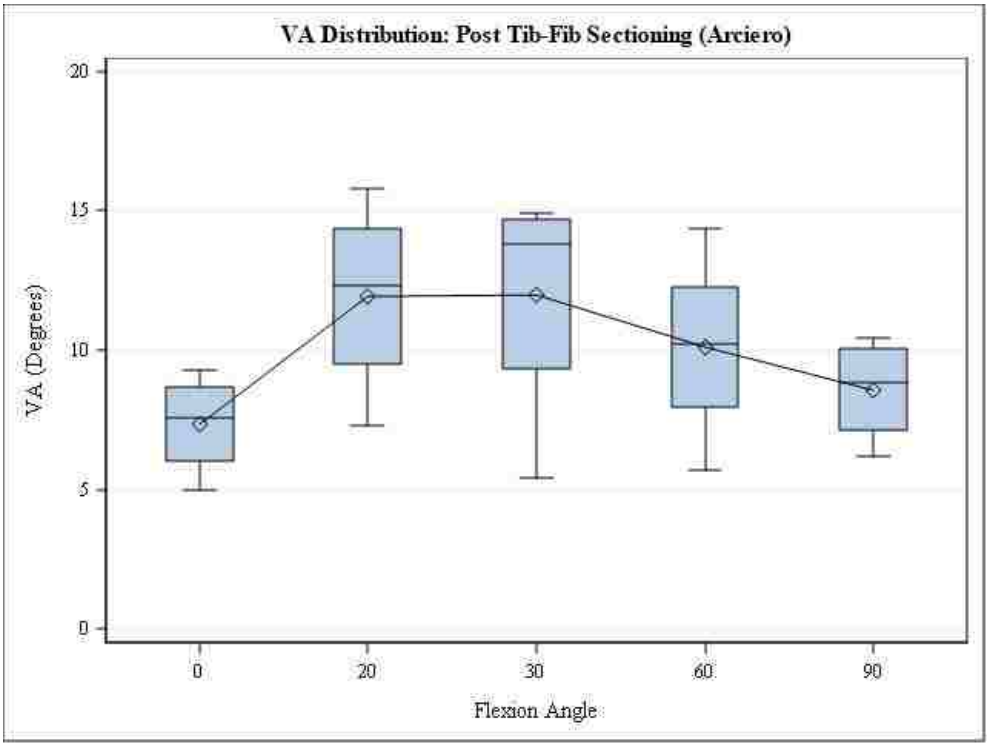

Figure 4.24: Mean post tib-fib sectioning VA distribution of Arciero specimens at 0°, 20°, 30°, 60°, and 90° of flexion.

Arciero VA Distribution: Post Tib-Fib Sectioning	
Flexion Angle	Mean ER (Degrees)
0	7.34
20	11.92
30	11.99
60	10.11
90	8.58

Table 4.19: Mean Arciero VA distribution at post tib-fib sectioning.

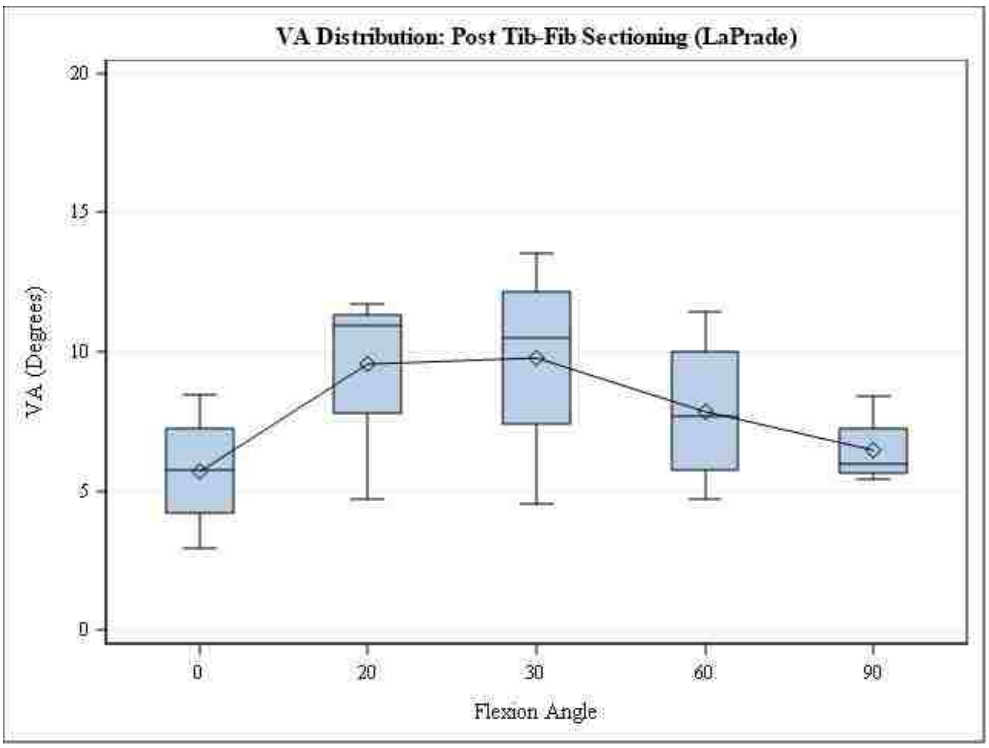

Figure 4.25: Mean post tib-fib sectioning VA distribution of LaPrade specimens at 0°, 20°, 30°, 60°, and 90° of flexion.

LaPrade VA Distribution: Post Tib-Fib Sectioning	
Flexion Angle	Mean VA (Degrees)
0	5.71
20	9.56
30	9.77
60	7.87
90	6.44

Table 4.20: Mean LaPrade VA distribution at post tib-fib sectioning.

Figure 4.26 shows the VA mean comparison profiles of the Arciero and LaPrade techniques. At all flexion angles, the LaPrade technique outperformed the Arciero technique. A Wilks' Lambda statistic of .0753 and P=0.1778 was found indicating that there is no statistical difference between the two profiles. A post hoc analysis

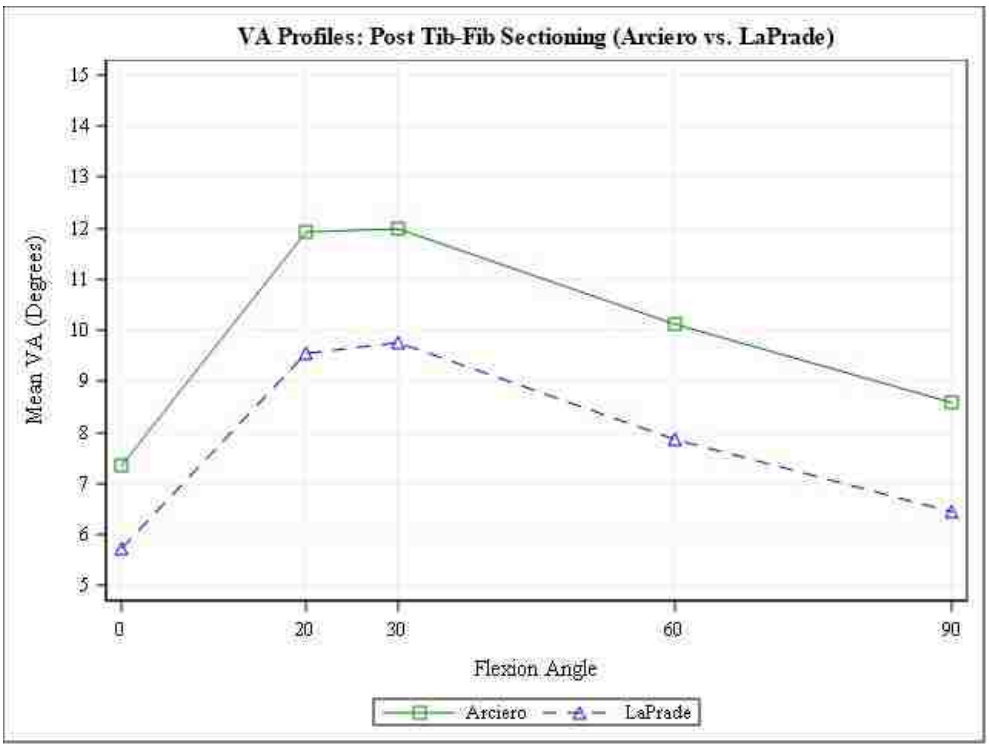

Figure 4.26: Arciero vs. LaPrade VA means at post tib-fib sectioning at 0°, 20°, 30°, 60°, and 90° of flexion.

using a parallel profile test revealed a value of P=.9962. This suggests that the two profiles are almost completely parallel across all flexion angles. This may indicate that there may be a difference but the sample size is too small for this case.

4.5 Post ACL Sectioning

Table 4.21 shows Specimen#1 mean ER and VA outcome measures at post ACL sectioning. The ER and VA outcome measures at post ACL sectioning were either similar or lower than values compared to the combined post reconstruction measures. All additional specimen mean ER and VA tables at post ACL sectioning can be found in Appendix D.5.

POST TIB-FIB SECTIONING: SPECIMEN#1 (MEANS)			
	Flexion Angle	**ER (Degrees)**	**VA (Degrees)**
LaPrade	0	7.90	5.65
	20	12.79	6.71
	30	19.74	9.77
	60	16.05	9.41
	90	15.64	9.92
Arciero	0	7.32	5.84
	20	13.92	6.47
	30	18.11	10.45
	60	14.63	9.08
	90	18.56	9.73

Table 4.21: Mean paired ER and VA data for Specimen#1 at 0°, 20°, 30°, 60°, and 90° of flexion.

4.5.1 External Rotation

Figure 4.27 and Table 4.22 show the Arciero ER profile distribution and mean values, respectively. Figure 4.28 and Table 4.23 show the LaPrade ER profile distribution and mean values, respectively.

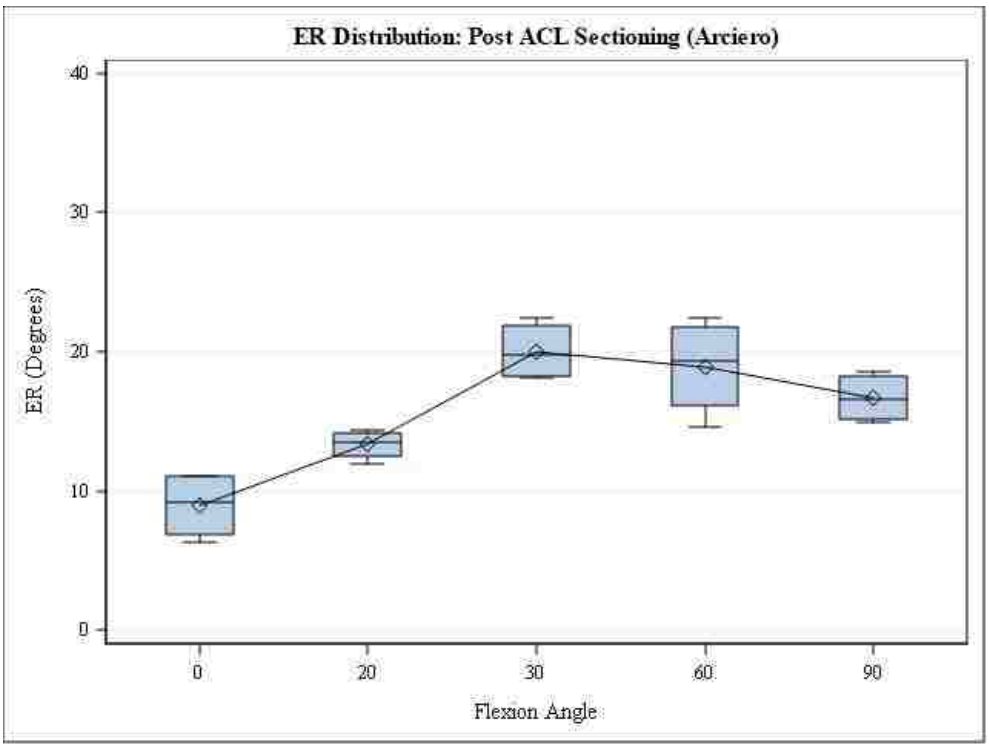

Figure 4.27: Mean post ACL sectioning ER distribution of Arciero specimens at 0°, 20°, 30°, 60°, and 90° of flexion.

Arciero ER Distribution: Post ACL Sectioning	
Flexion Angle	Mean ER (Degrees)
0	8.94
20	13.33
30	20.03
60	18.93
90	16.65

Table 4.22: Mean Arciero ER distribution at post ACL sectioning.

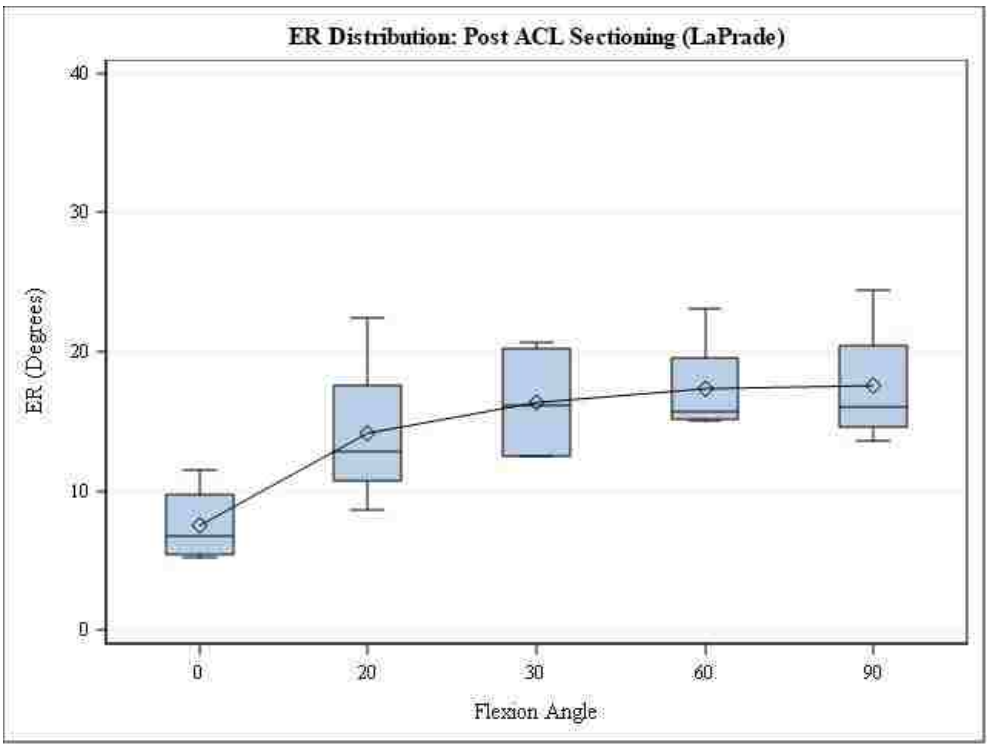

Figure 4.28: Mean post ACL sectioning ER distribution of LaPrade specimens at 0°, 20°, 30°, 60°, and 90° of flexion.

LaPrade ER Distribution: Post ACL Sectioning	
Flexion Angle	Mean ER (Degrees)
0	7.54
20	14.14
30	16.35
60	17.36
90	17.53

Table 4.23: Mean LaPrade ER distribution at post ACL sectioning.

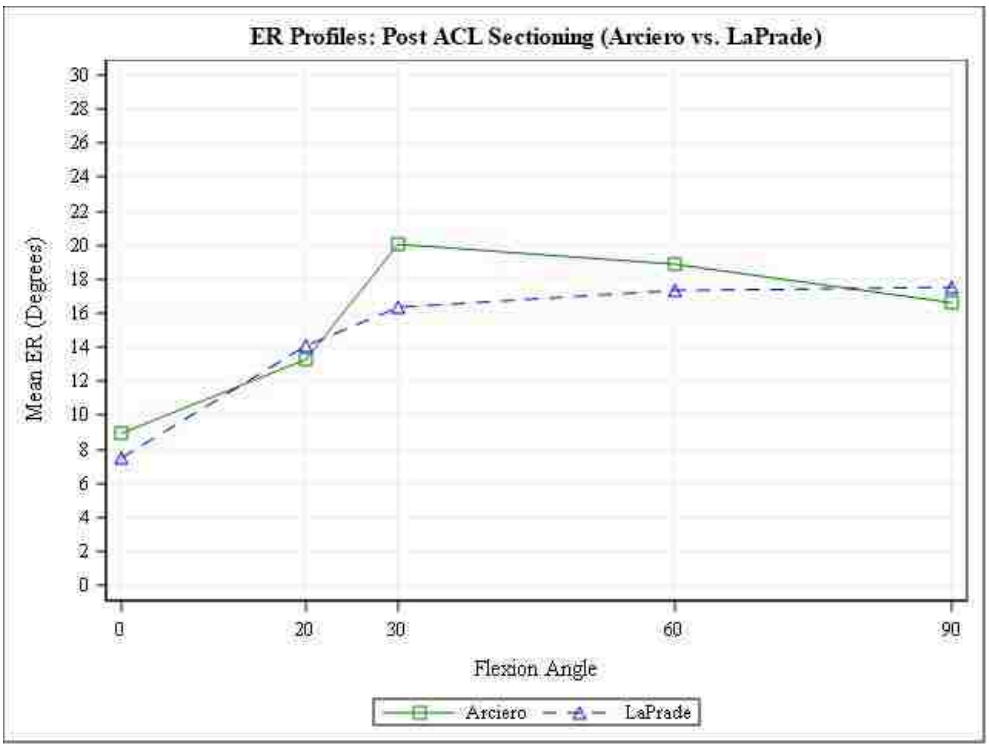

Figure 4.29: Arciero vs. LaPrade ER means at post ACL sectioning at 0°, 20°, 30°, 60°, and 90° of flexion.

At post ACL sectioning, rotational laxity across all flexion angles increased but the ER mean values were less than all post sectioning values. It is key to note that sectioning of the ACL did not destabilize the PLC to the degree that sectioning of the tibiofibular ligament did. A Wilks' Lambda statistic of .5313 and P=0.8496 was found between the two profiles indicating no statistical difference between the two profiles.

4.5.2 Varus Angulation

The VA distribution and means for the Arciero specimens can be seen in Figure 4.30 and Table 4.24. The VA distribution and means for the LaPrade specimens can be seen in Figure 4.31 and Table 4.25.

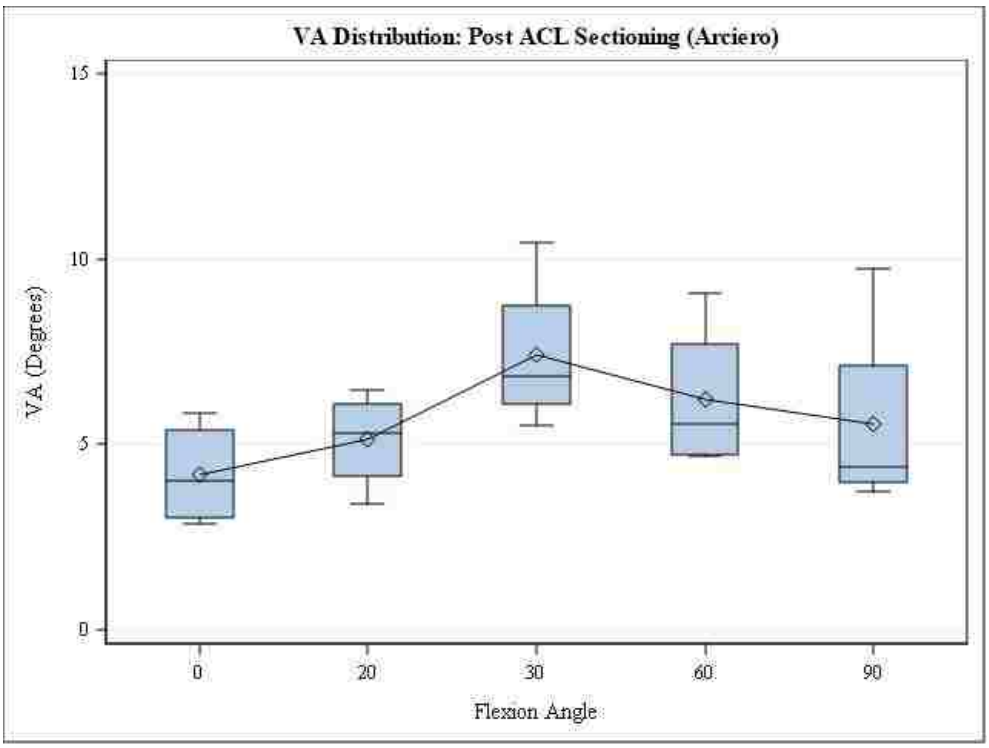

Figure 4.30: Mean post ACL sectioning VA distribution of Arciero specimens at 0°, 20°, 30°, 60°, and 90° of flexion.

Arciero VA Distribution: Post ACL Sectioning	
Flexion Angle	Mean VA (Degrees)
0	4.19
20	5.12
30	7.40
60	6.21
90	5.56

Table 4.24: Mean Arciero VA distribution at post ACL sectioning.

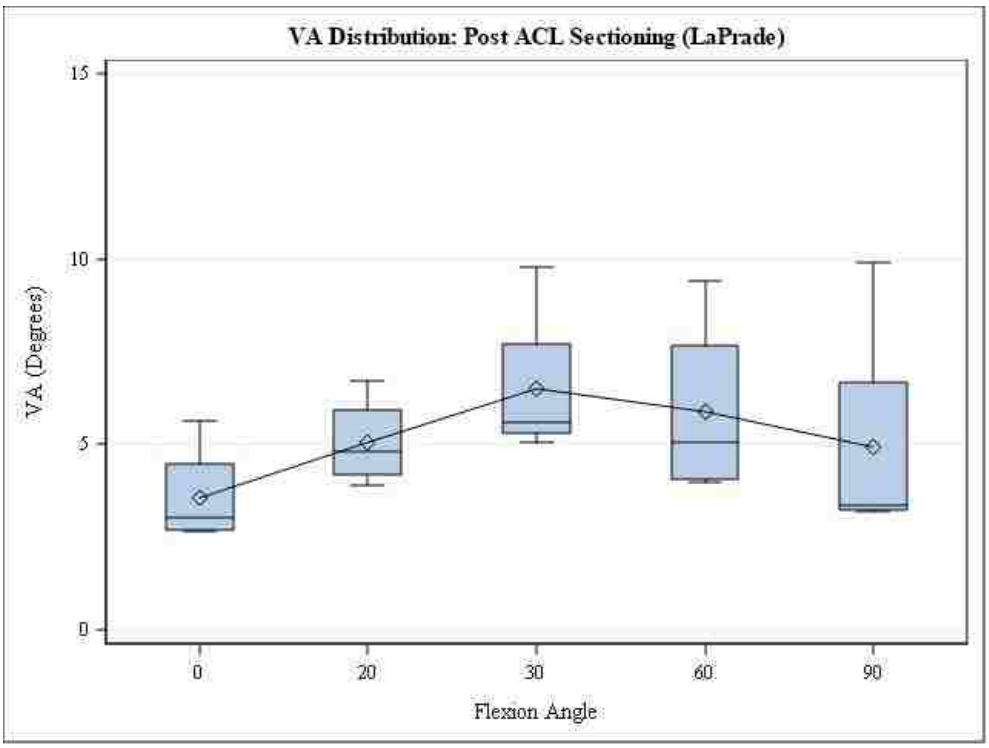

Figure 4.31: Mean post ACL sectioning VA distribution of LaPrade specimens at 0°, 20°, 30°, 60°, and 90° of flexion.

LaPrade VA Distribution: Post ACL Sectioning	
Flexion Angle	Mean VA (Degrees)
0	3.58
20	5.05
30	6.51
60	5.86
90	4.94

Table 4.25: Mean LaPrade VA distribution at post ACL sectioning.

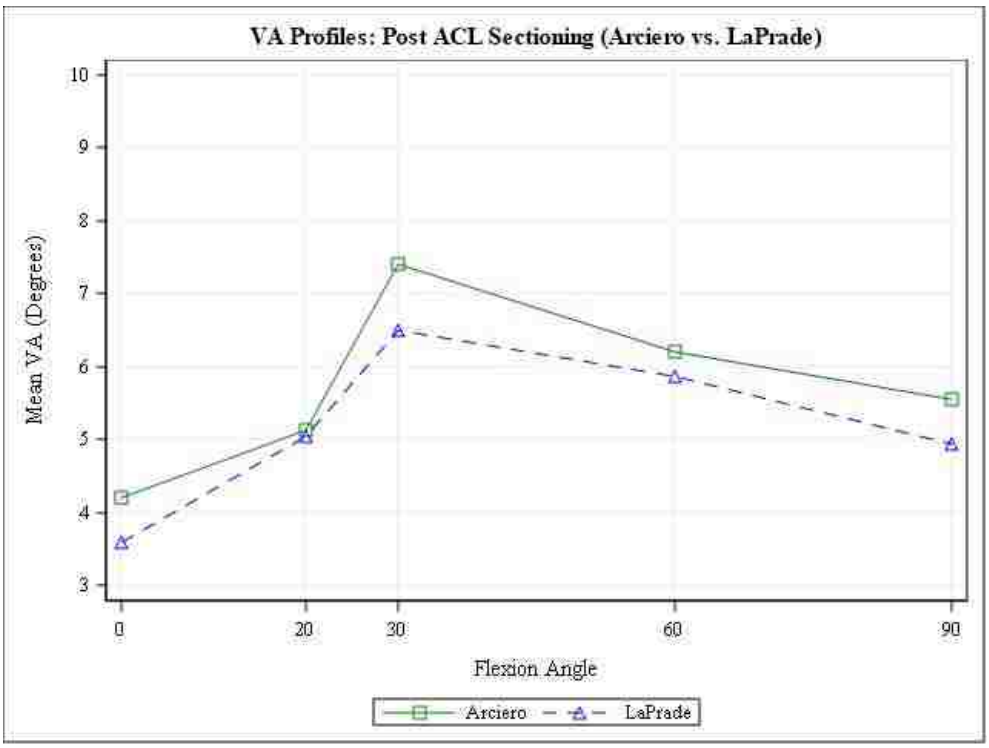

Figure 4.32: Arciero vs. LaPrade VA means at post ACL sectioning at 0°, 20°, 30°, 60°, and 90° of flexion.

A Wilks' Lambda statistic of 0.0836 and P=1962 was found indicating no statistical difference between the two profiles.

4.6 Paired Specimen Comparison

To further differentiate the Arciero and LaPrade techniques, a comparison of the two techniques for each matched pair was taken at all flexion angles for ER and VA at post reconstruction. The percentage of recovered ER/VA at post reconstruction for the two techniques were found and compared to each other. Equation 4.1 was used to determine the recovered ER/VA at each individual flexion angle by using the means at PS (Post Sectioning), PR (Post Reconstruction), and IT (Initial Testing). For

each flexion agle, the technique that restored the largest percentage of ER/VA was chosen to be superior at that instance. This procedure was repeated at all flexion angles for each matched pair. A maximum of nine instances for ER and VA at post reconstruction were measured. Table 4.26 shows the percentage comparison of recovered ER/VA for specimen#1 at post reconstruction for the Arciero and LaPrade techniques. All additional tables for all specimens can be found in Appendix .

$$Recovered\, ER/VA = (\frac{Mean\, at\, PS\, -\, Mean\, at\, PR}{Mean\, at\, PS\, -\, Mean\, at\, IT}) \cdot 100 \tag{4.1}$$

POST RECONSTRUCTION SPECIMEN#1			
	Flexion Angle	**% Recovered ER**	**% Recovered VA**
LaPrade	0	53.63	93.17
	20	115.50	107.70
	30	122.35	74.69
	60	130.81	111.15
	90	317.56	123.85
Arciero	0	198.75	92.41
	20	110.78	103.11
	30	130.91	75.36
	60	112.78	129.44
	90	90.30	91.33

Table 4.26: Percentage of recovered ER/VA Arciero vs. LaPrade comparison at post reconstruction for specimen#1.

A similar measure was investigated by solving for the percentage of ER/VA lost when the tibiofibular joint or ACL was sectioned. Equation 4.2 describes the ER/VA percentage lost after post tib-fib sectioning (PTFS) and post ACL sectioning (PACLS). At this measure, whichever technique lost the least amount of ER/VA (in terms of percentage) was declared superior at that instance. At post tib-fib sectioning and ACL sectioning, four instances were taken at these two phases. Tables were compiled which showed the number of instances in which the Arciero or LaPrade

technique fared better at post reconstruction, post tib-fib sectioning, and at post ACL sectioning. All additional tables for all specimens can be found in Appendix D.6..

$$Lost\ ER/VA = (\frac{Mean\ at\ PTFS/PACLS\ -\ Mean\ at\ PR}{Mean\ at\ PS\ -\ Mean\ at\ PR}) \cdot 100 \tag{4.2}$$

POST ACL SECTIONING SPECIMEN#1			
	Flexion Angle	**% Lost ER**	**% Lost VA**
LaPrade	0	-5.70	12.28
	20	0.36	19.37
	30	25.37	3.89
	60	14.89	4.88
	90	46.42	41.62
Arciero	0	70.59	8.41
	20	15.78	3.94
	30	32.84	10.44
	60	-4.85	3.97
	90	51.47	3.04

Table 4.27: Percentage of lost ER/VA Arciero vs. LaPrade comparison at post tib-fib/ACL sectioning for specimen#1.

Finally, a cumulative total of all instances at post reconstruction (Table 4.28), post tib-fib sectioning (Table 4.29), and post ACL sectioning (Table 4.30) were compiled with an aggregate total of 17 instances comparing the Arciero and LaPrade techniques. The aggregate total can be seen in Table 4.31.

POST RECONSTRUCTION RECOVERED ER (9/9)		
Flexion Angle	LaPrade	Arciero
0	6	3
20	6	3
30	6	3
60	4	5
90	4	5

POST RECONSTRUCTION RECOVERED VA (9/9)		
Flexion Angle	LaPrade	Arciero
0	6	3
20	8	1
30	3	6
60	6	3
90	8	1

Table 4.28: Arciero vs. LaPrade comparison of instances at post reconstruction for which technique proved superior (9 instances) at 0°, 20°, 30°, 60°, and 90° of flexion. Each row totals 9 instances.

POST TIB-FIB SECTIONING MINIMAL LOST ER (4/4)		
Flexion Angle	LaPrade	Arciero
0	1	3
20	3	1
30	2	2
60	2	2
90	2	2

POST TIB-FIB SECTIONING MINIMAL LOST VA (4/4)		
Flexion Angle	LaPrade	Arciero
0	4	0
20	3	1
30	4	0
60	3	1
90	3	1

Table 4.29: Arciero vs. LaPrade comparison of instances at post tib-fib sectioning for which technique proved superior (4 instances) at 0°, 20°, 30°, 60°, and 90° of flexion.

POST ACL SECTIONING MINIMAL LOST ER (4/4)		
Flexion Angle	LaPrade	Arciero
0	4	0
20	2	2
30	4	0
60	3	1
90	3	1

POST ACL SECTIONING MINIMAL LOST VA (4/4)		
Flexion Angle	LaPrade	Arciero
0	3	1
20	1	3
30	4	0
60	2	2
90	1	3

Table 4.30: Arciero vs. LaPrade comparison of instances at post ACL sectioning for which technique proved superior (4 instances) at 0°, 20°, 30°, 60°, and 90° of flexion.

OVERALL ER (17/17)		
Flexion Angle	LaPrade	Arciero
0	11	6
20	11	6
30	12	5
60	9	8
90	9	8

OVERALL VA (17/17)		
Flexion Angle	LaPrade	Arciero
0	13	4
20	12	5
30	11	6
60	11	6
90	12	5

Table 4.31: Aggregate total of instances at which the Arciero or LaPrade technique fared better at 0°, 20°, 30°, 60°, and 90° of flexion. The overall total consists of 9 instances at post reconstruction, 4 instances at post tib-fib sectioning, and 4 instances at post ACL sectioning.

Chapter 5

Computational Analysis

An additional method of analysis using a 3D computational model was generated to compare deformations in Arciero and LaPrade reconstructions under varus loading. Various platforms of software were used to create a 3D model of the knee joint. This included Mimics and 3-matic (Materialise, Ann Arbor, MI) software. Finally this 3D model was imported into ANSYS Workbench Academic 16.1 (ANSYS, Canonsbrug, PA, USA) where a 10 Nm varus moment was applied to the knee joint of an intact model, a model with simulated PLC deficiency, and with the simulated Arciero and LaPrade PLC reconstructions.

5.1 Mimics and 3-Matic

A lower extremity CT scan of a healthy 20 year old patient was scanned using a Phillips/Brilliance scanner. The 2D CT slices were imported into Mimic's where segmentation and a rendering of a 3D model was generated (Figure 5.1). The scanner operated at 120 kV and 188 mAs with an exposure of 200 (lux seconds). Slice thickness equaled 1 mm with a separation of 0.5 mm between slices. The entire CT

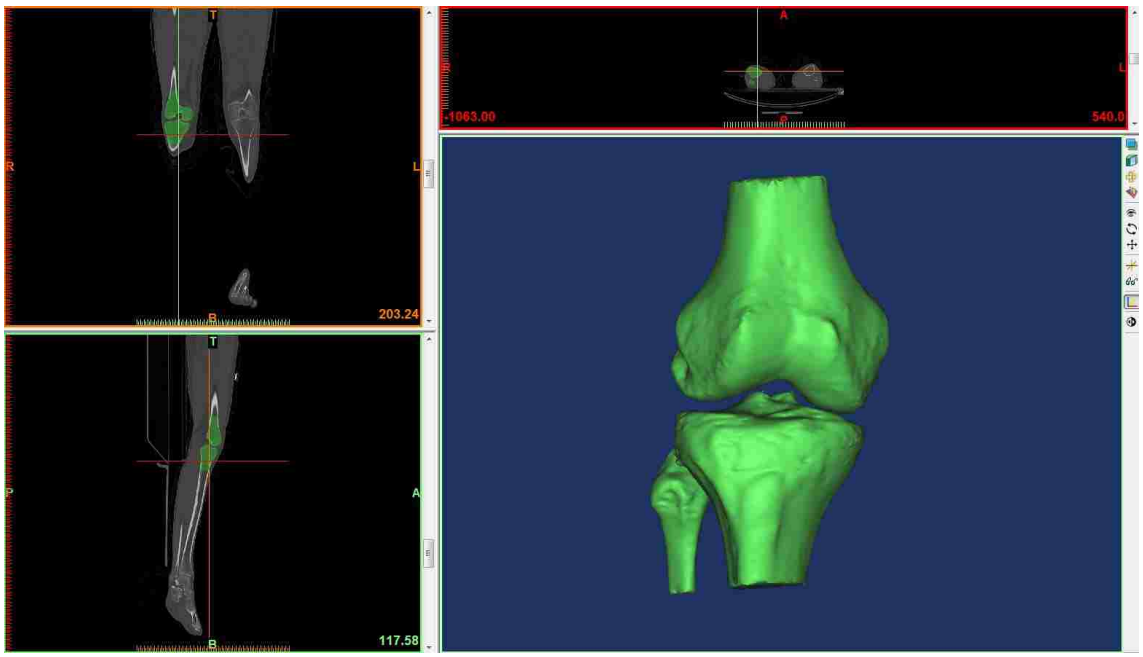

Figure 5.1: CT scan and segmentation of the knee joint. Top view of lower extremity (top left), side view of lower extremity (bottom left), axial view of the lower extremity (top right), and the 3D rendered image of the knee joint (bottom left).

scan consisted of a 512 x 512 pixel frame with a pixel size of 0.839844 mm. Using a predetermined threshold, the cortical bone was isolated from the scan and segmented in order to create a 2D "bone" mask of the lower extremity. This mask highlighted all cortical bone in the CT scan. For this model, the knee joint was the area of interest. The right knee was left highlighted and all cortical bone 6 cm proximal and distal to the knee joint was erased preserving only a rendering of the right knee joint. To simplify the model and reduce computational time, the medullary canals of the femur, tibia, and fibula were filled to create full solid models of the respective bones. Finally a rough solid 3D generated bone mask was created from the initial 2D mask. Smoothing, wrapping, and triangle reduction quality preserving techniques were used to smooth the rough model and eliminate sharp edges and pre-existing holes which can be seen in Figure 5.2. The model was then exported to 3-Matic where further quality preservation and meshing was performed.

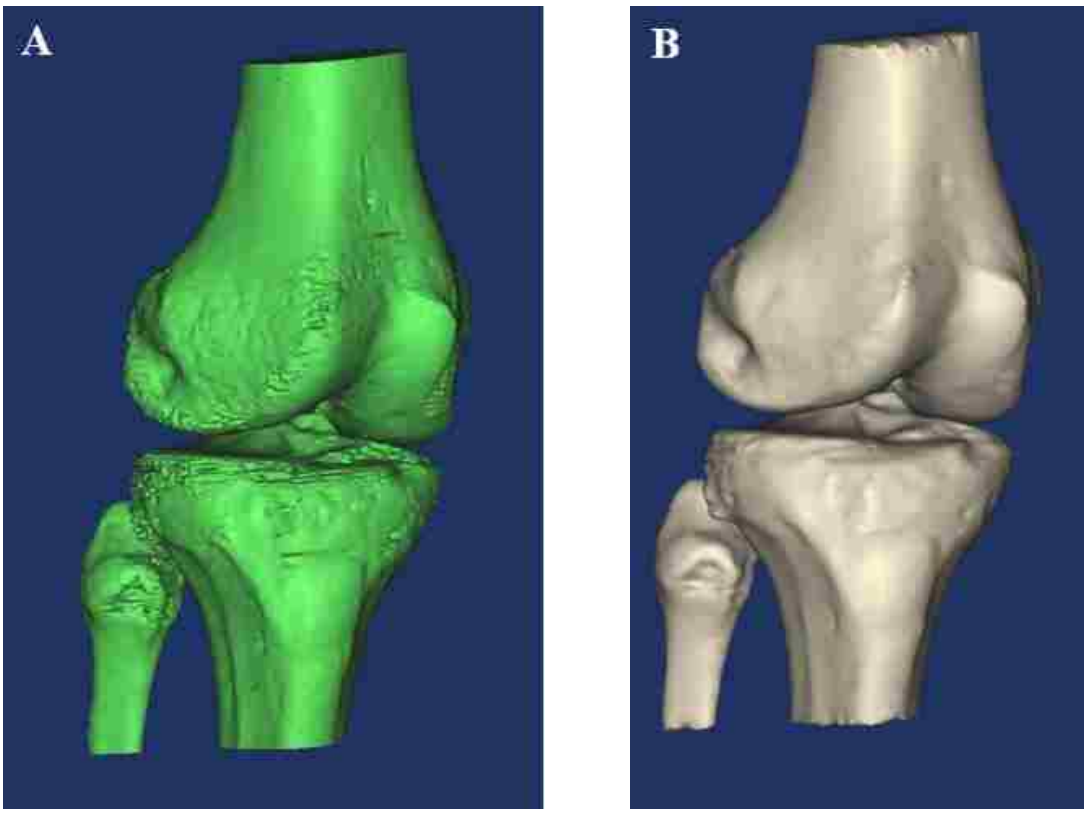

Figure 5.2: Initial rendering of the 3D generated knee joint with pre-existing holes and defects (left). Quality preserved rendering of the 3D generated knee joint with and defects and medullary canals of the femur, tibia, and fibula filled.

A uniform triangular mesh with a maximum edge length of 5.0 mm (coarse mesh) and a 2.5 mm (medium mesh) was created using 3-Matic software. The medium mesh was generated in the regions 3 cm distal and proximal from the tibial plateau which also included the proximal fibular head. This triangular mesh was used to represent the contours of the solid model which was then imported into ANSYS. The mesh from 3-Matic was not used for FEA in ANSYS. The final model was exported into ANSYS software for finite element analysis. The model and mesh can be seen in Figure 5.3, respectively.

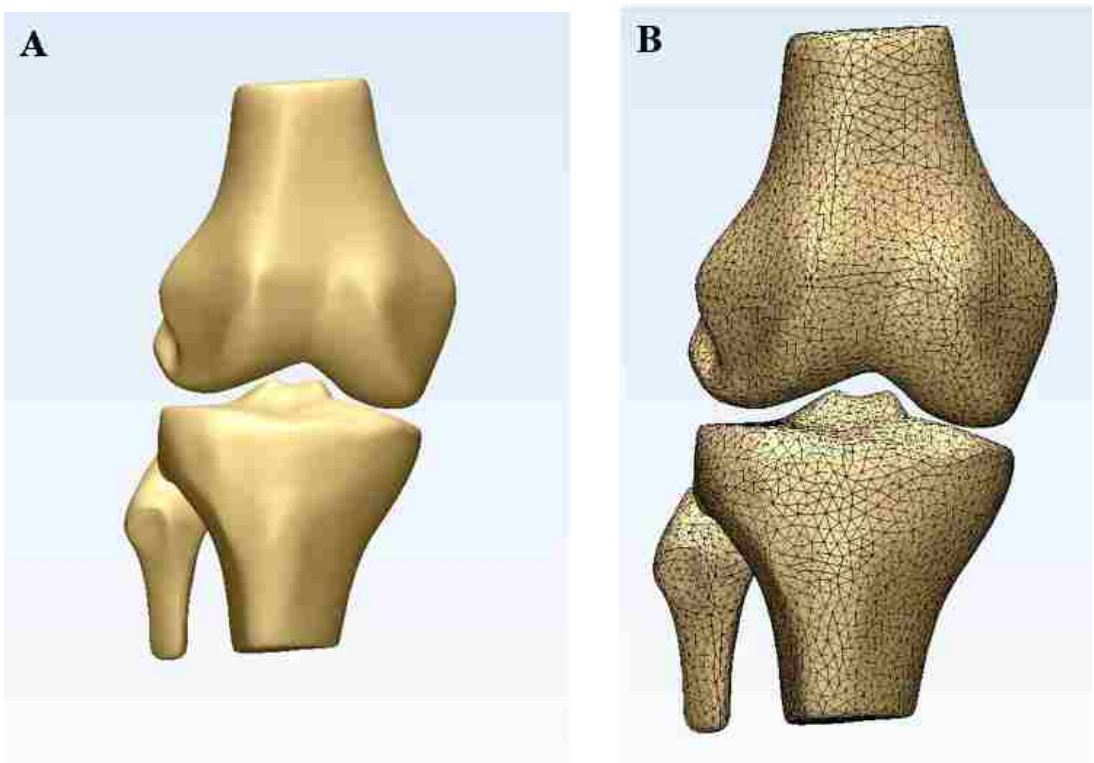

Figure 5.3: (A) Final model of the knee joint that was exported into ANSYS software for FEA analysis. (B) Final coarse and medium meshed model representing the contours of the femur, tibia, and fibula solid bodies.

5.2 ANSYS

Once imported, a static structural varus load simulation was conducted on the solid model of the knee joint at 0° of flexion. The geometry of the knee joint consisted of three solid bodies which included the femur, tibia, and fibula. All three solid bodies were assigned the material properties of cortical bone consisting of a density of 1900 kg/m^3, E = 1860 MPa, and a poisson's ratio of 0.3 [40,41]. The bounding box dimensions (x,y,z) in mm of the three solid bodies are as follows: femur (83.52 x 74.75 x 90.21) mm, tibia (73.24 x 62.26 x 74.15) mm, and the fibula (25.37 x 25.92 x 56.96) mm.

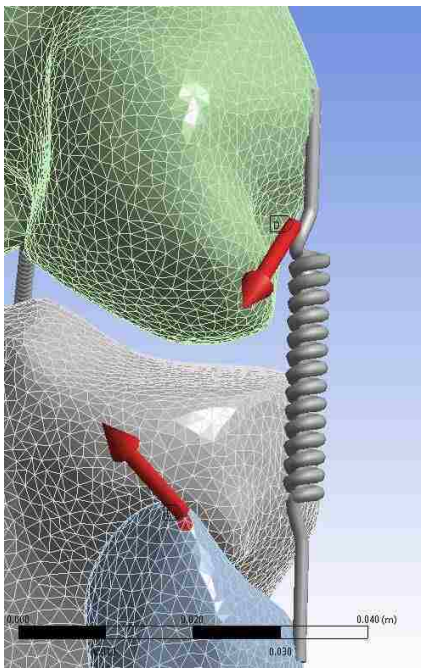

Figure 5.4: Intact model with the FCL spring and simulated forces representing the PLT and PFL.

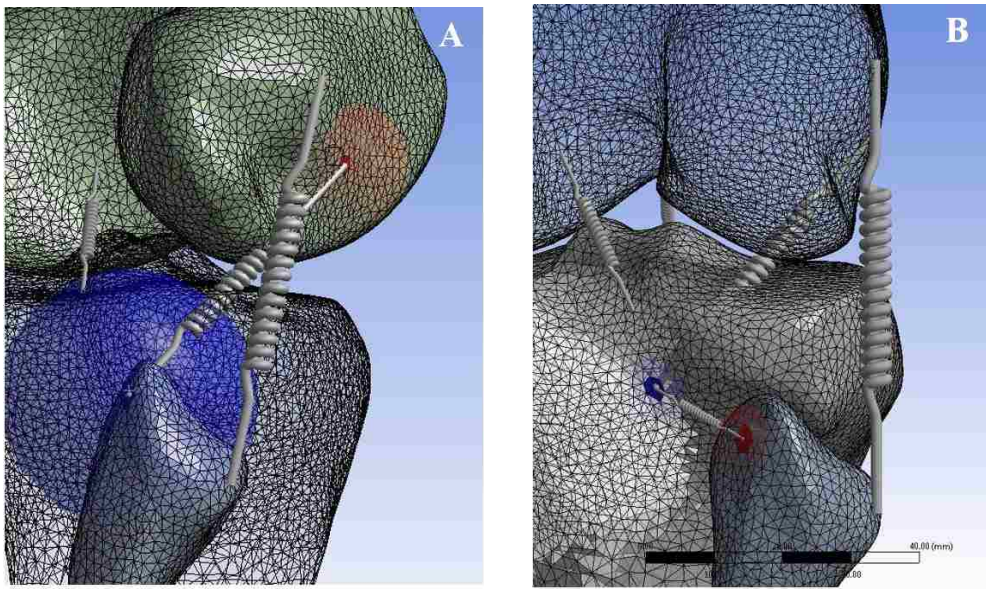

Figure 5.5: (A) Arciero reconstruction highlighting the FCL and PFL as springs with stiffnesses of 242 N/mm each, respectively. (B) LaPrade reconstruction highlighting the FCL, PLT, and PFL as springs with stiffnesses of 242 N/mm each.

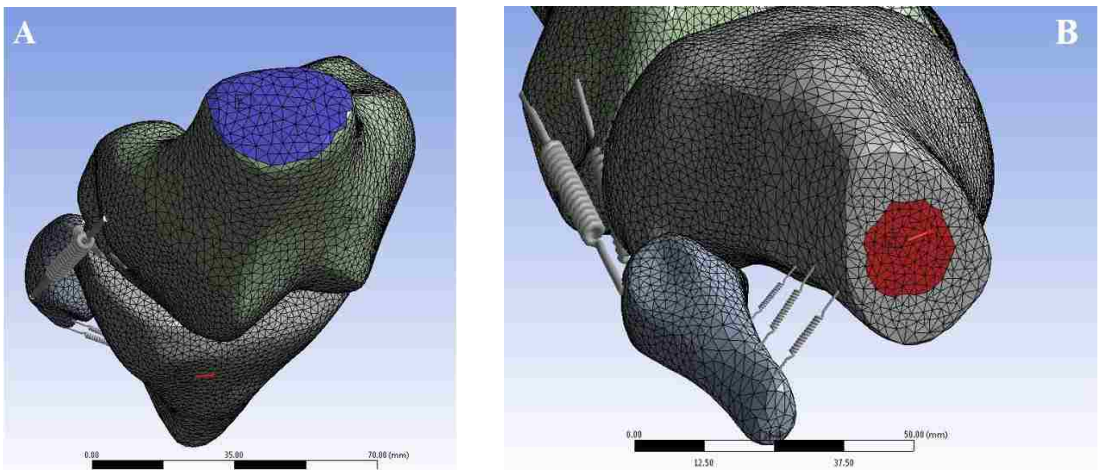

Figure 5.6: Fixed support (blue) at the head of the proximal femur preventing translation or rotation. (B) 142 Nm force applied at the articular surface of the distal tibia simulating a 10 Nm varus moment.

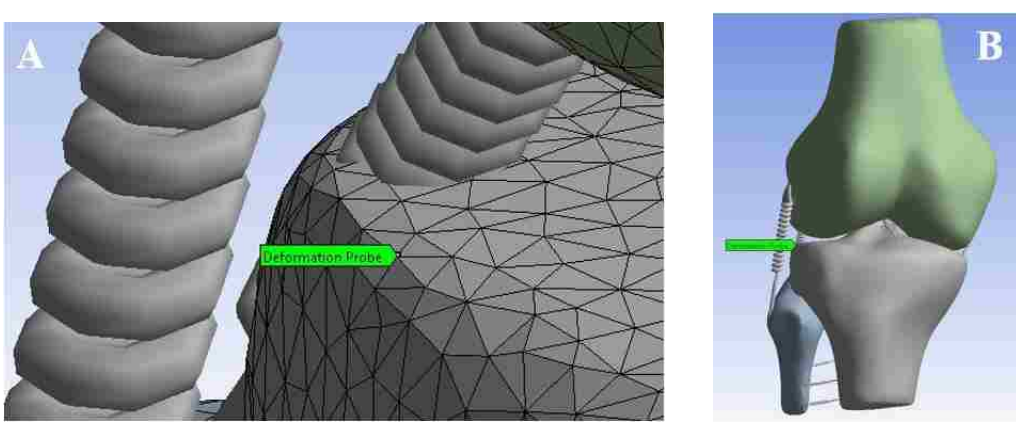

Figure 5.7: (A) Deformation probe placed at the most lateral aspect of the tibial plateau measuring the maximum displacement (z-direction) after a 10 N/m varus moment is applied. (B) Zoomed out image showing the location of the probe relative to the knee model.

Spring connections were assigned to the knee model to simulate the respective tendons and ligaments in the knee (Figure 5.8). The ACL was given a longitudinal stiffness of 242 N/mm, PCL: 400 N/mm, MCL: 200 N/mm, interosseous membrane: 13.1 N/mm, split achilles tendon allograft: 242 N/mm, and the FCL, PLT, and PFL

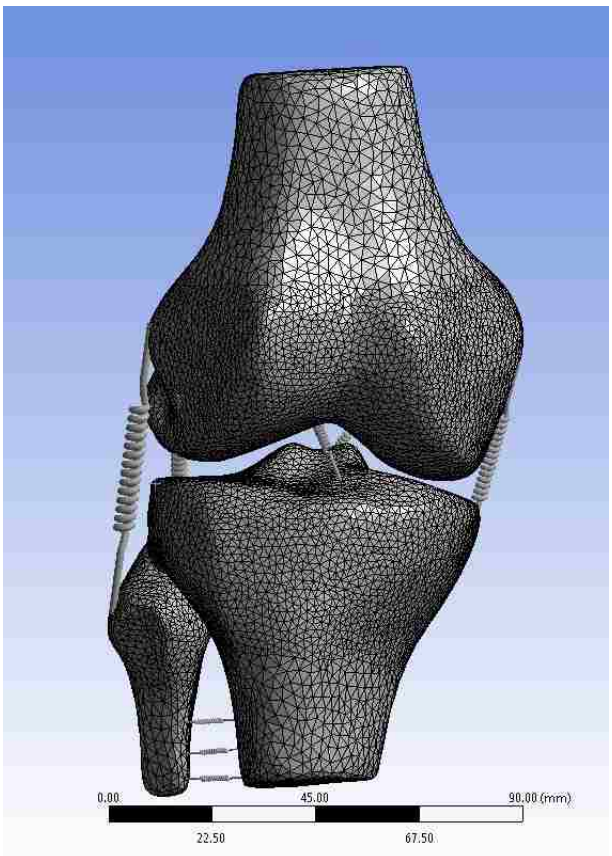

Figure 5.8: Model of the knee joint with spring connections simulating the PLC, MCL, ACL, and PCL. The model consists of three solid bodies: femur, tibia, and fibula.

were assigned a stifness of 33.5 N/mm, 28.6 N/mm, and 83.7 N/mm respectively [2,31,33,42,43]. An intact model was created to compare against the Arciero and LaPrade reconstruction post varus application (Figure 5.4). The intact model consisted of only an FCL spring at the posterolateral corner. The PLT and PFL were simulated using forces that created a vector simulating the tension of the popliteus muscle [4]. The magnitude of the PLT and PFL forces was equivalent to 44 N in the direction associated with the popliteus muscle. The directional force components of the PLT and PFL were (20, 30, -20) (N) and (2.5, 1, 2.5) (N), respectively. Next, a sectioned model was simulated with the absence all three primary structures of the

PLC:the FCL, PLT, and PFL. Figures 5.5(A) and 5.5(B) show the simulated Arciero and LaPrade reconstructions, respectively.

Two frictional contacts were assigned between the tibial plateau and the lateral and medial condyles of the distal femur with a coefficient of friction of 0.15 [4,29]. A bonded contact was assigned between the tibia and fibula at the tibiofibular ligament. Boundary conditions were assigned to simulate varus loading and external rotation about the knee joint. A fixed support was placed at the proximal femur to prevent any translation or rotation (Figure 5.6). For varus loading, a 142 N force was applied tangent to the articular surface of distal tibia in order to simulate a 10 Nm varus moment. A deformation probe was used to measure the displacement in the z-direction (vertical) for varus gapping at the posterolateral corner in mm (Figure 5.7). Finally the mesh of the final models were configured in a uniform triangular mesh with a minimum size length of 1 mm and max face size of 2 mm with a curvature normal angle of 30°. The final knee model had a total of 13,805 nodes and 24,347 elements.

Due to a larger deformation, adjustments needed to be made to the sectioned knee model in order for the simulation to converge. A larger pinball radius (20 mm) had to be configured at the contact region between the medial condyle and tibial plateau. Also the automatic time step had to be reconfigured by changing the number of substeps from one to ten. At each substep, the varus load was incrementally increased by 1 Nm until a 10 Nm varus moment was applied to the PLC. Only the sectioned model needed this configuration. The intact, Arciero, and LaPrade models converged without these configurations.

5.3 Computational Results

Results for the Arciero, LaPrade, and intact models for VA can be seen in Table 5.1.

VA DISPLACEMENT (mm) **Z-DIRECTION**			
INTACT	**SECTIONED**	**ARCIERO**	**LAPRADE**
1.389	7.081	1.423	1.322

Table 5.1: Computational results showing the displacement (z-direction) in the PLC after a 10 Nm had been simulated.

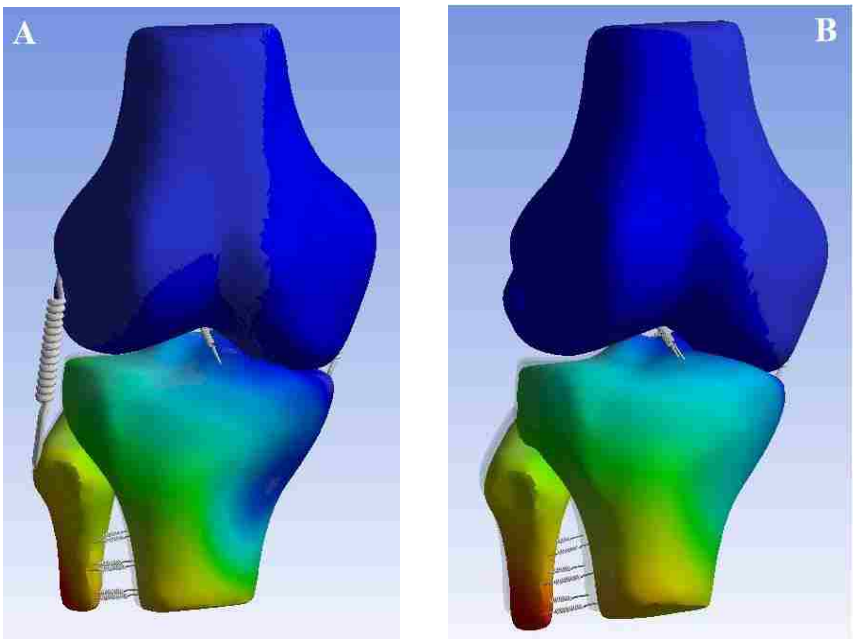

Figure 5.9: Total deformation of (A) Intact (1.389 mm) and (B) Sectioned (7.081 mm) models post VA.

The respective deformation and displacements for the intact, sectioned, Arciero, and LaPrade reconstructions can be seen in Figures 5.9 and 5.10. The gray shadows in the deformation models show the initial position while the colored models show the final position of the model after varus loading. The intact, Arciero, and LaPrade

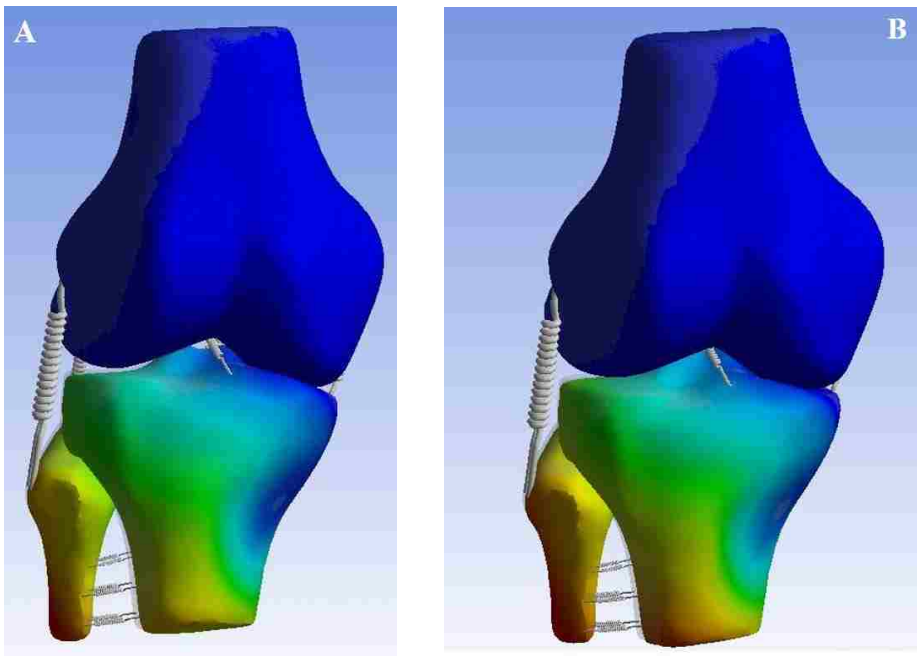

Figure 5.10: Total deformation of (A) Arciero and (B) LaPrade models post VA. At the deformation probe, LaPrade showed the lowest displacement in the z-direction (1.322 mm) as compared to Arciero (1.423 mm).

outcome measures generate similar results. This supports our experimental data suggesting that the Arciero and LaPrade reconstructions successfully re-stabilize the posterolateral corner at 0° of flexion.

Chapter 6

Conclusions

As of recently, the biomechanical function of the Posterolateral Corner (PLC) and its injury has garnered the attention of medical community. Because of its complexity, many well known orthopedic surgeons have developed their own unique methods of reconstruction to re-stabilize the PLC. Research has demonstrated that the function of the PLC is to resist external rotation (ER) and varus gapping (VA) about the lateral compartment of the knee. Studies have compared the varying PLC reconstruction techniques by determining which reconstruction method best restores these two biomechanical functions, ER and VA. The Arciero and LaPrade techniques are two of the most used and well known PLC reconstructions but they have never been compared to one another from a biomechanical perspective. The purpose of this thesis was to investigate which method best restored stability to the PLC, with the inclusion of an injury to the tibiofibular ligament or ACL.

Originally two matched pairs were used for preliminary tests and eight matched pairs were to be used for the study. The two preliminary matched pairs were included for data analysis and one of the eight matched pairs had considerable arthritis in the knee which prevented full extension at 0° of flexion. As a result this matched pair was

not used. In total, nine paired specimens were subjected to torsional and varus loads at four different phases: initial testing, post sectioning, post reconstruction, and post tib-fib/ACL sectioining. Also, at each phase, each paired specimen underwent torsional and varus loads at 0°, 20°, 30°, 60°, and 90° of flexion. For every matched pair, one leg was reconstructed with the Arciero technique while the contralateral leg was reconstructed with the LaPrade technique.

Initial testing of the Arciero and LaPrade matched paired specimens showed no dissimilarity between their ER and VA profiles. This allowed the study to establish a baseline with which to compare the sectioned specimens against their respective reconstructions. MANOVA determined that there was significance between the initial and sectioned specimens with P=0.0165 using Wilks' Lambda statistic with a significance level of 5%. At post reconstruction, post tib-fib sectioning, and post ACL sectioning, no statistical difference was found between the two reconstruction profiles with regards to ER and VA despite the LaPrade technique displaying slightly better outcome measures at all phases. All P values at these phases of the study were greater that P>0.05. A post-hoc parallel profile test was conducted to investigate if the two reconstructions profiles showed parallelism and if a consistent difference across all flexion angles was found at all phases of the study. This test showed that the two techniques displayed parallelism (P>>0.05) for both ER and VA measures at post reconstruction, post tib-fib sectioning, and post ACL sectioning. This implies that the study may have been underpowered and that a larger sample size may yield significance between the two reconstruction methods.

The greatest difference between the Arciero and LaPrade specimens was at the post tib-fib sectioning phase. No statistical significance was found but the post-hoc parallel profile test indicates that a larger sample size may have revealed a statistical difference. The Arciero techniques lack of a PLT reconstruction may be the reason why the LaPrade technique showed slightly better outcome measures.

Other studies have highlighted the importance of the popliteus complex such as LaPrade et. al., McCarthy et. al., and Plaweski et. al. [1,2,23,38] respectively. Also the stability of the tibiofibular ligament has been addressed by Jahara et. al. [26] where he suggests that the integrity of any PLC reconstruction is extremely reliant upon a stable tibiofibular ligament. Our data shows no significant difference at tib-fib sectioning but the difference in measures between the Arciero and LaPrade profiles suggests that the addition of the PLT reconstruction provides added stability to the PLC.

Another test was conducted by comparing the number of instances the Arciero or LaPrade technique yielded superior outcome measures for a single matched pair at individual degrees of flexion by solving for the percentage of restored ER and VA at post reconstruction. Additionally, the percentage of ER and VA that was lost due to sectioning of the tibiofibular ligament or ACL was also used. At post reconstruction, the LaPrade technique outscored the Arciero technique in seven of the ten categories. At post tib fib sectioning, LaPrade outscored Arciero in six of the ten categories and both reconstructions tied in three of the ten categories. Finally at post ACL sectioning, LaPrade outscored Arciero in six of the ten categories and tied in two. Although the LaPrade technique yielded better outcome measures with regards to this comparison, it does not indicate that this technique is superior. Both techniques were able to restore stability the PLC close to initial conditions in terms of ER and VA.

The purpose of our computational model was to quantify the displacement post varus loading and determine if the orientation of the reconstructed ligaments contributed to less varus displacement. We can review this by first looking at the outcome measure of the sectioned PLC. The sectioned model showed partial destabilization of the PLC. According to Cooper et al [8], the displacement of the sectioned model (7.081 mm) is comparable to a grade II PLC injury. He states that a torn PLC

should generate more than 10 mm of displacement at the lateral joint line when a varus moment is applied. Our simulation may not have achieved this because of over constraint, lack of true soft tissue geometry, and/or in clinical settings, clinicians may apply lesser or greater varus loads based on their preference for diagnosis. But in relation to the intact and reconstructed models, the sectioned model proves the value of a stable PLC. Our computational model supports our experimental data suggesting that both the Arciero and LaPrade reconstructions are capable of restoring varus instability to the PLC equal or close to initial conditions. Our experimental data showed no statistical difference between the two reconstructions and the intact state. This is mimicked in our computational results where the greatest difference between the intact and reconstructed models is 0.101 mm of deformation at the posterolateral corner. Like our experimental results, the LaPrade technique showed slightly better outcome measures than Arciero but this is negligible due to the difference being 0.101 mm. This is achieved because the geometry of the LaPrade technique more closely resembles the orientation of the native PLC with the only difference being insertion sites of the PLT and PFL. Whereas the only similarity the Arciero and intact PLC share is the orientation of the FCL. The simulated PFL of the Arciero technique acts more like a pseudo FCL but rather it is oriented at approximately 70° and inserts at the origin of the PLT. Also the LaPrade technique uses the femur, tibia, and fibula as points of connection to stabilize the PLC whereas Arciero only uses the femur and fibula to stabilize the PLC. This analyses is limited due to our simulation being executed only at 0° of flexion, we cannot state which technique's orientation re-stabilizes the PLC without further simulations involving ER loads and at varying degrees of flexion.

6.1 Future Work

Due to the limited number of specimens, this study was underpowered and was unable to show statistical significance between the Arciero and LaPrade PLC reconstructions at any phase of the study. A larger sample size is needed for future work. Further analysis should be conducted using computational models that analyze the Arciero and LaPrade reconstructions for both ER and VA at 0°, 20°, 30°, 60°, and 90° of flexion. We hope that this thesis brings to light more understanding of the PLC and allows surgeons to select the technique they prefer based on their preference and training without concern for surgical outcomes affecting PLC stability.

Appendices

Appendix A

Early Renderings

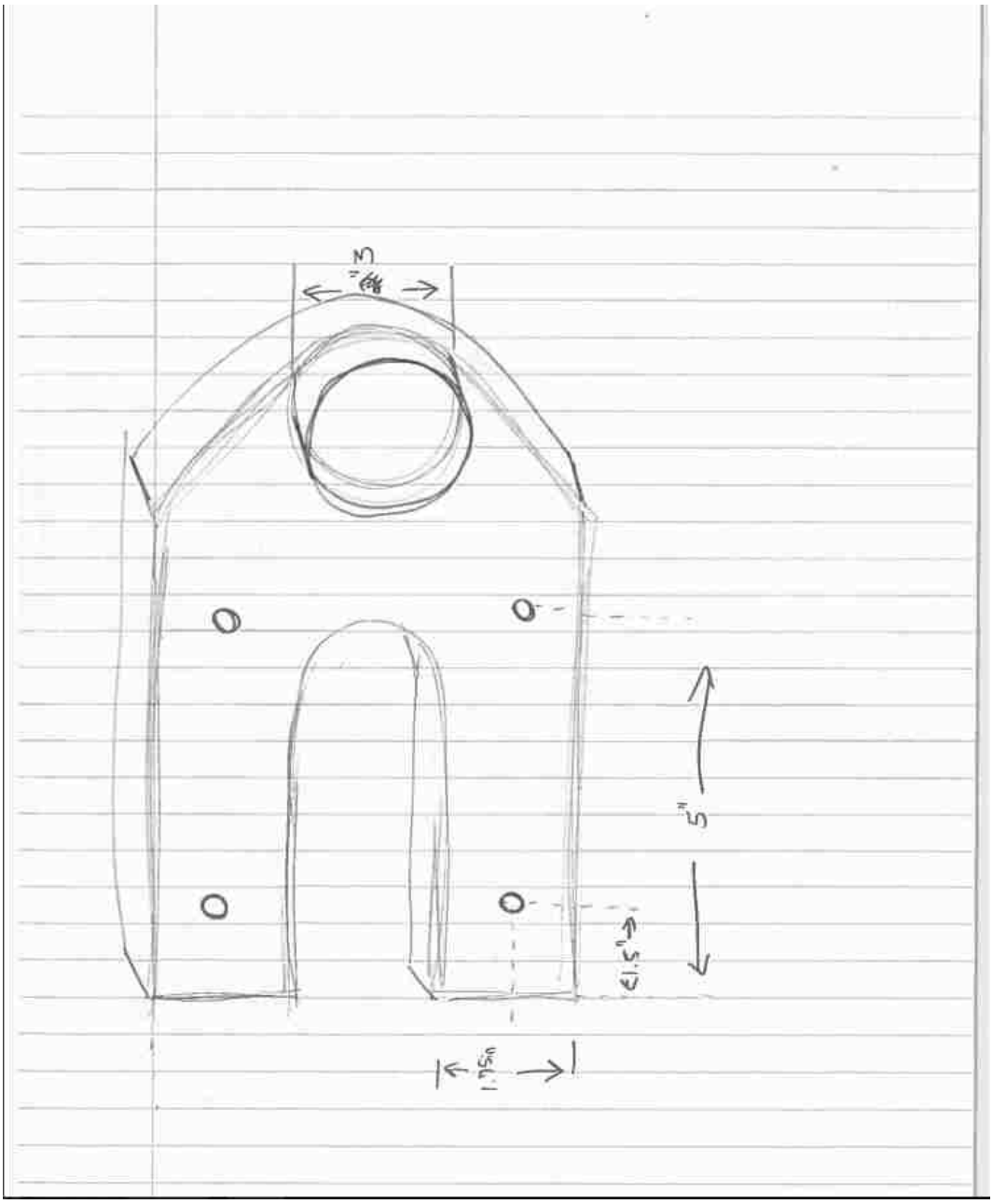

Figure A.1: Initial rendering of the dial plate

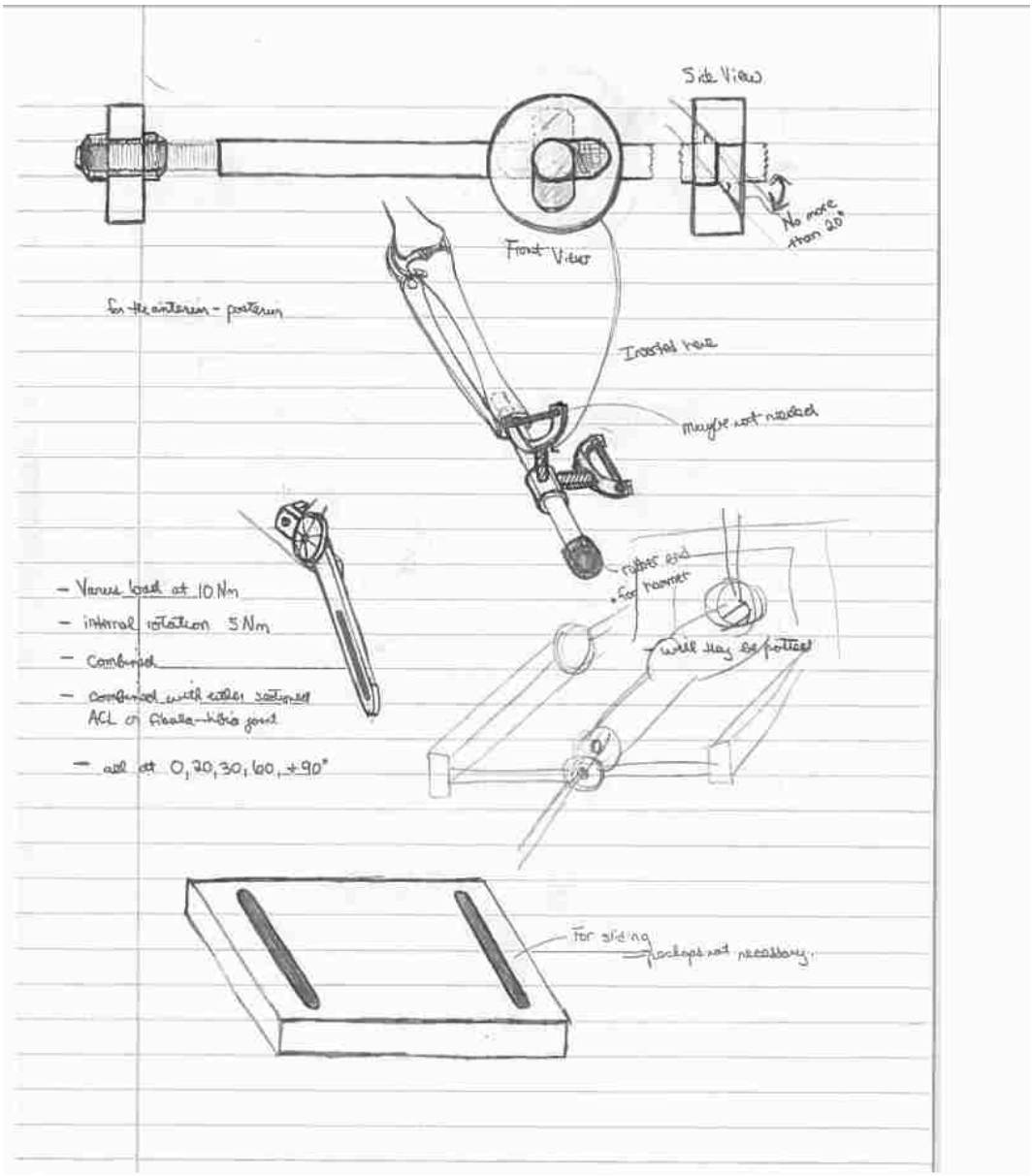

Figure A.2: Initial rendering of the end piece and fixture with the specimen mounted

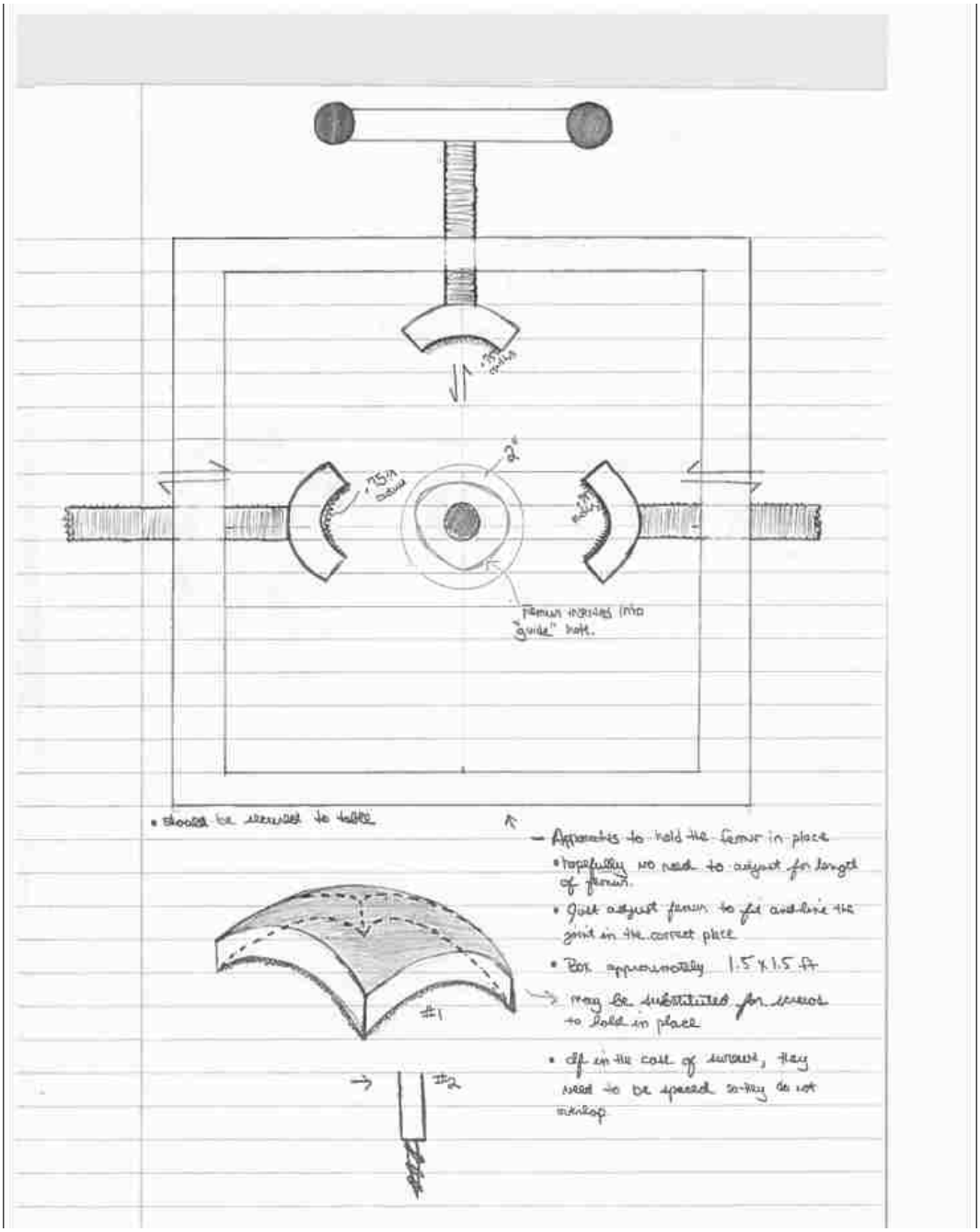

Figure A.3: Initial rendering of the mechanism that would fix the proximal femur into the testing fixture

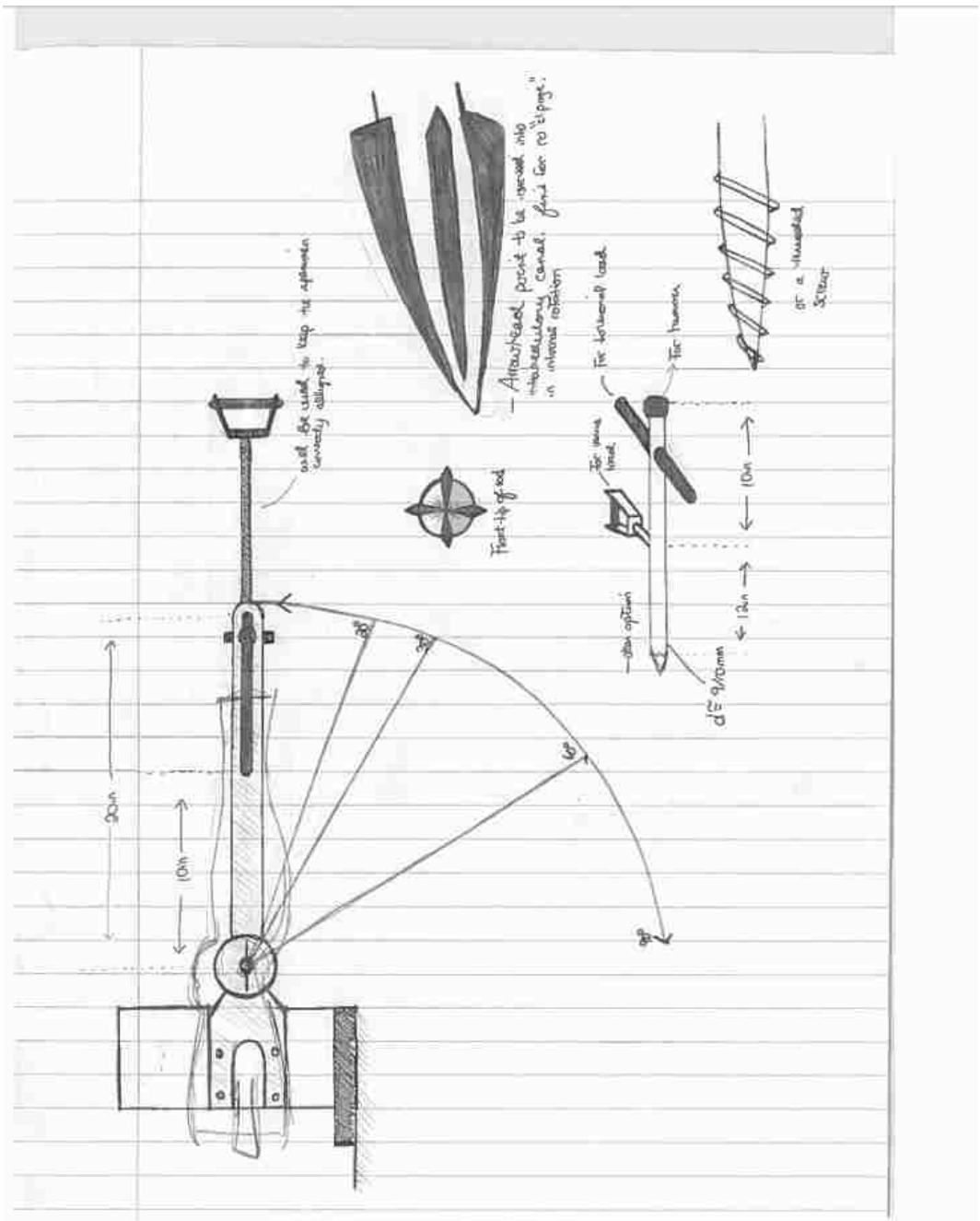

Figure A.4: Initial rendering of the rod. Also rotation about the dial plate that would allow varing degrees of flexion

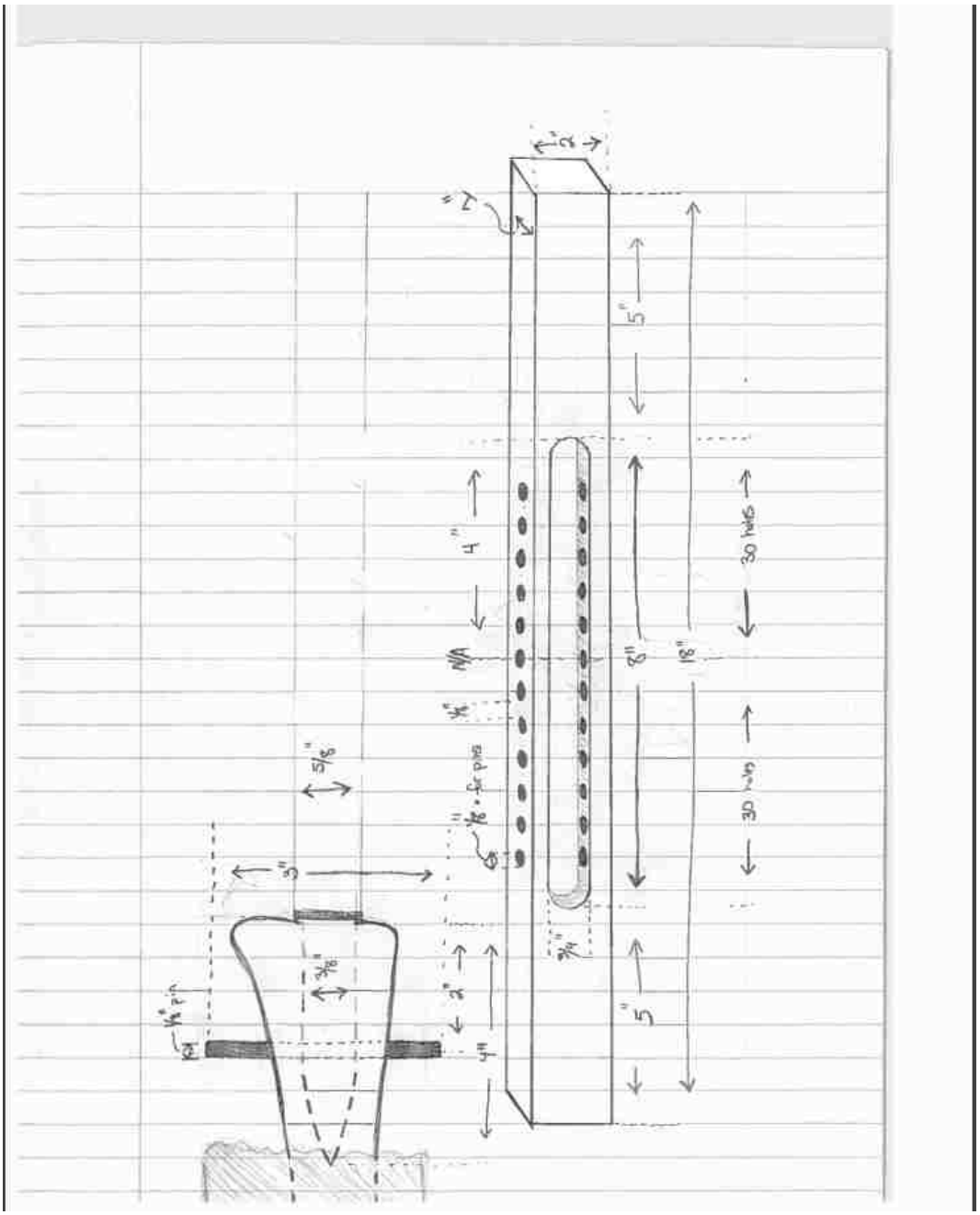

Figure A.5: Initial rendering of the end piece and fixation of the rod into the distal tibia

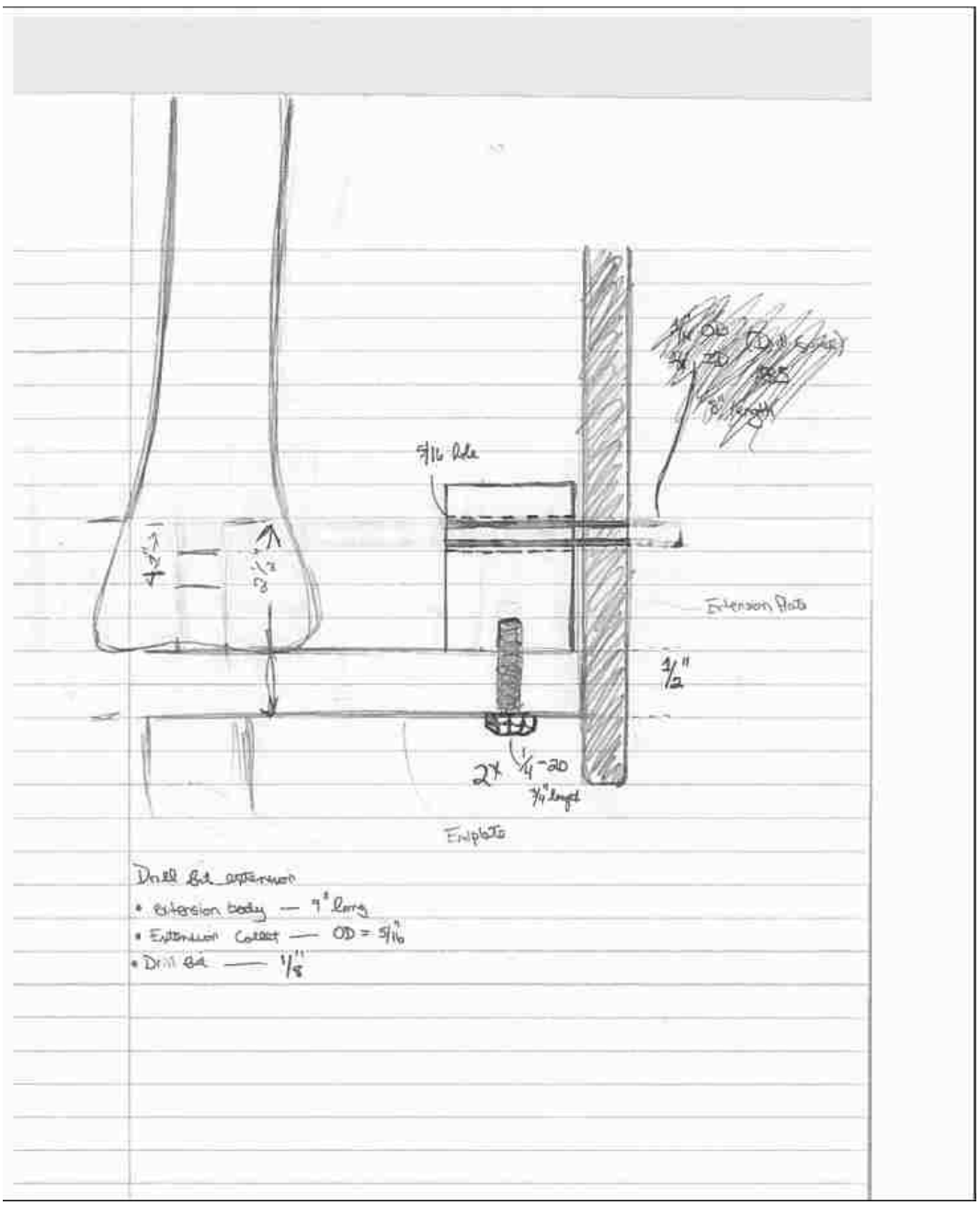

Figure A.6: Initial rendering of the distal tibia and its location relative to the end piece. Also, the idea of a drill guide being used

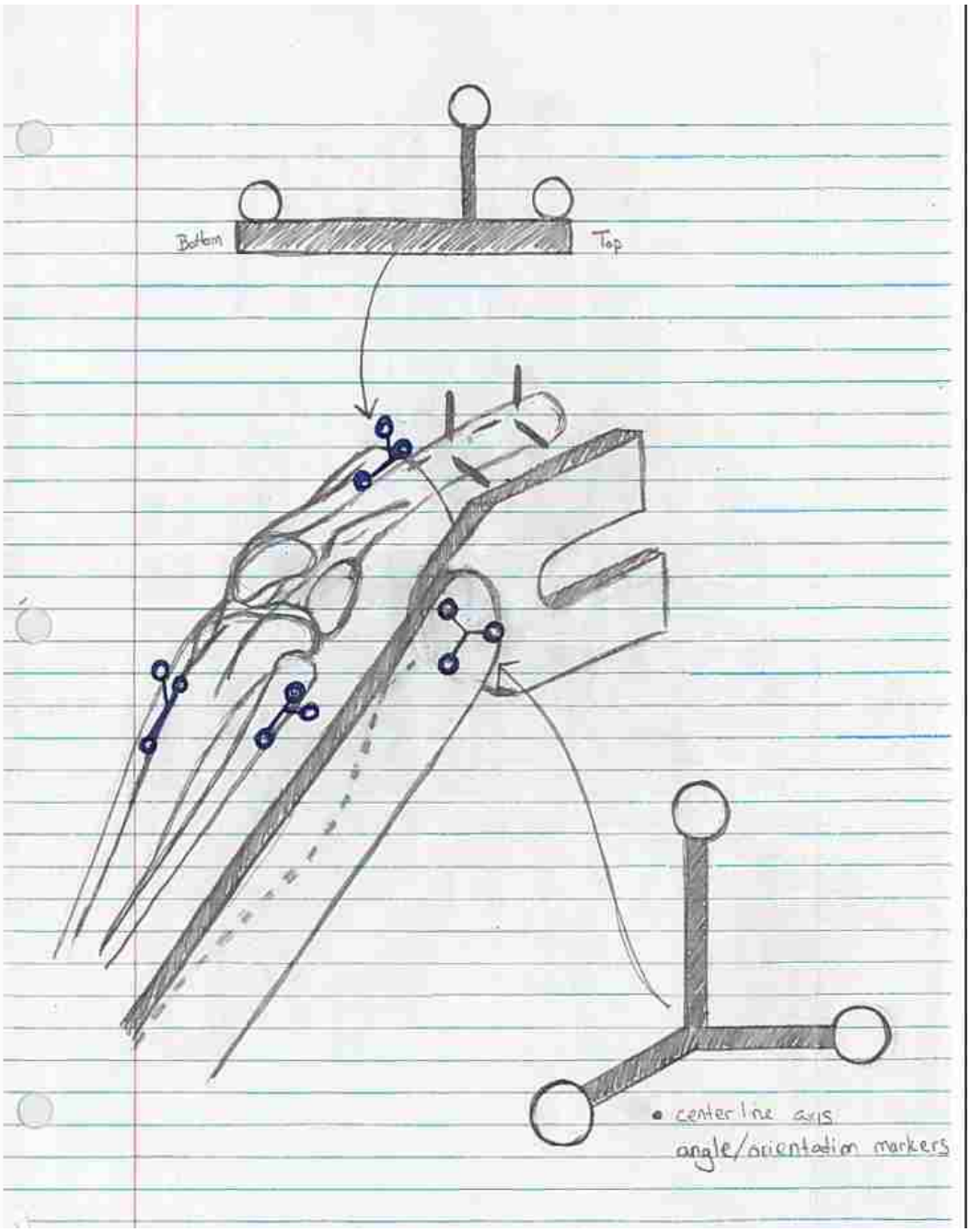

Figure A.7: Initial rendering of the marker sets and their location relative to the specimen

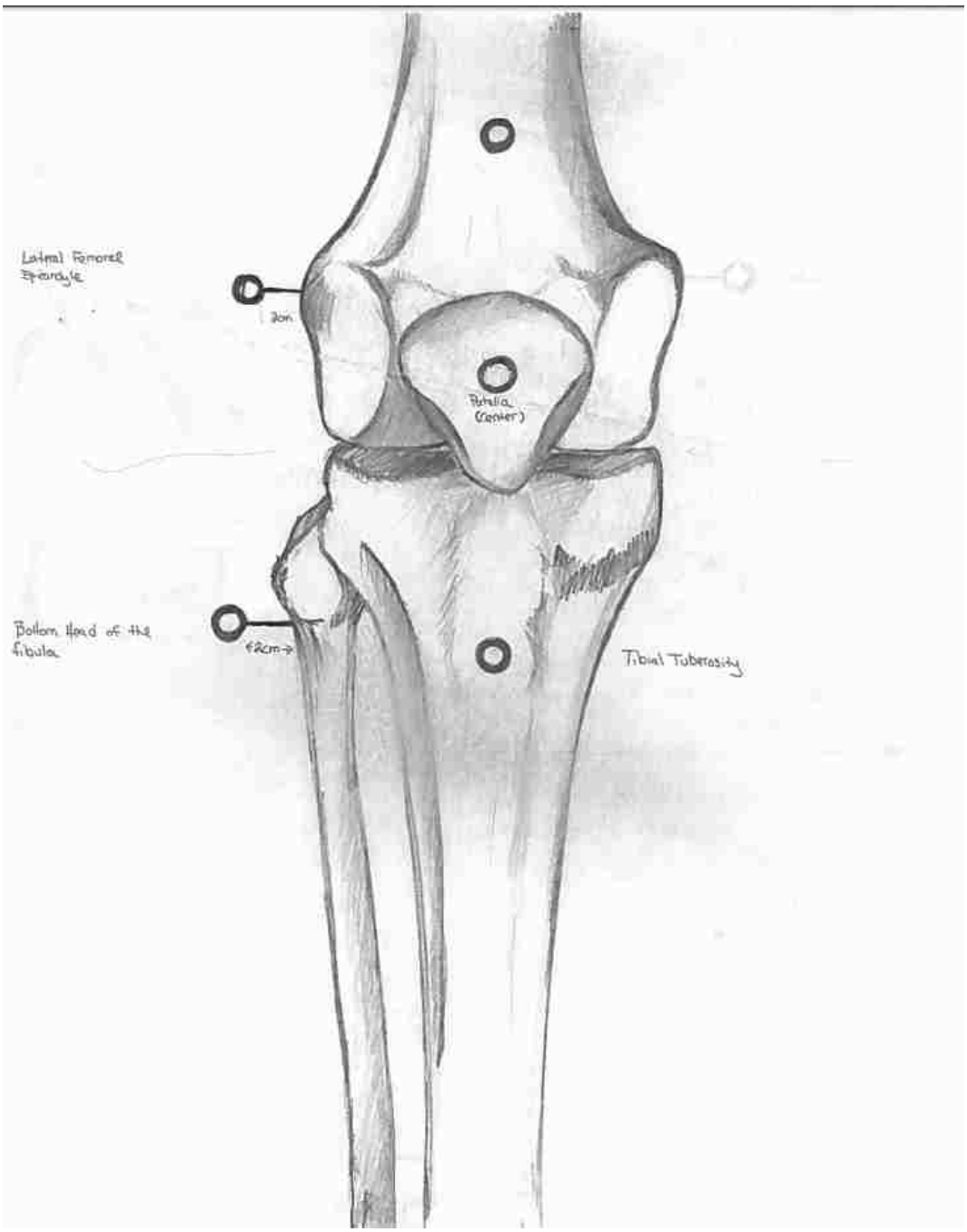

Figure A.8: Initial rendering of the anterior tibia and the locations of the marker sets

Appendix B

Computer Aided Drawings

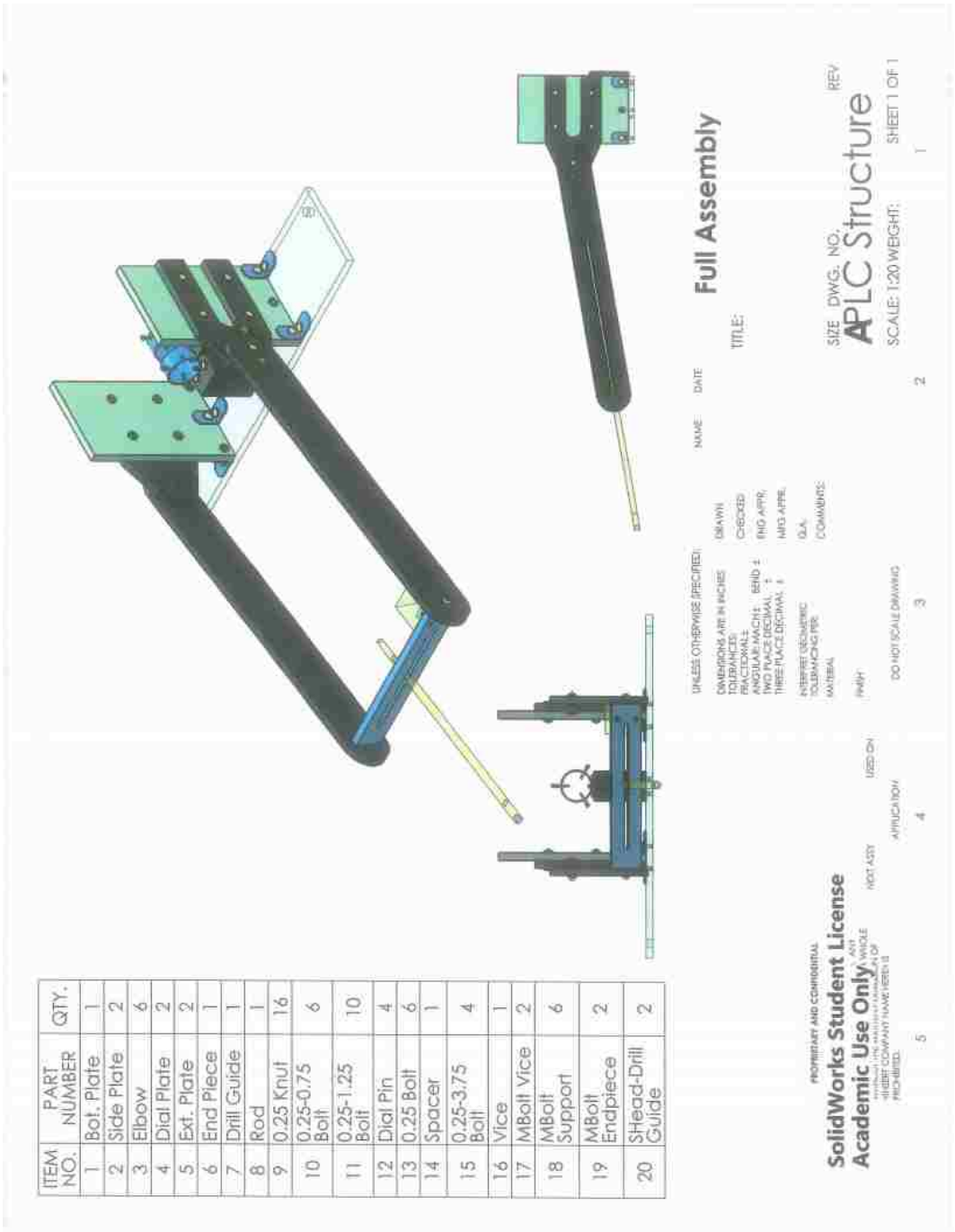

ITEM NO.	PART NUMBER	QTY.
1	Bot. Plate	1
2	Side Plate	2
3	Elbow	6
4	Dial Plate	2
5	Ext. Plate	2
6	End Piece	1
7	Drill Guide	1
8	Rod	1
9	0.25 Knut	16
10	0.25-0.75 Bolt	6
11	0.25-1.25 Bolt	10
12	Dial Pin	4
13	0.25 Bolt	6
14	Spacer	1
15	0.25-3.75 Bolt	4
16	Vice	1
17	MBolt Vice	2
18	MBolt Support	6
19	MBolt Endpiece	2
20	SHead-Drill Guide	2

Figure B.1: Drawing of the complete PLC Testing Fixture

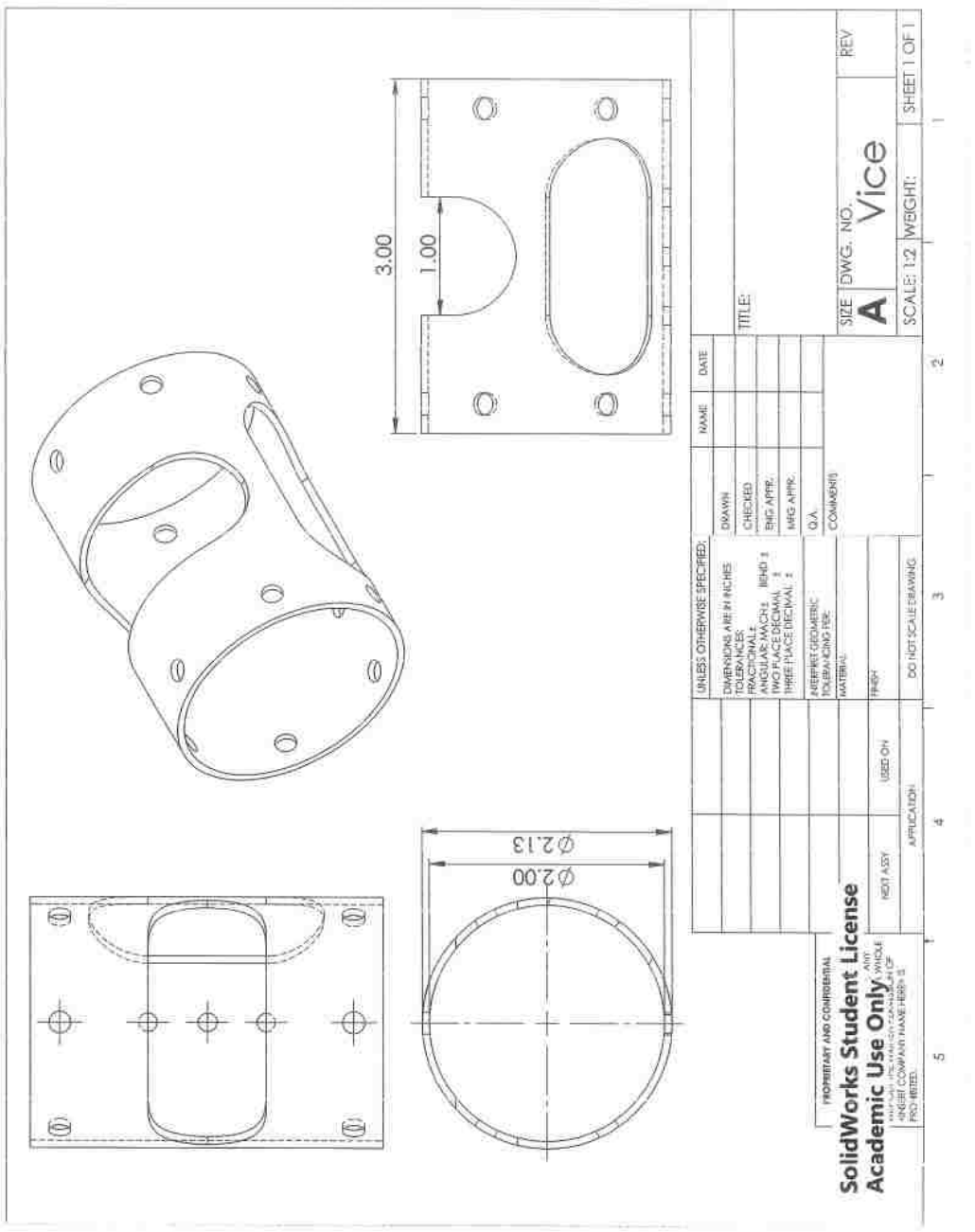

Figure B.2: Drawing of the Vice

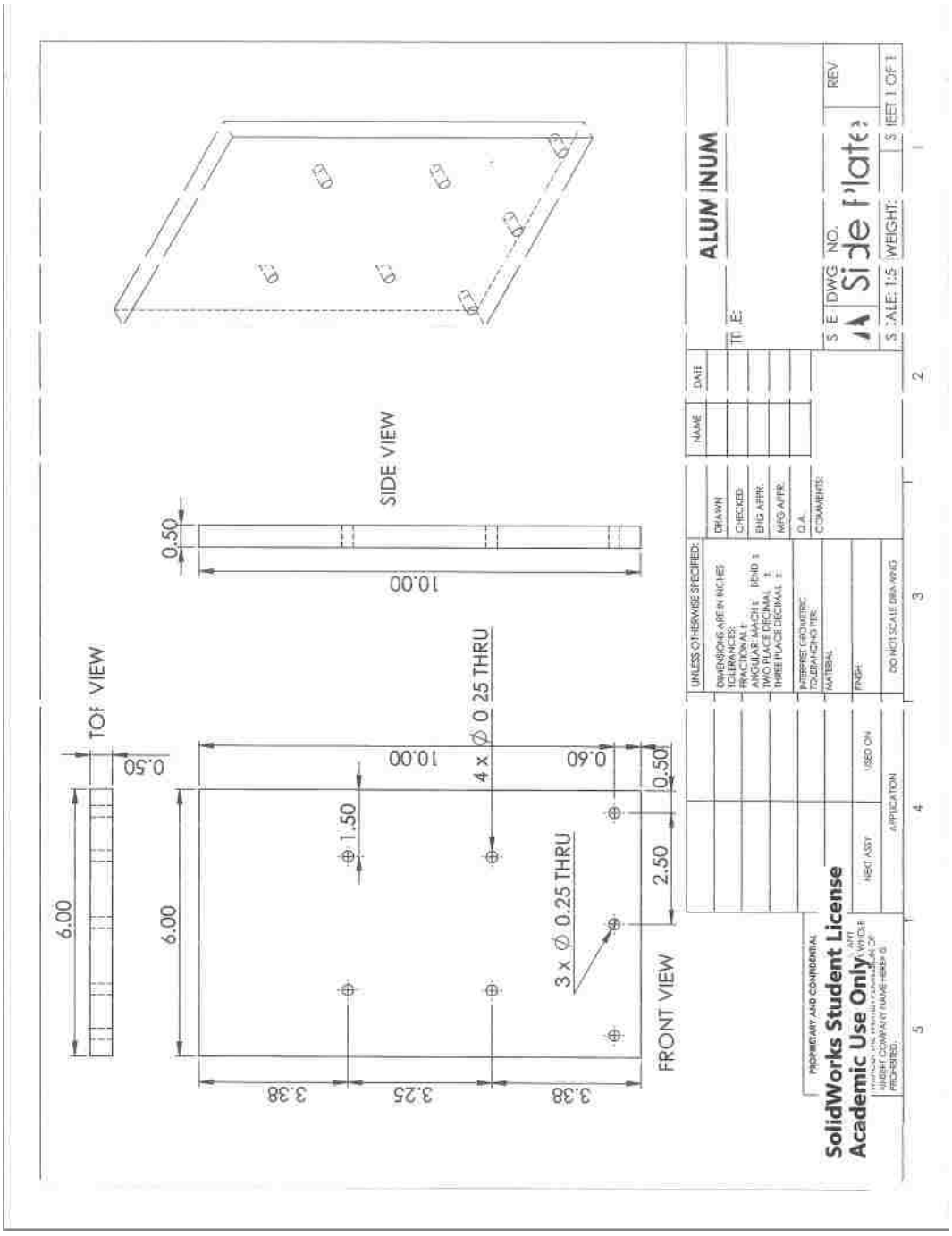

Figure B.3: Drawing of a single Side Plate

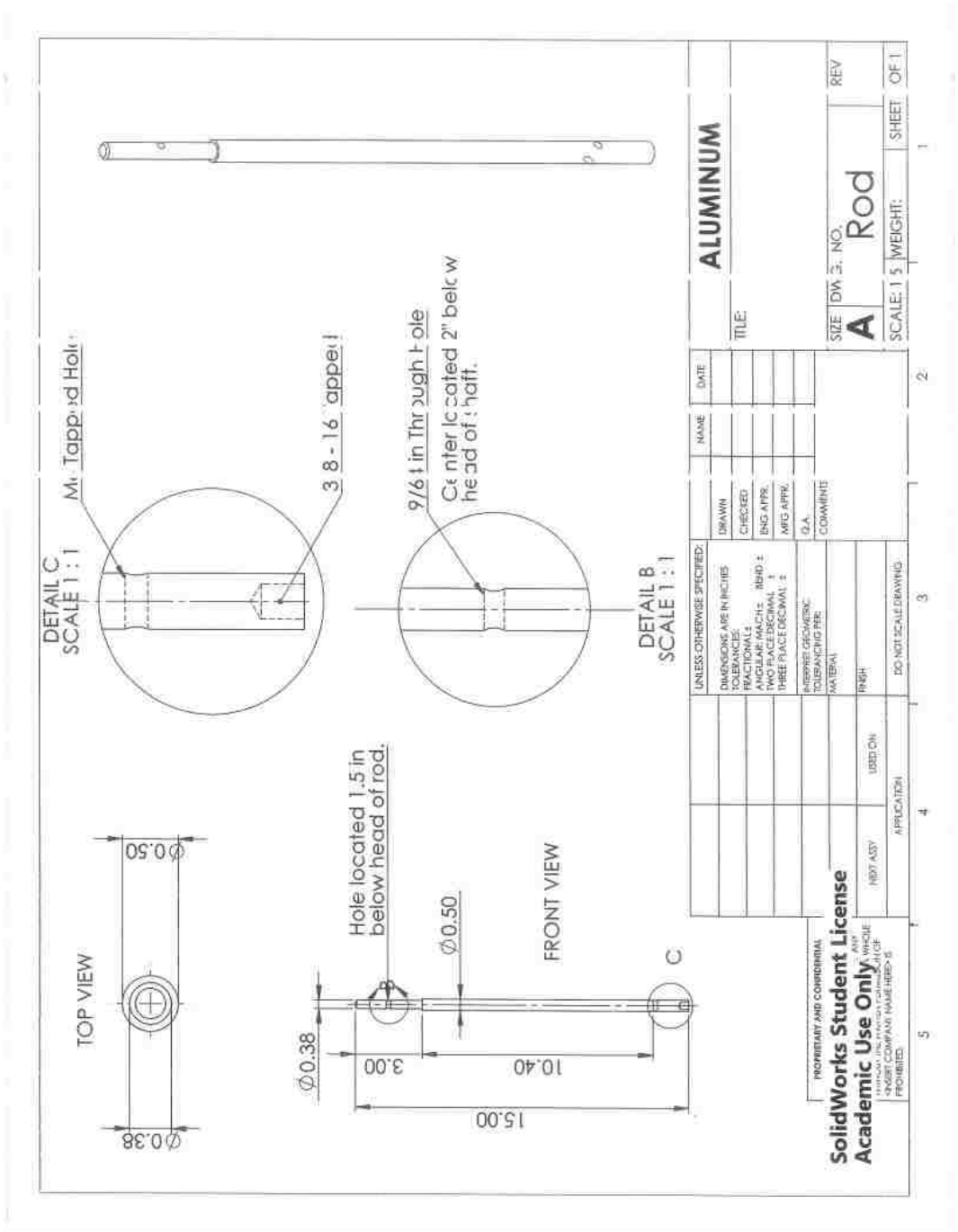

Figure B.4: Drawing of the Rod

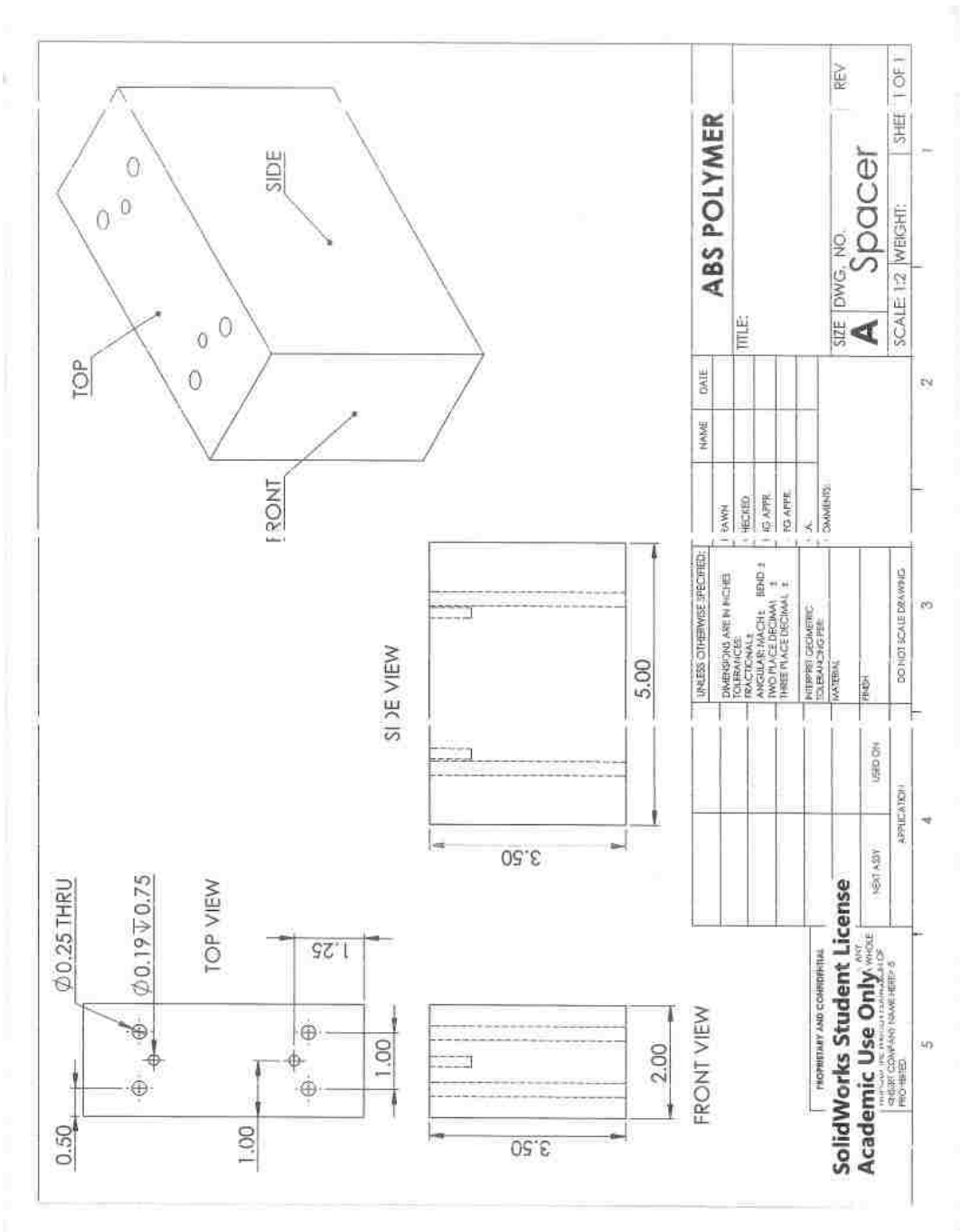

Figure B.5: Drawing of the Spacer

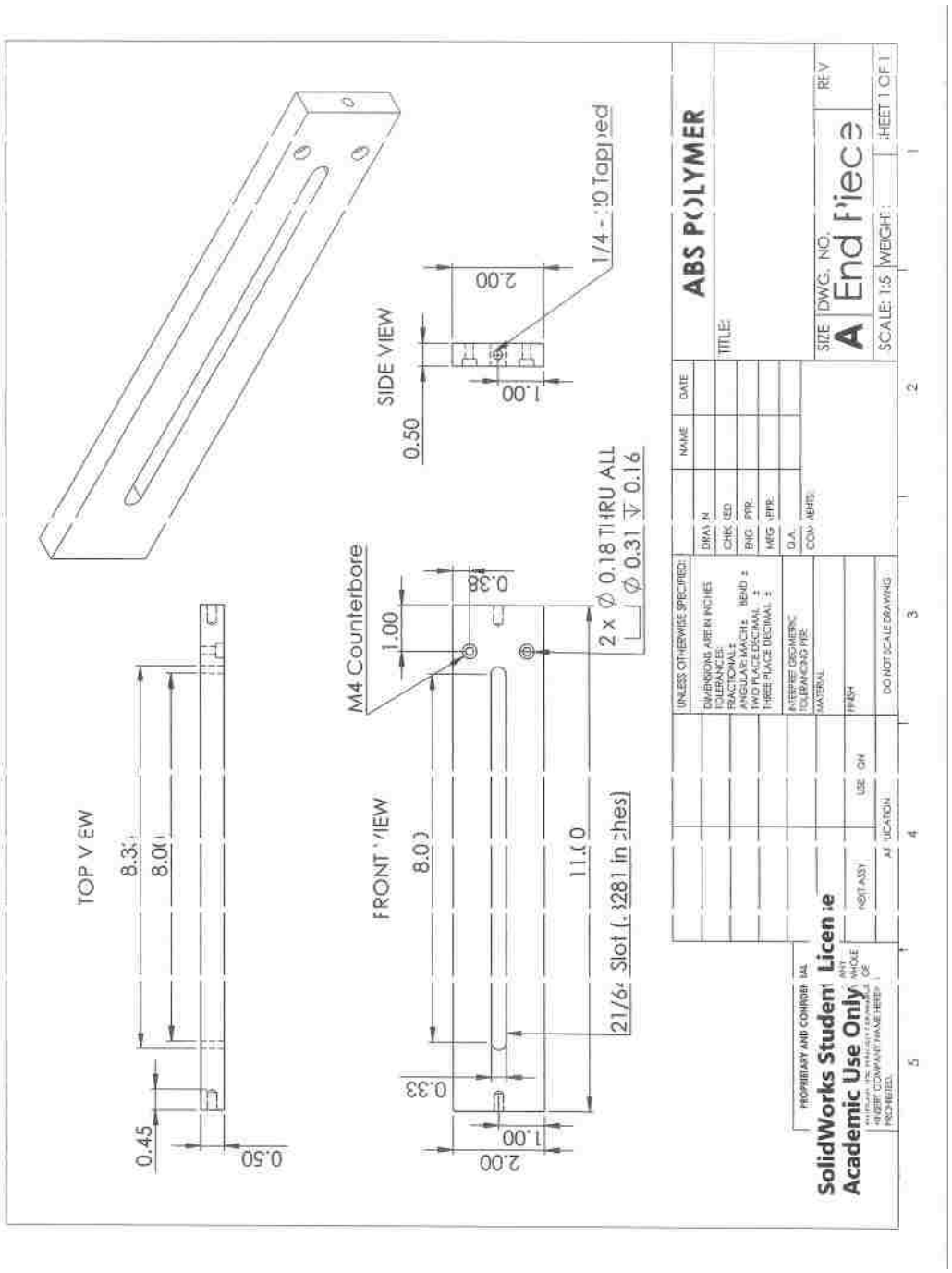

Figure B.6: Drawing of the End Piece

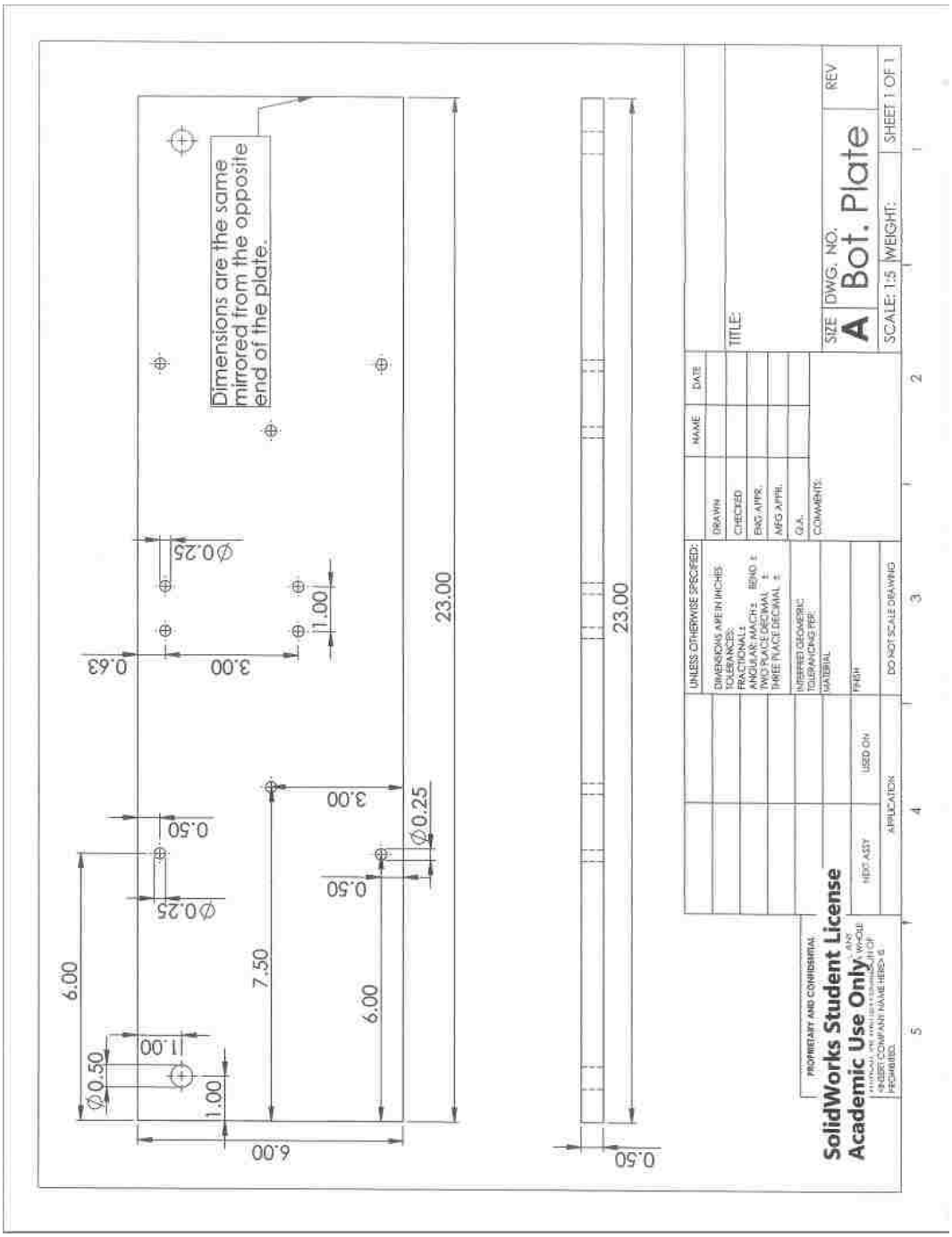

Figure B.7: Drawing of the Base Plate

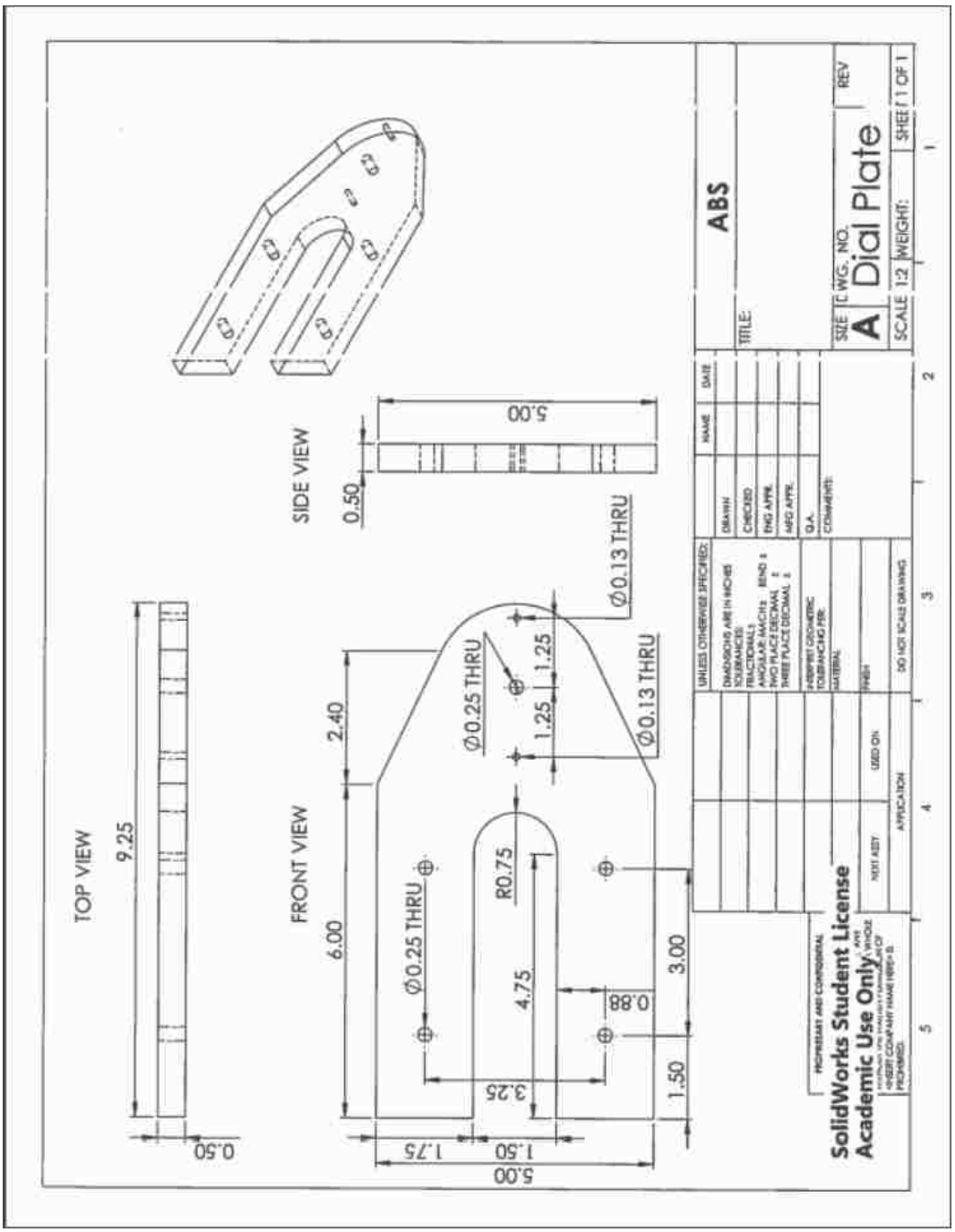

Figure B.8: Drawing of the Dial Plate

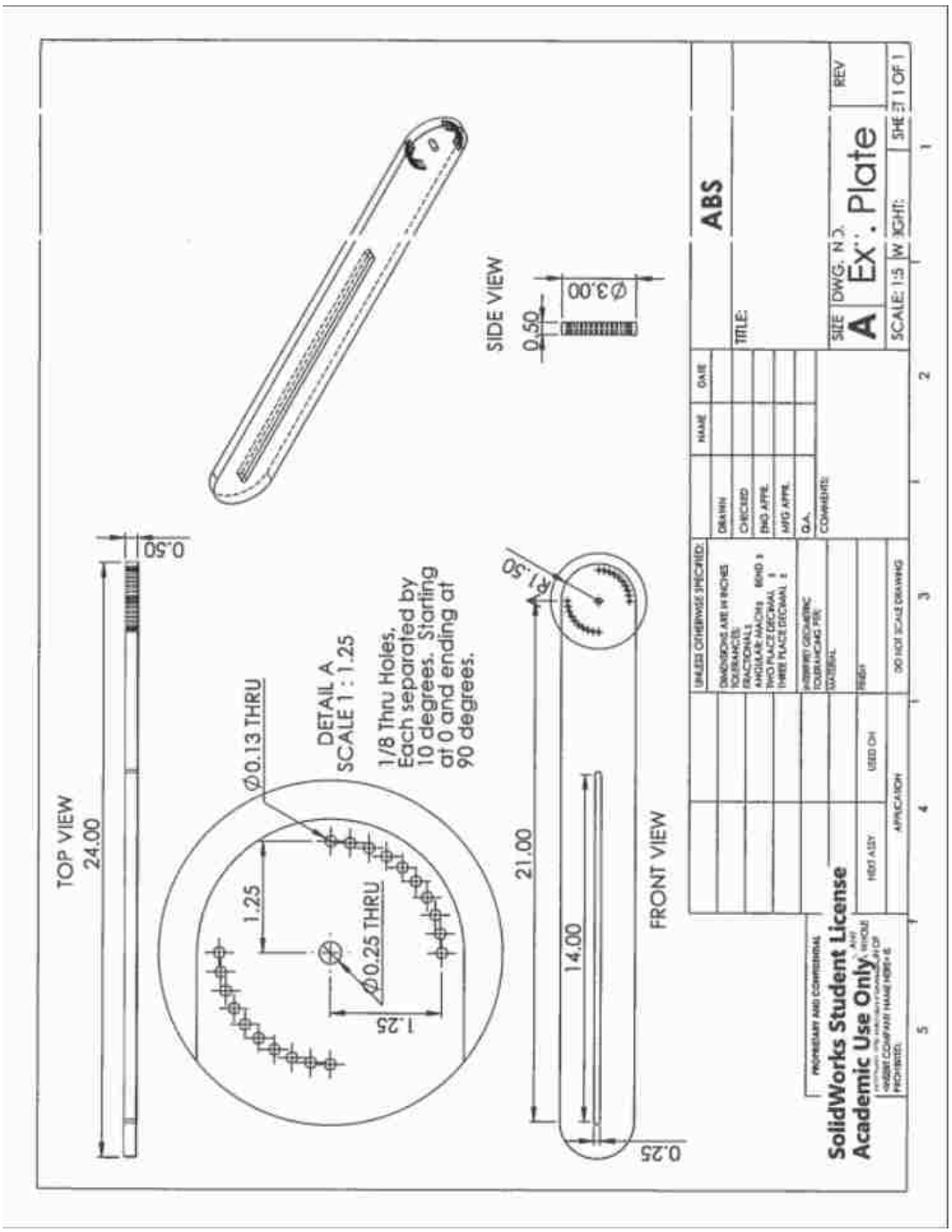

Figure B.9: Drawing of Extension Plate

Appendix C

MATLAB®code

```
% Arciero v LaPrade Posterolateral Corner Data Analysis
clc
clear

%%%%%%%%%%%%%%%%%%%%%%%%%%%%%%%%%%%%%%%%%%%%%%%%%%%%%%%%%%%%%%%%%%%%%%%%
%                      INPUT VARIABLES                                  %
%%%%%%%%%%%%%%%%%%%%%%%%%%%%%%%%%%%%%%%%%%%%%%%%%%%%%%%%%%%%%%%%%%%%%%%%

% These are the inputs for the Tibia and Origin positions in (x,y,z)
% Tibia = [Tx,Ty,Tz],  Origin = [Ox,Oy,Oz], Displaced Tibia = [TDx,TDy,TDz]
% I have kept the inputs because it takes just as much time to input the
% positions as it does to import each file that calls upon the data.  Also
% because when defining rigid bodies, if they are not defined in the same
% order for every calibration then the individual cells that it calls upon
% will be incorrect.  Also each take has differing times, prevents from
% pre-selecting an individual cell for the displaced positions.

prompt = 'Flexion Angle = ';    % This will adjust the origin maker set.
theta = input(prompt);

prompt1 = 'Initial External Rotation = ';
prompt2 = 'Final External Rotation = ';
prompt4 = 'Tx = ';
prompt5 = 'Ty = ';
prompt6 = 'Tz = ';
prompt13 = 'TDx = ';
prompt14 = 'TDy = ';
prompt15 = 'TDz = ';
prompt7 = 'Ox = ';
prompt8 = 'Oy = ';
prompt9 = 'Oz = ';

Tx = input(prompt4);
Ty = input(prompt5);
Tz = input(prompt6);
Ox = input(prompt7);
Oy = input(prompt8);
Oz = input(prompt9);

TDx = input(prompt13);
TDy = input(prompt14);
TDz = input(prompt15);

Tib = [Tx Ty Tz];    % ORIGINAL TIBIA POSITION IN GLOBAL COORDINATES
Ori = [Ox Oy Oz];    % ORIGINAL ORIGIN POSITION IN GLOBAL COORDINATES
TibD = [TDx TDy TDz];  % DISPLACED TIBIA POSITIONIN GLOBAL COORDINATES

ER = abs(input(prompt2)-input(prompt1));  % EXTERNAL ROTATION IN DEGREES

%%%%%%%%%%%%%%%%%%%%%%%%%%%%%%%%%%%%%%%%%%%%%%%%%%%%%%%%%%%%%%%%%%%%%%%%
%              DETERMINING THE FLEXION ANGLE                            %
%%%%%%%%%%%%%%%%%%%%%%%%%%%%%%%%%%%%%%%%%%%%%%%%%%%%%%%%%%%%%%%%%%%%%%%%

% This accounts for the Origin marker set not being directly in line with
```

```
% joint line.  The distance of the marker set from the joint line is known
% to equal (2 inches = 50.8 mm).  This adjusts the marker set at different
% flexion angles.

% This also accounts for the amount of translation in the y direction
% (local coordinates of the tibia marker set, not global).

if theta == 0
    Ori_N = Ori + [165.1 0 50.8];  % 0 degree flexion angle
    delY = Tib(2)-TibD(2);

    elseif theta == 20
        Ori_N = Ori + [165.1 +17.3736 47.7266];  % 20 degree flexion angle
        delY = (cos(theta)*Tib(2))-(cos(theta)*TibD(2));

    elseif theta == 30
        Ori_N = Ori + [165.1 25.4 43.99];  % 30 degree flexion angle
        delY = (cos(theta)*Tib(2))-(cos(theta)*TibD(2));

    elseif theta == 60
        Ori_N = Ori + [165.4 43.99 25.4];  % 60 degree flexion angle
        delY = (cos(theta)*Tib(2))-(cos(theta)*TibD(2));

    elseif theta == 90
        Ori_N = Ori + [165.4 50.8 0];  % 90 degree flexion angle
        delY = Tib(3)-TibD(3);

end

%%%%%%%%%%%%%%%%%%%%%%%%%%%%%%%%%%%%%%%%%%%%%%%%%%%%%%%%%%%%%%%%%%%%%%%%%%%%
%                   DETERMING NEW VECTORS                                  %
%%%%%%%%%%%%%%%%%%%%%%%%%%%%%%%%%%%%%%%%%%%%%%%%%%%%%%%%%%%%%%%%%%%%%%%%%%%%

Ori_F = Ori_N - Ori_N;           % This should make the Ori_F = [0 0 0]

TIBo = Tib - Ori_N;              % Readjusts the orignal tibia position
                                 % based on the new Origin [0 0 0]

TIBd = TibD - Ori_N;             % Readjusts the displaced tibia position
                                 % based on the new Origin [0 0 0]

%%%%%%%%%%%%%%%%%%%%%%%%%%%%%%%%%%%%%%%%%%%%%%%%%%%%%%%%%%%%%%%%%%%%%%%%%%%%
%%%%%%%%%%%%%%%%%%%%%%%%%%%%%%%%%%%%%%%%%%%%%%%%%%%%%%%%%%%%%%%%%%%%%%%%%%%%

% This determines the distance between the Origin centroid and the tibia
% centroid.  The distances are averaged in the case that for whatever
% reason should the lengths change, an average distance is calculated.
% Both distances should be very close to each other.

Distance = sqrt((Ori_F(1)-TIBo(1))^2+(Ori_F(2)-TIBo(2))^2+(Ori_F(2)-TIBo(3))^2);

delX = abs(TIBd(1)-TIBo(1));   % This is the total tranlation of the tibia
                               % marker set in the x-direction only.
```

```
%%%%%%%%%%%%%%%%%%%%%%%%%%%%%%%%%%%%%%%%%%%%%%%%%%%%%%%%%%%%%%%%%%%%%%%%
%                          VARUS ANGULATION                             %
%%%%%%%%%%%%%%%%%%%%%%%%%%%%%%%%%%%%%%%%%%%%%%%%%%%%%%%%%%%%%%%%%%%%%%%%

% This takes the absolute value of the the arc tangent between translation
% in the x direction with the known distance between the origin and tibia.

Varus_Angulation = (atan((delX-Added_X)/Distance))*180/pi          % In degrees
VA = (atan((delX)/Distance))*180/pi
```

Appendix D

Specimen Raw Data

D.1 Initial Testing

INITIAL TESTING: SPECIMEN #1 (MEANS)			
	Flexion Angle	**ER (Degrees)**	**VA (Degrees)**
LaPrade	0	6.44	4.56
	20	14.73	5.76
	30	18.79	7.44
	60	17.26	9.71
	90	16.79	8.69
Arciero	0	6.66	4.70
	20	13.07	6.41
	30	16.48	8.05
	60	17.00	10.30
	90	14.68	9.16

Table D.1: Mean paired ER and VA data for Specimen #1 at 0°, 20°, 30°, 60°, and 90° of flexion.

INITIAL TESTING: SPECIMEN #2 (MEANS)			
	Flexion Angle	**ER (Degrees)**	**VA (Degrees)**
LaPrade	0	2.10	1.95
	20	7.55	3.87
	30	15.07	4.21
	60	15.48	5.52
	90	13.00	4.17
Arciero	0	2.54	2.07
	20	8.44	3.70
	30	14.75	4.37
	60	13.46	4.17
	90	11.20	3.48

Table D.2: Mean paired ER and VA data for Specimen #2 at 0°, 20°, 30°, 60°, and 90° of flexion.

INITIAL TESTING: SPECIMEN #3 (MEANS)			
	Flexion Angle	**ER (Degrees)**	**VA (Degrees)**
LaPrade	0	4.53	2.18
	20	11.55	6.94
	30	16.99	6.21
	60	19.88	4.13
	90	17.39	3.65
Arciero	0	4.97	2.33
	20	11.38	5.26
	30	17.42	5.88
	60	20.38	4.47
	90	16.55	3.62

Table D.3: Mean paired ER and VA data for Specimen #3 at 0°, 20°, 30°, 60°, and 90° of flexion.

INITIAL TESTING: SPECIMEN #4 (MEANS)			
	Flexion Angle	**ER (Degrees)**	**VA (Degrees)**
LaPrade	0	5.51	2.86
	20	14.91	4.70
	30	15.90	4.73
	60	12.83	3.45
	90	13.07	2.68
Arciero	0	6.18	2.56
	20	12.52	4.35
	30	13.07	4.87
	60	21.98	3.59
	90	23.61	2.78

Table D.4: Mean paired ER and VA data for Specimen #4 at 0°, 20°, 30°, 60°, and 90° of flexion.

INITIAL TESTING: SPECIMEN #5 (MEANS)			
	Flexion Angle	**ER (Degrees)**	**VA (Degrees)**
LaPrade	0	5.59	3.16
	20	15.16	4.82
	30	18.26	3.81
	60	11.89	4.24
	90	16.57	4.70
Arciero	0	8.93	3.68
	20	14.74	5.64
	30	16.74	4.66
	60	21.99	4.44
	90	20.44	5.98

Table D.5: Mean paired ER and VA data for Specimen #5 at 0°, 20°, 30°, 60°, and 90° of flexion.

INITIAL TESTING: SPECIMEN #6 (MEANS)			
	Flexion Angle	**ER (Degrees)**	**VA (Degrees)**
LaPrade	0	12.21	5.56
	20	19.12	7.63
	30	16.70	9.64
	60	21.20	10.40
	90	22.89	5.91
Arciero	0	11.28	5.23
	20	18.10	7.77
	30	17.74	8.74
	60	18.69	9.80
	90	29.78	6.13

Table D.6: Mean paired ER and VA data for Specimen #6 at 0°, 20°, 30°, 60°, and 90° of flexion.

INITIAL TESTING: SPECIMEN #7 (MEANS)			
	Flexion Angle	**ER (Degrees)**	**VA (Degrees)**
LaPrade	0	6.22	9.29
	20	9.3	9.82
	30	11.37	9.57
	60	15.25	9.88
	90	23.97	6.70
Arciero	0	9.28	9.50
	20	16.76	11.52
	30	17.38	12.71
	60	19.87	8.72
	90	25.62	6.15

Table D.7: Mean paired ER and VA data for Specimen #7 at 0°, 20°, 30°, 60°, and 90° of flexion.

INITIAL TESTING: SPECIMEN #8 (MEANS)			
	Flexion Angle	**ER (Degrees)**	**VA (Degrees)**
LaPrade	0	13.51	13.59
	20	15.35	18.37
	30	18.62	12.36
	60	18.17	15.68
	90	18.69	9.74
Arciero	0	10.88	11.48
	20	15.89	11.59
	30	17.48	13.14
	60	25.06	15.54
	90	37.84	7.86

Table D.8: Mean paired ER and VA data for Specimen #8 at 0°, 20°, 30°, 60°, and 90° of flexion.

INITIAL TESTING: SPECIMEN #9 (MEANS)			
	Flexion Angle	**ER (Degrees)**	**VA (Degrees)**
LaPrade	0	7.94	7.07
	20	13.32	8.95
	30	12.93	12.44
	60	12.67	14.50
	90	12.08	12.29
Arciero	0	7.91	7.37
	20	13.97	8.42
	30	13.28	13.51
	60	15.44	13.20
	90	15.17	13.86

Table D.9: Mean paired ER and VA data for Specimen #9 at 0°, 20°, 30°, 60°, and 90° of flexion.

D.2 Post Sectioning

POST SECTIONING: SPECIMEN#2 (MEANS)			
	Flexion Angle	**ER (Degrees)**	**VA (Degrees)**
LaPrade	0	7.20	5.68
	20	24.71	6.52
	30	25.51	6.79
	60	21.38	7.29
	90	15.44	6.58
Arciero	0	7.69	5.60
	20	22.32	6.42
	30	24.00	7.05
	60	20.91	7.16
	90	14.75	6.60

Table D.10: Mean paired post sectioning ER and VA data for Specimen #2 at 0°, 20°, 30°, 60°, and 90° of flexion.

POST SECTIONING: SPECIMEN#3 (MEANS)			
	Flexion Angle	**ER (Degrees)**	**VA (Degrees)**
LaPrade	0	18.09	5.64
	20	22.91	8.35
	30	25.25	7.83
	60	28.80	9.30
	90	23.87	7.11
Arciero	0	14.66	5.12
	20	24.34	7.68
	30	23.93	8.50
	60	28.73	9.95
	90	25.56	8.22

Table D.11: Mean paired post sectioning ER and VA data for Specimen #3 at 0°, 20°, 30°, 60°, and 90° of flexion.

POST SECTIONING: SPECIMEN#4 (MEANS)			
	Flexion Angle	**ER (Degrees)**	**VA (Degrees)**
LaPrade	0	7.69	6.10
	20	22.51	9.14
	30	45.52	7.55
	60	45.17	6.20
	90	32.13	5.57
Arciero	0	7.88	4.96
	20	15.94	8.88
	30	20.49	7.81
	60	27.66	6.22
	90	25.46	4.95

Table D.12: Mean paired post sectioning ER and VA data for Specimen #4 at 0°, 20°, 30°, 60°, and 90° of flexion.

POST SECTIONING: SPECIMEN#5 (MEANS)			
	Flexion Angle	**ER (Degrees)**	**VA (Degrees)**
LaPrade	0	7.26	6.34
	20	21.30	6.05
	30	23.58	5.82
	60	24.58	5.51
	90	43.36	7.82
Arciero	0	10.25	6.71
	20	18.38	6.98
	30	29.41	5.94
	60	35.33	6.35
	90	24.96	10.99

Table D.13: Mean paired post sectioning ER and VA data for Specimen #5 at 0°, 20°, 30°, 60°, and 90° of flexion.

POST SECTIONING: SPECIMEN#6 (MEANS)			
	Flexion Angle	**ER (Degrees)**	**VA (Degrees)**
LaPrade	0	15.05	9.73
	20	26.64	14.70
	30	32.73	15.76
	60	34.09	13.76
	90	36.07	7.06
Arciero	0	17.16	8.83
	20	27.61	14.48
	30	27.97	14.21
	60	31.41	12.70
	90	40.40	7.16

Table D.14: Mean paired post sectioning ER and VA data for Specimen #6 at 0°, 20°, 30°, 60°, and 90° of flexion.

POST SECTIONING: SPECIMEN#7 (MEANS)			
	Flexion Angle	**ER (Degrees)**	**VA (Degrees)**
LaPrade	0	12.89	12.08
	20	21.44	14.95
	30	21.07	14.22
	60	30.02	13.60
	90	32.78	11.88
Arciero	0	12.14	12.47
	20	20.12	15.61
	30	35.94	14.97
	60	41.91	13.86
	90	40.62	11.80

Table D.15: Mean paired post sectioning ER and VA data for Specimen #7 at 0°, 20°, 30°, 60°, and 90° of flexion.

POST SECTIONING: SPECIMEN#8 (MEANS)			
	Flexion Angle	**ER (Degrees)**	**VA (Degrees)**
LaPrade	0	27.45	17.75
	20	23.61	20.67
	30	30.82	16.73
	60	36.24	17.60
	90	37.40	12.85
Arciero	0	15.81	12.91
	20	24.84	14.43
	30	32.06	14.75
	60	43.11	15.93
	90	50.30	11.24

Table D.16: Mean paired post sectioning ER and VA data for Specimen #8 at 0°, 20°, 30°, 60°, and 90° of flexion.

POST SECTIONING: SPECIMEN#9 (MEANS)			
	Flexion Angle	**ER (Degrees)**	**VA (Degrees)**
LaPrade	0	10.11	14.76
	20	13.06	28.81
	30	16.97	22.10
	60	21.17	23.19
	90	12.79	19.13
Arciero	0	12.51	15.82
	20	13.43	28.66
	30	15.80	28.43
	60	21.75	24.27
	90	24.24	21.26

Table D.17: Mean paired post sectioning ER and VA data for Specimen #9 at 0°, 20°, 30°, 60°, and 90° of flexion.

D.3 Post Reconstruction

POST RECONSTRUCTION: SPECIMEN #2 (MEANS)			
	Flexion Angle	**ER (Degrees)**	**VA (Degrees)**
LaPrade	0	4.68	1.95
	20	13.34	2.84
	30	12.73	5.68
	60	14.77	3.50
	90	12.06	2.80
Arciero	0	6.06	2.19
	20	10.21	3.25
	30	14.33	5.24
	60	12.60	4.02
	90	13.33	3.62

Table D.18: Mean paired post reconstruction ER and VA data for Specimen #2 at 0°, 20°, 30°, 60°, and 90° of flexion.

POST RECONSTRUCTION: SPECIMEN#3 (MEANS)			
	Flexion Angle	**ER (Degrees)**	**VA (Degrees)**
LaPrade	0	3.92	2.32
	20	7.56	3.57
	30	8.42	5.36
	60	14.10	4.30
	90	16.53	2.54
Arciero	0	2.48	2.37
	20	11.37	4.56
	30	17.66	6.12
	60	17.99	4.61
	90	12.02	4.14

Table D.19: Mean paired post reconstruction ER and VA data for Specimen #3 at 0°, 20°, 30°, 60°, and 90° of flexion.

POST RECONSTRUCTION: SPECIMEN#4 (MEANS)			
	Flexion Angle	**ER (Degrees)**	**VA (Degrees)**
LaPrade	0	8.97	2.56
	20	17.92	4.36
	30	23.91	3.85
	60	27.34	3.43
	90	19.96	2.56
Arciero	0	7.35	3.14
	20	15.18	4.60
	30	16.41	4.10
	60	19.28	3.62
	90	16.38	2.85

Table D.20: Mean paired post reconstruction ER and VA data for Specimen #4 at 0°, 20°, 30°, 60°, and 90° of flexion.

POST RECONSTRUCTION: SPECIMEN#5 (MEANS)			
	Flexion Angle	**ER (Degrees)**	**VA (Degrees)**
LaPrade	0	4.94	2.62
	20	17.54	4.11
	30	17.12	3.65
	60	23.36	3.79
	90	23.91	2.75
Arciero	0	8.28	3.43
	20	15.70	5.50
	30	16.21	3.63
	60	18.16	4.53
	90	20.11	4.50

Table D.21: Mean paired post reconstruction ER and VA data for Specimen #5 at 0°, 20°, 30°, 60°, and 90° of flexion.

POST RECONSTRUCTION: SPECIMEN#6 (MEANS)			
	Flexion Angle	**ER (Degrees)**	**VA (Degrees)**
LaPrade	0	11.13	5.03
	20	16.15	10.21
	30	19.03	9.59
	60	25.88	6.30
	90	25.35	5.38
Arciero	0	11.81	5.00
	20	20.38	11.01
	30	19.04	9.65
	60	21.89	5.10
	90	33.04	5.03

Table D.22: Mean paired post reconstruction ER and VA data for Specimen #6 at 0°, 20°, 30°, 60°, and 90° of flexion.

POST RECONSTRUCTION: SPECIMEN#7 (MEANS)			
	Flexion Angle	**ER (Degrees)**	**VA (Degrees)**
LaPrade	0	8.42	4.12
	20	20.73	9.34
	30	16.25	10.93
	60	20.55	10.85
	90	21.78	8.96
Arciero	0	10.26	4.89
	20	17.67	10.45
	30	20.65	11.97
	60	23.64	12.25
	90	31.17	8.75

Table D.23: Mean paired post reconstruction ER and VA data for Specimen #7 at 0°, 20°, 30°, 60°, and 90° of flexion.

POST RECONSTRUCTION: SPECIMEN#8 (MEANS)			
	Flexion Angle	**ER (Degrees)**	**VA (Degrees)**
LaPrade	0	12.90	7.23
	20	17.75	9.88
	30	20.59	7.09
	60	25.00	7.97
	90	25.95	5.46
Arciero	0	12.39	8.01
	20	25.90	11.29
	30	28.55	10.42
	60	30.55	10.31
	90	35.28	6.44

Table D.24: Mean paired post reconstruction ER and VA data for Specimen #8 at 0°, 20°, 30°, 60°, and 90° of flexion.

POST RECONSTRUCTION: SPECIMEN#9 (MEANS)			
	Flexion Angle	**ER (Degrees)**	**VA (Degrees)**
LaPrade	0	6.15	12.65
	20	14.56	18.76
	30	14.82	24.74
	60	13.62	18.08
	90	13.35	18.51
Arciero	0	5.27	12.61
	20	13.36	19.66
	30	14.54	19.48
	60	19.24	25.15
	90	16.34	21.65

Table D.25: Mean paired post reconstruction ER and VA data for Specimen #9 at 0°, 20°, 30°, 60°, and 90° of flexion.

D.4 POST TIB-FIB SECTIONING

POST TIB-FIB SECTIONING: SPECIMEN#6 (MEANS)			
	Flexion Angle	**ER (Degrees)**	**VA (Degrees)**
LaPrade	0	15.15	6.00
	20	30.57	10.98
	30	33.71	10.70
	60	35.59	6.75
	90	27.88	5.40
Arciero	0	13.54	8.03
	20	34.42	15.80
	30	38.89	13.21
	60	22.42	5.72
	90	30.97	6.21

Table D.26: Mean paired post tib-fib sectioning ER and VA data for Specimen #6 at 0°, 20°, 30°, 60°, and 90° of flexion.

POST TIB-FIB SECTIONING: SPECIMEN#7 (MEANS)			
	Flexion Angle	**ER (Degrees)**	**VA (Degrees)**
LaPrade	0	9.50	5.45
	20	25.84	10.86
	30	20.65	13.56
	60	23.25	11.41
	90	21.33	8.43
Arciero	0	9.90	7.09
	20	18.44	11.69
	30	23.15	14.94
	60	30.47	14.35
	90	36.08	10.44

Table D.27: Mean paired post tib-fib sectioning ER and VA data for Specimen #7 at 0°, 20°, 30°, 60°, and 90° of flexion.

POST TIB-FIB SECTIONING: SPECIMEN#8 (MEANS)			
	Flexion Angle	**ER (Degrees)**	**VA (Degrees)**
LaPrade	0	13.50	8.46
	20	20.50	11.71
	30	22.05	10.29
	60	29.19	8.63
	90	26.22	6.01
Arciero	0	18.76	9.27
	20	23.15	12.93
	30	24.53	14.40
	60	28.17	10.23
	90	32.90	9.65

Table D.28: Mean paired post tib-fib sectioning ER and VA data for Specimen #8 at 0°, 20°, 30°, 60°, and 90° of flexion.

D.5 POST ACL SECTIONING

POST ACL SECTIONING: SPECIMEN#2 (MEANS)			
	Flexion Angle	**ER (Degrees)**	**VA (Degrees)**
LaPrade	0	5.58	2.65
	20	12.75	3.89
	30	12.48	5.57
	60	15.29	4.17
	90	13.57	3.40
Arciero	0	6.34	2.88
	20	14.42	3.41
	30	18.35	6.63
	60	17.64	4.67
	90	14.98	3.73

Table D.29: Mean paired post ACL sectioning ER and VA data for Specimen #2 at 0°, 20°, 30°, 60°, and 90° of flexion.

POST ACL SECTIONING: SPECIMEN#3 (MEANS)			
	Flexion Angle	**ER (Degrees)**	**VA (Degrees)**
LaPrade	0	5.22	2.71
	20	8.63	5.16
	30	12.59	5.65
	60	15.01	5.93
	90	16.48	3.18
Arciero	0	11.03	3.16
	20	12.00	4.90
	30	22.42	7.03
	60	22.45	6.31
	90	15.23	4.53

Table D.30: Mean paired post ACL sectioning ER and VA data for Specimen #3 at 0°, 20°, 30°, 60°, and 90° of flexion.

POST ACL SECTIONING: SPECIMEN#4 (MEANS)			
	Flexion Angle	**ER (Degrees)**	**VA (Degrees)**
LaPrade	0	11.51	3.34
	20	22.41	4.45
	30	20.62	5.05
	60	23.11	3.97
	90	24.46	3.30
Arciero	0	11.08	4.90
	20	13.00	5.71
	30	21.25	5.53
	60	21.01	4.79
	90	17.86	4.25

Table D.31: Mean paired post ACL sectioning ER and VA data for Specimen #4 at 0°, 20°, 30°, 60°, and 90° of flexion.

D.6 PAIRED SPECIMEN COMPARISON

D.6.1 Post Reconstruction Paired Comparison

POST RECONSTRUCTION SPECIMEN #2			
	Flexion Angle	**% Recovered ER**	**% Recovered VA**
LaPrade	0	49.36	99.91
	20	65.75	134.47
	30	122.40	42.88
	60	112.05	214.31
	90	138.81	151.00
Arciero	0	35.02	96.41
	20	87.27	116.81
	30	104.54	67.50
	60	111.49	105.01
	90	39.85	95.62

Table D.32: Mean post reconstruction paired specimen comparison for Specimen #2 at 0°, 20°, 30°, 60°, and 90° of flexion.

POST RECONSTRUCTION SPECIMEN #3			
	Flexion Angle	**% Recovered ER**	**% Recovered VA**
LaPrade	0	104.50	95.77
	20	135.12	340.14
	30	203.58	152.88
	60	164.80	96.77
	90	113.16	131.89
Arciero	0	125.75	98.45
	20	100.04	128.97
	30	96.22	90.72
	60	128.70	97.51
	90	150.31	88.69

Table D.33: Mean post reconstruction paired specimen comparison for Specimen #3 at 0°, 20°, 30°, 60°, and 90° of flexion.

POST RECONSTRUCTION SPECIMEN #4			
	Flexion Angle	**% Recovered ER**	**% Recovered VA**
LaPrade	0	-58.74	109.47
	20	60.38	107.79
	30	72.95	131.40
	60	55.12	100.85
	90	63.88	101.32
Arciero	0	30.84	75.85
	20	22.14	94.52
	30	54.99	126.05
	60	147.61	98.91
	90	490.33	97.07

Table D.34: Mean post reconstruction paired specimen comparison for Specimen #4 at 0°, 20°, 30°, 60°, and 90° of flexion.

POST RECONSTRUCTION SPECIMEN #5			
	Flexion Angle	**% Recovered ER**	**% Recovered VA**
LaPrade	0	176.61	116.85
	20	61.28	158.40
	30	121.48	108.00
	60	9.59	136.22
	90	72.60	162.42
Arciero	0	149.29	108.39
	20	73.59	110.39
	30	104.21	180.98
	60	128.72	95.24
	90	107.39	129.73

Table D.35: Mean post reconstruction paired specimen comparison for Specimen #5 at 0°, 20°, 30°, 60°, and 90° of flexion.

POST RECONSTRUCTION SPECIMEN #6			
	Flexion Angle	**% Recovered ER**	**% Recovered VA**
LaPrade	0	138.14	112.84
	20	139.43	63.52
	30	85.48	100.82
	60	63.72	222.12
	90	81.32	147.08
Arciero	0	91.01	106.45
	20	76.09	51.70
	30	87.30	83.31
	60	74.83	262.14
	90	69.23	206.45

Table D.36: Mean post reconstruction paired specimen comparison for Specimen #6 at 0°, 20°, 30°, 60°, and 90° of flexion.

POST RECONSTRUCTION SPECIMEN #7			
	Flexion Angle	**% Recovered ER**	**% Recovered VA**
LaPrade	0	67.07	285.87
	20	5.87	109.43
	30	49.77	70.70
	60	64.11	73.99
	90	124.88	56.40
Arciero	0	65.79	255.12
	20	72.78	126.23
	30	82.39	132.92
	60	82.91	31.28
	90	62.99	54.09

Table D.37: Mean post reconstruction paired specimen comparison for Specimen #7 at 0°, 20°, 30°, 60°, and 90° of flexion.

POST RECONSTRUCTION SPECIMEN #8			
	Flexion Angle	**% Recovered ER**	**% Recovered VA**
LaPrade	0	104.36	253.02
	20	71.00	470.54
	30	83.84	220.58
	60	62.23	501.02
	90	61.21	237.24
Arciero	0	69.36	342.41
	20	-11.75	110.72
	30	24.10	269.25
	60	69.56	-3647.59
	90	120.54	142.20

Table D.38: Mean post reconstruction paired specimen comparison for Specimen #8 at 0°, 20°, 30°, 60°, and 90° of flexion.

POST RECONSTRUCTION SPECIMEN #9			
	Flexion Angle	**% Recovered ER**	**% Recovered VA**
LaPrade	0	182.64	27.45
	20	577.61	50.61
	30	53.02	-27.30
	60	88.84	58.77
	90	-78.36	8.95
Arciero	0	157.58	38.02
	20	-11.19	44.47
	30	50.16	60.01
	60	39.86	-7.98
	90	87.02	-5.28

Table D.39: Mean post reconstruction paired specimen comparison for Specimen #9 at 0°, 20°, 30°, 60°, and 90° of flexion.

D.6.2 Post Tib-Fib/ACL Paired Comparison

POST ACL SECTIONING SPECIMEN #2			
	Flexion Angle	**% Lost ER**	**% Lost VA**
LaPrade	0	-35.65	17.73
	20	-5.97	28.71
	30	-1.96	-9.97
	60	7.77	17.75
	90	44.71	14.91
Arciero	0	14.94	20.27
	20	34.80	5.15
	30	41.55	76.75
	60	60.67	20.78
	90	116.6	3.91

Table D.40: Mean tib-fib/acl sectioned paired specimen comparison for Specimen #2 at 0°, 20°, 30°, 60°, and 90° of flexion.

POST ACL SECTIONING SPECIMEN #3			
	Flexion Angle	**% Lost ER**	**% Lost VA**
LaPrade	0	-9.15	11.66
	20	6.97	33.24
	30	24.78	11.71
	60	6.19	32.53
	90	-0.73	13.88
Arciero	0	70.25	28.61
	20	4.82	11.02
	30	75.90	38.24
	60	41.50	31.75
	90	23.70	9.48

Table D.41: Mean tib-fib/acl sectioned paired specimen comparison for Specimen #3 at 0°, 20°, 30°, 60°, and 90° of flexion.

POST ACL SECTIONING SPECIMEN #4			
	Flexion Angle	**% Lost ER**	**% Lost VA**
LaPrade	0	197.71	22.13
	20	97.66	1.87
	30	-15.25	32.53
	60	-23.73	19.70
	90	37.03	22.42
Arciero	0	713.46	96.38
	20	-287.93	25.92
	30	118.67	38.42
	60	20.61	45.19
	90	16.24	66.68

Table D.42: Mean tib-fib/acl sectioned paired specimen comparison for Specimen #4 at 0°, 20°, 30°, 60°, and 90° of flexion.

POST TIB-FIB SECTIONING SPECIMEN #5			
	Flexion Angle	**% Lost ER**	**% Lost VA**
LaPrade	0	149.21	8.87
	20	-98.79	31.24
	30	-75.40	40.92
	60	-334.68	53.23
	90	-4.54	62.71
Arciero	0	44.95	47.53
	20	261.96	121.02
	30	51.58	77.76
	60	60.63	310.89
	90	182.74	54.44

Table D.43: Mean tib-fib/acl sectioned paired specimen comparison for Specimen #5 at 0°, 20°, 30°, 60°, and 90° of flexion.

POST TIB-FIB SECTIONING SPECIMEN #6			
	Flexion Angle	**% Lost ER**	**% Lost VA**
LaPrade	0	102.52	20.61
	20	137.47	16.97
	30	107.13	18.07
	60	118.29	5.95
	90	23.56	1.35
Arciero	0	32.38	79.22
	20	194.03	137.81
	30	222.407	78.107
	60	5.48	8.20
	90	-28.20	55.31

Table D.44: Mean tib-fib/acl sectioned paired specimen comparison for Specimen #6 at 0°, 20°, 30°, 60°, and 90° of flexion.

POST TIB-FIB SECTIONING SPECIMEN #7			
	Flexion Angle	**% Lost ER**	**% Lost VA**
LaPrade	0	24.22	16.79
	20	716.45	27.05
	30	91.16	79.81
	60	28.56	20.56
	90	-4.09	-18.22
Arciero	0	-19.18	29.11
	20	31.43	24.09
	30	16.36	99.07
	60	37.35	130.68
	90	51.96	55.48

Table D.45: Mean tib-fib/acl sectioned paired specimen comparison for Specimen #7 at 0°, 20°, 30°, 60°, and 90° of flexion.

POST TIB-FIB SECTIONING SPECIMEN #8			
	Flexion Angle	**% Lost ER**	**% Lost VA**
LaPrade	0	4.12	11.68
	20	47.04	17.01
	30	14.25	33.17
	60	37.24	6.88
	90	2.42	7.39
Arciero	0	186.25	25.71
	20	261.34	52.24
	30	-114.22	91.87
	60	-18.99	1.88
	90	-15.82	66.94

Table D.46: Mean tib-fib/acl sectioned paired specimen comparison for Specimen #8 at 0°, 20°, 30°, 60°, and 90° of flexion.

POST TIB-FIB SECTIONING SPECIMEN #9			
	Flexion Angle	**% Lost ER**	**% Lost VA**
LaPrade	0	5.58	240.32
	20	152.71	47.89
	30	-67.65	-133.13
	60	-1.39	139.62
	90	227.76	-678.50
Arciero	0	17.70	154.15
	20	-2382.98	-19.73
	30	-4.89	-0.50
	60	6.06	839.03
	90	33.97	2471.48

Table D.47: Mean tib-fib/acl sectioned paired specimen comparison for Specimen #9 at 0°, 20°, 30°, 60°, and 90° of flexion.

Bibliography

[1] LaPrade, F. Robert, Ly V., Thuan., "The Posterolateral Attachments of the Knee, A Qualitative and Quantitative Morphologic Analysis of the Fibular Collateral Ligament, Popliteus Tendon, Popliteofibular Ligament, and Lateral Gastrocnemius Tendon" *Am J Sports Med.* 2003;854-860

[2] Laprade, F. Robert, Morgan M., Patrick., "The Anatomy of the Posterior Aspect of the Knee, An Anatomic Study" *J Bone Joint Surg.* 2007

[3] LaPrade, F. Robert, Bollom S., Timothy., "Mechanical Properties of the Posterolateral Structures of the Knee" *Am J Sports Med.* 2005;1386-1391

[4] Kim, H. Yoon, Purevsuren, Tserenchimed., Contribution of posterolateral corner structures to knee joint translational and rotational stabilities: A computational study" *Journal of Engineering in Medicine.* 2013;227(9)968-975

[5] Sanchez II, R. Anthony, Sugalski, T. Matthew., "Anatomy and Biomechanics of the Lateral Side of the Knee" *Sports Med Arthrosc Rev.* 2006(14)

[6] Vinson, N. Emily, Major, M. Nancy., "The Posterolateral Corner of the Knee" *American Journal of Roentgenology.* 2008;190: 449-458

[7] Davies, Hywel, Unwin, Andrew., "The posterolateral corner of the knee Anatomy, biomechanics and management of injuries" *Injury, Int. J. Care Injured.* 2004;35:68-75

[8] Cooper, M. Jonathan, McAndrews, T. Peter., "Posterolateral Corner Injuries of the Knee: Anatomy, Diagnosis, and Treatment" *Sports Med Arthrosc Rev.* 2006(14)

[9] Lunden, B. Jason, Bzdusek, J. Peter., "Current Concepts in the Recognition and Treatment of Posterolateral Corner Injuries of the Knee" *J Orthop Sports Phys Ther.* 2010;40(8):502-516

[10] Arciero, A. Robert., "Technical Note: Anatomic Posterolateral Corner Knee Reconstruction" *Arthroscopy: The Journal of Arthroscopic and Related Surgery.* 2005;(21)1147.e1-1147.e5

[11] LaPrade, F. Robert, Johansen, Steinar., "An Analysis of an Anatomical Posterolateral Knee Reconstruction: An In Vitro Biomechanical Study and Development of a Surgical Technique" *Am J Sports Med.* 2004;(32)

[12] Ho, P. Eric, Lam, Mak-Ham., "Comparison of 2 Surgical Techniques for Reconstructing Posterolateral Corner of the Knee: A Cadaveric Studyy Evaluated by Navigation System" *The Journal of Arthroscopic and Related Surgery.* 2011;(27):89-96

[13] LaPrade, F. Robert, Heikes, Christie., "The Reproducibility and Repeatability of Varus Stress Radiographs in the Assessment of Isolated Fibular Collateral Ligament and Grade-III Posterolateral Knee Injuries, An in Vitro Biomechanical Study" *J Bone Joint Surg Am.* 2008;(90):2069-2076

[14] Clancy Jr, W.G. P.B. Rauh, Jasper, L.E., "Biomechanical evaluation of two reconstruction techniques for posterolateral instability of the knee" *J Bone Joint Surg [Br]* 2010;92-B:1460-1465

[15] Yoon, H. Kyoung, Lee, H. Jung., "Comparison of Clinical Results of Anatomic Posterolateral Corner Reconstruction for Posterolateral Rotary Instability of the Knee With or Without Popliteal Tendon Reconstruction" *Am J Sports Med.* 2011;39:2421

[16] Geeslin, G. Andrew, LaPrade, F. Robert., "Outcomes of Treatment of Acute Grade-III Isolated and Combined Posterolateral Knee Injuries" *J Bone Joint Surg Am.* 2011;(93):1672-1683

[17] Fanelli, C. Gregory, Edson, J. Craig., "Combined Posterior Cruciate Ligament-Posterolateral Reconstructions With Achilles Tendon Allograft and Biceps Femoris Tendon Tenodesis: 2-to 10-Year Follow-Up" *The Journal of Arthroscopic and Related Surgery.* 2004;(20):339-345

[18] Bolog Nicolae, Hodler Juerg., "MR imaging of the posterolateral corner of the knee" *Skeletal Radiology.* 2007;(36)715-728

[19] LaPrade, F. Robert, Griffith. J. Chad., "Improving Outcomes for Posterolateral Knee Injuries" *Journal of Orthopedic Research.* 2014;DOI:10.1002/jor.22572

[20] Nau Thomas, Chevalier Yan., "Comparison of 2 Surgical Techniques of Posterolateral Corner Reconstruction of the Knee" *Am J Sports Med.* 2005;(33)No.12

[21] Kanamori Akihiro, Mi Lee J., "A biomechanical analysis of two reconstructive approaches to the posterolateral corner of the knee" *Knee Surg Sports Traumatol Arthrosc* 2003;(11):312-317

[22] Engebretsen Lars, Wijdicks, A. Coen., "Evaluation of simulated pivot-shift test: a biomechanical study" *Knee Surg Sports Traumatol Arthros.* 2012;(20)698-702

[23] McCarthy Mark, Camarda Lawrence., "Anatomic Posterolateral Knee Reconstructions Require a Popliteofibular Ligament Reconstruction Through a Tibial Tunnel" *Am J Sports Med* 2010;(38):1674

[24] Djian P., "Posterolateral knee reconstruction" *Orthopedics and Traumatology: Surgery and Research.* 2015;S159-S170

[25] Terry, C. Glenn, LaPrade, F. Robert., "The Posterolateral Aspect of the Knee, Anatomy and Surgical Approach" *Am J Sports Med.* 1996;(24):6

[26] Jabara, Michael., Bradley, Jeffrey., Merrick, Michael., "Is Stability of the Proximal Tibiofibular Joint Important in the Multiligament-injured Knee?" *Clin Orthop Relat Res.* 2014; 427:2691-2697

[27] Crespo, Bernardo., James, W. Evan., Metsavaht, Leonardo., LaPrade, F. Robert., "Injuries to Posterolateral Corner of the Knee: a Comprehensive Review from Anatomy to Surgical Treatment" *Rev Bras Ortop.* 2014; 50(4):363-70

[28] LaPrade, F. Robert., Moulton, G. Samuel., Nitri, Marco., Mueller, Werner., Engebretsen, Lars., "Clinically Relevant Anatomy and what Anatomic Reconstruction Means" *Knee Surg Sports Traumatol Arthrosc.* 2015; (10):2950-9

[29] Shin, Miyatake., Eiji, Kondo., Tsung-Yuan, Tsai., Hirschmann, Michael., Halewood, Camilla., Bent, W. Jakobsen., Kazunor, Yasuda., Amis, A. Andrew., "Biomechanical Comparisons Between 4-Strand and Modified Larson 2-Strand Procedures for Reconstruction of the Posterolateral Corner of the Knee" *Am J Sports Med.* 2011; 39:146

[30] Besier, TF., Lloyd, DG., Ackland, TR., Cochrane, JL., "Anticipatory Effects on Knee Joint Loading during Running and Cutting Maneuvers" *Med Sci Sports Exerc.* 2001; 33:1176-1181

[31] Boden BP, Dean GS, Feagin JA Jr, Garrett WE Jr., "Mechanisms of Anterior Cruciate Ligament Injury" *Orthopedics.* 2000; 23:573-578

[32] Renstrom P, Ljungqvist A, Arendt E, Beynnon B, Fukubayashi T, Garrett W, Georgoulis T, Hewett TE, Johnson R, Krosshaug T, Mandelbaum B, Micheli L, Myklebust G, Roos E, Roos H, Schamasch P, Shultz S, Werner S, Wojtys E, Engebretsen L., "Non-contact ACL Injuries in female athletes: an International Olympic Committee current concepts statement." *Br J Sports Med* 2008; 42:394-412

[33] Sonin AH, Fitzgerald SW , Friedman H , Hoff FL , Hendrix RW , Rogers LF., "Posterior Cruciate Ligament Injury: MR Imaging Diagnosis and Patterns of Injury." *Radiology* 1994; 190(2):455-8

[34] Mo F, Arnoux PJ , Zahidi O , Masson C., "Injury Thresholds of Knee Ligaments under lateral-medial shear loading: an Experimental Study" *Traffic Injury Prevention.* 2013; 14(6):623-9

[35] Cram 2014. Gorummd J. Accessed January 2016. www.cram.com/flashcards

[36] Sports Injury Clinic "Proximal Tibiofibular Joint Dislocation". Accessed January 2016. www.sportsinjuryclinic.net/sports-injuries/knee-pain/tibiofibular-joint-dislocation

[37] ACLSolutions "What is the ACL". Accessed January 2016. www.aclsolutions.com/theacl1.php

[38] Serbino Jose, Da Mota Roberto, Pereira Cesar., "Posterolateral anatomical reconstruction restored varus but not rotational stability: A biomechanical study with cadavers" *Knee, The, Elsevier ClinicalKey Journals.* 2015; 499-505

[39] Plaweski S, Belvisi B, Moreau-Gaudry A,. "Reconstruction of the Posterolateral Corner after Sequential Sectioning Restores Knee Stability" *Orthopedic Journal of Sports Medicine* 2015;3(2):2325967 115570560

[40] Fares Qeadan (2015). On MANOVA using STATA, SAS & R. A short course in biostatistics for the Mountain West Clinical Translational Research Infrastructure Network (grant 1U54GM104944) and UNM Clinical & Translational Science Center (CTSC) (grant UL1TR001449). University of New Mexico Health Sciences Center. Albuquerque, New Mexico

[41] Dieter Christian, Wirtz, Schiffers Norbert, Pandorf Thomas, Radermacher Klaus,. "Critical evaluation of known bone material properties to realize anisotropic FE-simulation of the proximal femur" *Journal of Biomechanics* 2000;1325-1330

[42] Rho Jae-Young, Roy II Marcel, Tsui Ting, Pharr George,. "Elastic properties of microstructural components of human bone tissue as measured by nanoindentation" *Journal of Biomedical Materials Research* 1999;Volume 45:48-54

[43] YI Wian-hong, Jun PAN, GUO Xiao-shan,. "Anatomical and biomechanical study on the interosseous membrane of the cadaveric forearm" *Chinese Journal of Tramatology* 2011;14(3):147-150

[44] A. Thambyah, B.P. Pereira,. "Mechanical Contribution of the Fibula to Torsion Stiffness in the Lower Extremity" *Clinical Anatomy"* 2006;19:615-620

[45] Dragomir-Daescu D, Salas C, Uthamaraj S, Rossman T,. "Quantitative computed tomography-based finite element analysis predictions of femoral strength and stiffness depend on computed tomography settings" *J Biomech.* 2015;48(1):153-61

[46] Dragomir-Daescu D, Op Den Buijs J, McEligot S, Dai Y, Entwistle RC, Salas C, Melton LJ 3rd,. "Robust QCT/FEA models of proximal femur stiffness and fracture load during a sideways fall on the hip" *Ann Biomed Eng.* 2011;39(2):742-55